

**JAERI-Tech  
98-055**



**DESIGN & ANALYSIS OF ITER SHIELD BLANKET**

**December 1998**

**Junji OHMORI, Toshihisa HATANO, Kouichiro EZATO, Shigemitsu HARA\*,  
Hidenori MIURA\*\*, Toshimasa KURODA, Kazuyuki FURUYA, Satoshi SATO,  
Mikio ENOEDA, Hideyuki TAKATSU and Yoshiyuki OHARA**

**日本原子力研究所  
Japan Atomic Energy Research Institute**

本レポートは、日本原子力研究所が不定期に公刊している研究報告書です。

入手の問い合わせは、日本原子力研究所研究情報部研究情報課（〒319-1195 茨城県那珂郡東海村）あて、お申し越してください。なお、このほかに財団法人原子力弘済会資料センター（〒319-1195 茨城県那珂郡東海村日本原子力研究所内）で複写による実費頒布をおこなっております。

**This report is issued irregularly.**

**Inquiries about availability of the reports should be addressed to Research Information Division, Department of Intellectual Resources, Japan Atomic Energy Research Institute, Tokai-mura, Naka-gun, Ibaraki-ken 319-1195, Japan.**

**© Japan Atomic Energy Research Institute, 1998**

編集兼発行 日本原子力研究所

Design & Analysis of ITER Shield Blanket

Junji OHMORI<sup>+</sup>, Toshihisa HATANO, Kouichiro EZATO, Shigemitsu HARA\*,  
Hidenori MIURA\*\*, Toshimasa KURODA, Kazuyuki FURUYA, Satoshi SATO,  
Mikio ENOEDA, Hideyuki TAKATSU<sup>++</sup> and Yoshiyuki OHARA

Department of Fusion Engineering Research  
Naka Fusion Research Establishment  
Japan Atomic Energy Research Institute  
Naka-machi, Naka-gun, Ibaraki-ken

(Received November 11, 1998)

This report includes electromagnetic analyses for ITER shielding blanket modules, fabrication methods for the blanket modules and the back plate, the design and the fabrication methods for port limiter have been investigated. Studies on the runaway electron impact for Be armor have been also performed.

Electro-magnetic analysis has been carried out for the shield blanket module to evaluate the effect of the slot on the first wall. Two models are applied to the analyses for stainless steel shield block of the #7 and the #9 module. The depth and the number of slots are simulated by changing the resistivity of the slotted SS. The relation between the reduction of electro-magnetic force and the increase of the resistivity are evaluated, and the number and the depth of slot are proposed.

The fabrication procedure for shield blanket module has been proposed using multi-layered HIP process. The shield modules are divided into several pieces in order to machine them. The pieces are machined for the grooves of cooling tubes, then bent to shape 3-D curved shaping. It is necessary to assemble them precisely for bonding by HIP at the same time. Issues are pointed out for the fabrication.

Fabrication procedure of the double wall back plate has been developed associated with machining procedure and welding concept. Welding jigs and fixtures, and the heat

---

+ Department of ITER Project

++ Office of ITER Project Promotion

\* Hitachi, Ltd.

\*\* Kawasaki Heavy Industry, Ltd.

treatment condition of back plate sectors are also presented for the assembly. The welding concept for connecting the rib to the inner wall is discussed and it is concluded that the through wall e-beam welding which needs less machining time is the most efficient welding method. The back plate shrinkage and deformation for splice plate welding are estimated. For the reference port limiter design, a compact support structure in the equatorial port and alternative vertical plate designs have been proposed. The support system meets the alignment and the support requirement under the electro-magnetic impulse loads. As to the vertical plate design, bolt connection between FWs and a vertical plate and bolt assembly of vertical plates are designed from the view point of fabrication. The fabrication procedures of the vertical plate is also discussed for low cost fabrication.

The thermal response of the First wall Be armor to the volumetric heat generation due to the runaway electrons impact is investigated. Using the energy deposition density, i.e. the volumetric heat generation due to the runaway electrons the maximum temperature and the melting region at the Be armor are also calculated.

**Keywords :** ITER, Blanket, Shield, First Wall, Runaway Electron

## ITER遮蔽ブランケットの設計と解析

日本原子力研究所那珂研究所核融合工学部

大森 順次<sup>+</sup>・秦野 歳久・江里幸一郎・原 重充\*  
三浦 秀徳\*\* 黒田 敏公・古谷 一幸・佐藤 聡  
榎枝 幹男・高津 英幸<sup>++</sup>・小原 祥裕

(1998年11月11日受理)

ITERの遮蔽ブランケットに対する電磁力解析、モジュールおよびバックプレートの製作方法、ポートリミターの設計と製作方法の検討を行った。また、逃走電子によるベリリウム第一壁の熱解析等を行った。

電磁力解析は、ブランケットモジュールについて第一壁に設けるスリットの影響を評価するために行った。代表的な#7モジュールと#9モジュールについて2つのモデルを用いた。スリットの深さと数はステンレスの抵抗値を変えることで模擬し、抵抗値の増加と電磁力の減少との関係を求め、スリットの数と深さを提案した。

遮蔽ブランケットの製作方法は、多層HIPによる方法を提案した。シールドモジュールは機械加工のため数個の部分に分けられる。各部分は冷却管の溝加工の後、3次元形状に曲げられる。各部分は1回のHIPによって接合する。さらに、製作上の問題点を指摘した。

2重壁のバックプレートの製作手法は、機械加工と溶接に関して検討し、組立のために必要な溶接治具、固定具、バックプレートセクターの熱処理条件等を示した。内壁とリブの接続の溶接法を検討した結果、壁を貫通するEB溶接が機械加工時間が少なく、最も有効である。さらに、溶接に用いる間隔片の収縮量と変形量も評価した。

ポートリミターの設計では、現在の設計に対する水平ポート内のリミター支持構造と代替設計を提案した。支持構造は、組立精度と電磁力の支持条件を満たしている。リミターの垂直板の設計では、第一壁とのボルト接続と垂直板のボルト組立を、製作の上から設計し、垂直板の低コストの製作手法も検討した。

逃走電子によるベリリウム第一壁の熱応答を検討した。エネルギー密度である体積発熱量を用いて、ベリリウム表面の最大温度、溶融深さを求めた。

---

那珂研究所：〒311-0193 茨城県那珂郡那珂町向山801-1

+ ITER開発室

++ ITER業務推進室

\* (株)日立製作所

\*\* 川崎重工業株式会社

This is a blank page.

## Contents

1. Introduction .....	1
2. Objectives .....	2
3. Electromagnetic Analysis of Shield Blanket Modules .....	3
3.1 Analytical Conditions .....	3
3.2 Analytical Results .....	8
3.3 Conclusions .....	24
4. Module Fabrication Procedure .....	25
4.1 Fabrication Procedures .....	25
4.2 Problems for Module Fabrication .....	26
5. Back Plate Fabrication Procedure .....	46
5.1 Design Concept .....	46
5.2 Fabrication Procedure .....	47
5.3 Annealing Process to Remove Residual Stress .....	49
5.4 Prevention of Welding Deformation .....	49
5.5 Estimation of Welding Deformation .....	50
6. Port Limiter Design .....	63
6.1 Support Structure .....	63
6.2 Fabrication .....	72
7. Studies on the Runaway Electron Effects on FW.....	89
7.1 Outline of EGS4 Code System and its Validation .....	89
7.2 Thermal Analyses of the Runaway Electron Impact on FW.....	89
7.3 Heat Generation inside of FW due to the Runaway Electron Impact .....	90
7.4 Thermal Response of FW due to the Runaway Electron Impact .....	91
7.5 Summary .....	91
8. Summary .....	96
Acknowledgement .....	97
References .....	97

## 目 次

1. 緒 言 .....	1
2. 目 的 .....	2
3. シールドブランケットモジュールの電磁解析 .....	3
3.1 解析条件 .....	3
3.2 解析結果 .....	8
3.3 結 論 .....	24
4. モジュールの製作方法 .....	25
4.1 製作手法 .....	25
4.2 モジュール製作の問題点 .....	26
5. バックプレートの製作手法 .....	46
5.1 設計概念 .....	46
5.2 製作手法 .....	47
5.3 残留応力除去の焼鈍手法 .....	49
5.4 溶接歪みの防止 .....	49
5.5 溶接歪みの評価 .....	50
6. ポートリミターの設計 .....	63
6.1 支持構造 .....	63
6.2 製 作 .....	72
7. 第一壁への迷走電子の検討 .....	89
7.1 EDS4コードの概要と妥当性 .....	89
7.2 第一壁への迷走電子衝突の熱解析 .....	89
7.3 迷走電子衝突による第一壁内の熱発生 .....	90
7.4 迷走電子衝突による第一壁の熱応答 .....	91
7.5 ま と め .....	91
8. ま と め .....	96
謝 辞 .....	97
参考文献 .....	97



## 1 . Introduction

This report was presented for ITER shield blanket design. ITER design has been performed during CDA (Conceptual Design Activities) and EDA ( Engineering Design Activities). For EDA design work, The report includes electromagnetic analyses for shield blanket modules, fabrication methods for the shield blanket modules and the back plate, the design and the fabrication methods for port limiter, and studies on the runaway electron impact for Be armor.

Electro-magnetic analysis has been carried out for the shield blanket module to evaluate the effect of the slot on the first wall in order to educe the electro-magnetic force. The fabrication procedure for shield blanket module and the back plate has been developed associated with machining procedure and welding concept. The designs and fabrication methods of port limiter which is located in equatorial port have been proposed.

The runaway electron effects on First Wall with Be armor were parametrically investigated by thermal analysis.

## 2. Objectives

The objective of this report is to perform mechanical design and analysis to further advance the current reference design of the shield blanket system. The shield blanket system is intended to remove the surface heat flux from the plasma and from bulk heating by the neutrons and to protect the superconducting coils and other ex-vessel components from excessive nuclear heating and radiation damage. The current design for the shield blanket features mechanically, hydraulically attached modules with beryllium first wall.

### 1) Electromagnetic Analysis

Perform electromagnetic analysis to define the electromagnetic forces in the shield blanket modules based on the current reference shield blanket system. Perform 3-D eddy current and EM load analyses incorporating the blanket modules, the back plate and the vacuum vessel with external coil systems and plasma. Examine further the effect of slots on EM load reduction.

### 2) Module Fabrication Procedure

Develop detailed module fabrication procedure, including fabrication methods to be applied and fabrication route of the blanket modules for the current reference shield blanket system. This study is to incorporate penetration holes in the module for front-access hydraulic connection and disconnection.

### 3) Back Plate Fabrication Procedure

Develop detailed back plate fabrication procedure based on the current reference shield blanket system. This study is to incorporate the double-walled back plate configuration and reinforcement ribs at the outboard region.

### 4) Port Limiter Design

Develop port limiter design, including study of fabrication route.

### 5) Analysis of Run-Away Electron Effects on the First Wall

Perform 3-D run-away electron analysis for the reference first wall. Perform 2-D thermo-mechanical analysis to obtain temperature and stress responses during run-away electron bombardment events.

### 3. Electromagnetic analysis of Shield Blanket Modules

Electromagnetic analysis has been carried out for the blanket modules to investigate the effect of the slot on the module surface.

#### 3.1 Analytical Conditions

The effects of the slot depth and number from the FW surface to the DS-Cu were evaluated by induced current and electromagnetic forces. The analyses have been carried out for #7 module because of maximum radial moment, and for #9 module because of maximum radial pulling force. The analysis conditions are as follows:

Model	Box-Shell, Torus 1/2 Sector(9°)
Code	EDDYCAL
Parameter	
Number of Slot	1, 10, 20 (per module)
Depth of Slot	0, 5, 15 (for Type I)
	0, 10, 50 (for Type II)

The analysis model and parameters are shown in Figs. 3.1-1 ~ 3.1-3 and Tables 3.1-1, 3.1-2. The 3-D shape modules were modeled by shell elements.

Two models are applied to the analyses. One has the element thickness of 20 mm on the plasma-side shield block (called Type I) which corresponds to the distance from FW to the first row of cooling tube. The other has the element thickness of 100 mm (called Type II) which corresponds to the skin depth for the 50 ms plasma disruption. The depth of slots are simulated by changing the resistivity of the slotted 316SS. The numbers of slots per module are 1 and 20, except for the slot depth of 15 mm for Type I because of the CPU time limit.

Table 3.1-1 Materials and Thickness of Blanket Structural Components

Component	Material	Thickness
Blanket		
First Wall	DS-Cu	5mm
Shield Block (Plasma Side)	SS316	20mm (Type I) 100mm (Type II)
Side Wall	SS316	100mm
End Wall	SS316	100mm
Top/Bottom Plate	SS316	100mm
Back Plate		
Inner Skin	SS316	50mm
Outer Skin	SS316	70mm
Vacuum Vessel		
Inner Skin	SS316	40mm
Outer Skin	SS316	40mm

Table 3.1-2 Plasma Disruption Conditions

Plasma Current	21MA
Major Radius	7.90m
Minor Radius	2.90m
Decay Time	50msec
Decay Mode	Centered Disruption
Blanket Thickness	0.40m

SDRC EAS VI: FE\_Modeling\_&\_Analysis  
02-DEC-97 14:51:12  
Units : SI  
Display: No stored Option  
Model Bar: 1-MAIN  
Associated Workset: 2-WORKING\_SET2

Database: none  
/view : ISOMETRIC (modified)  
Tech: Post Processing  
Model: 2-FWDET1

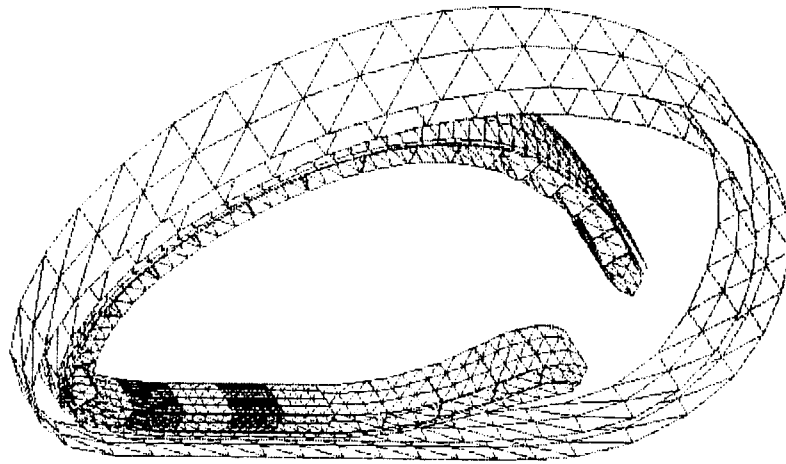


Fig. 3.1-1 Calculation model for electromagnetic analysis (whole view)

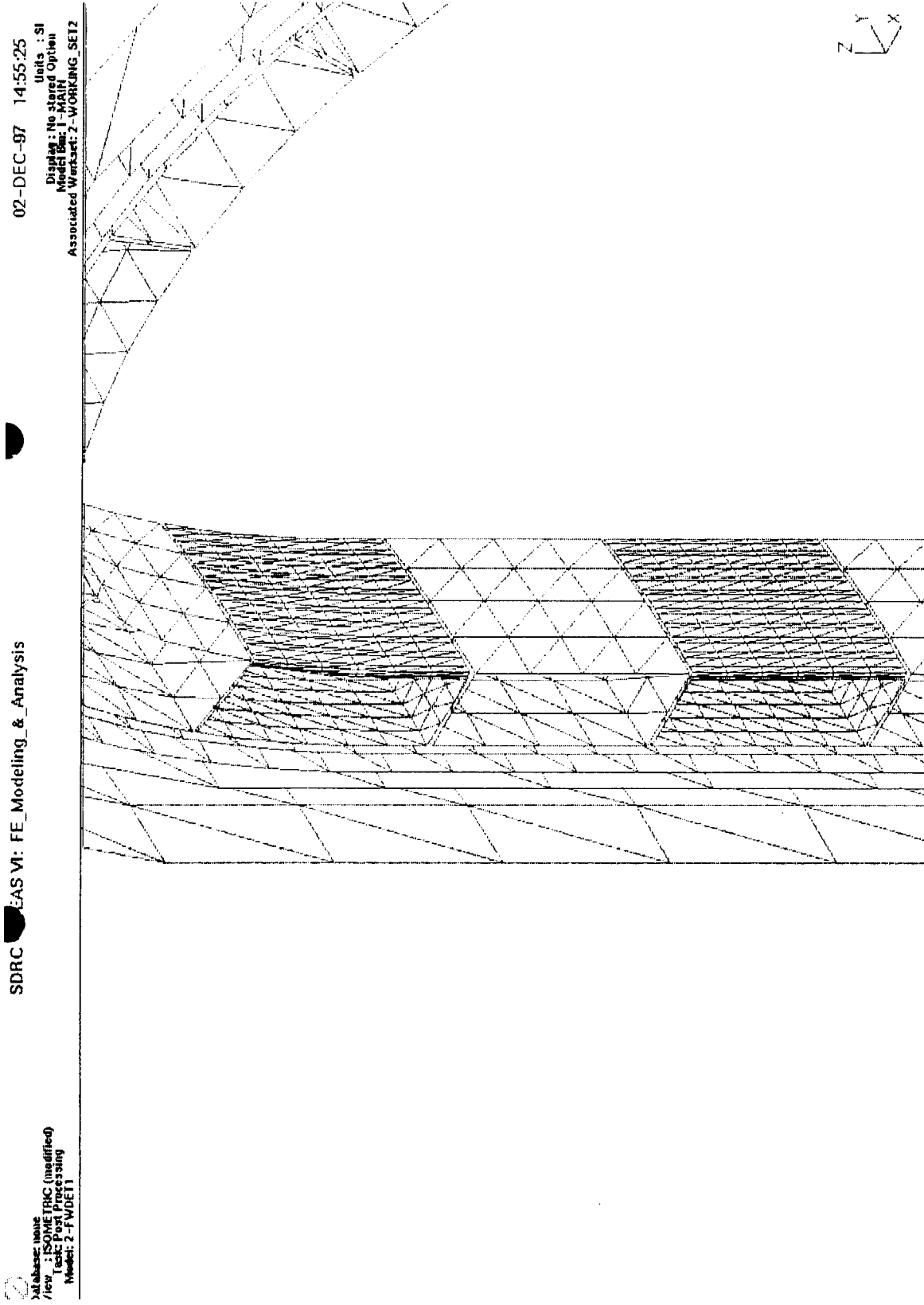


Fig. 3.1-2 Calculation model for electromagnetic analysis (Zoom-up of inboard)

22-DEC-97 14:30:05  
Units : SI  
Display : No stored Option  
Model Base : 1 - MAIN  
Associated Worksheet : WORKING\_SET4

SDRC EAS VI: FE\_Modeling\_ & Analysis

2  
Modelbase: none  
New Tech: ELECTRIC (unofficial)  
Tech: Post Processing  
Model: 4-FWDET10

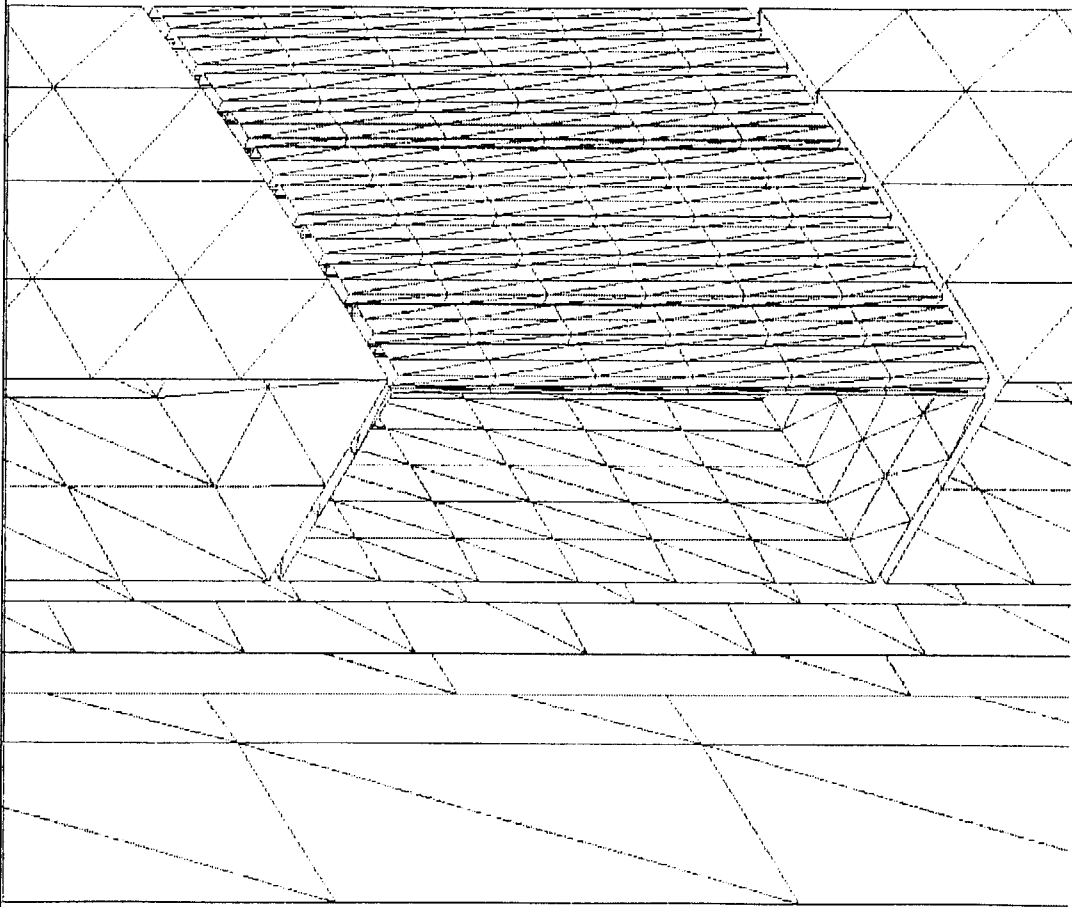


Fig. 3.1-3 Calculation model for electromagnetic analysis (Zoom-up of #7 module)

## 3.2 Analytical Results

### 3.2.1 Results of analyses for Type I cases

The model of Type I has the element thickness of 20mm on the plasma-side shield block which corresponds to the distance from FW to the first row of cooling tube.

#### 3.2.1.1 Results for #7 module

The induced currents, the electro-magnetic forces on the side wall and the pulling forces on the first wall for the #7 module are shown in Figs. 3.2.1-1~3.2.1-3. The horizontal axis of these figures is the relative resistance normalized by the first wall resistance without slot. The equivalent circuit of the first wall with slot is shown in Fig. 3.2.1-4. The resistivities of DS-Cu and 316SS had been used from the value of the ITER Material Assessment Report (IMAR) and the temperature at the first wall was assumed to be 250 °C.

The induced currents and the electro-magnetic forces decreased with the increase of the number of slots. In the case of normalized resistance of 6.5, which corresponds to the slotted first wall at every cooling channel, induced currents and shearing forces decreased to about 20 ~ 50% of that of no slotted first wall by extrapolation of exponential functions.

The pulling forces on the first wall depends on the current in DS-Cu of the first wall and they reduces two order less than of no slotted first wall in the case of the slot depth of 15mm into SS. In case of one slot, the induced current on side wall became about 75% of that of no slotted first wall even if the slot depth is 15mm. In case of 20 slots, the induced current is about 50% if the slot depth is 15mm. As the number of slot increases, the deep slot is required to reduce the electro-magnetic force

The value of normalized resistance vs. slot depth is shown in Fig. 3.2.1-5. The increase of normalized resistance is small at the slot depth of more than 5 mm, as the number of slot increases. When normalized resistance is about 5 or more, the induced current and electro-magnetic force decrease to less than 50%. It is difficult to slot around the front access holes. 50 slots is required to reduce the electro-magnetic force to 50% with the slot depth of 2 mm into SS. 10 slots is enough to reduce the force to 25%.

#### 3.2.1.2 Results for #9 module



The induced current and electro-magnetic force on side wall of #9 module are shown in Figs. 3.2.1-6 and 3.2.1-7. In the #9 module, the induced current to poloidal direction appears due to the change of the magnetic field caused by plasma current, because the external shape of plasma does not match with the poloidal curvature of the first wall surface. A current pattern in the first wall of the #9 module is an eddy shape and the gradient of the induced current to the poloidal direction is observed on side wall.

Induced current and pulling force on the DS-Cu of #9 module first wall decreased with increasing the slot depth. However, reduction of the induced current and the electro-magnetic force are small, and they increase in the case of many slots because of the addition of the induced current in poloidal direction in the shield block. Slotting is not effective to reduce the electro-magnetic force on the #9. Slotting should be limited only in the effective module for cost reduction.

### 3.2.2 Results of analyses for Type II cases

The model of Type II has the element thickness of 100mm on the plasma-side shield block which corresponds to the skin depth of 50 ms plasma disruption.

#### 3.2.2.1 Results for # 7 module

The induced currents, the electro-magnetic forces on the side wall and the pulling forces on the first wall for the #7 module are shown in Figs. 3.2.2-1 ~ 3.2.2-3. The induced current in 316SS is several times larger than that of Type I, although that in DS-Cu is a little bit lower. That is because the shield block elements are thicker and their resistance is smaller than those of Type I.

In the case of one slot, the induced current to the toroidal direction in DS-Cu does not decrease much with increasing the slot depth in SS. For the slot depth of more than 50 mm the induced current decreases in DS-Cu. As the number of slot increases, the deep slot become effective for the induced current reduction. However, even if first wall are slotted in depth of 10 mm at every all cooling channel(normalization resistance 2.15), the reduction of electro-magnetic force is only 20~30% by extrapolation of slot depth.

The electro-magnetic shearing force decrease to about 50% in the cases of slot depth of 0 and 10 mm. The shearing force in a side wall is the summation of that of the shield block region and the first wall region. The shearing force is proportional to the radial distance between elements that cross the magnetic field. Current

reduction of the first wall DS-Cu is larger than that of the side wall of shield block. The distance between DS-Cu element and SS shield is larger than that of Type I. Those effects made the electro-magnetic shearing force small.

Although the induced current in DS-Cu decreases, the pulling force increases in the elements. The deep slot makes it difficult for the induced current to flow into a shield block. The flow pattern of the induced current is the circulation in DS-Cu elements. The pulling force becomes large by the interaction between the induced current and the poloidal/toroidal magnetic field. For a lot of slots, the increase of the pulling force is not much because of canceling the force between adjacent slots.

The increase of normalized resistance (see Fig. 3.2.2-4) becomes small with the increase of the number of slots. Induced current and electro-magnetic force decrease to 20~30% at the normalized resistance of 2. The normalized resistance saturates at the depth of about 10 mm and the number of slot of 30. It is acceptable that the number of slot is 10 ~20 and the depth is 2 mm same as Type I.

#### **3.2.2.2 Results for # 9 module**

The analyses results for the #9 module are shown in Figs. 3.2.2-5, 3.2.2-6. Induced current and electro-magnetic force increase except in the first wall DS-Cu. This reason is similar to that of Type I. Slotting is not effective to reduce the electro-magnetic force for #9 module.

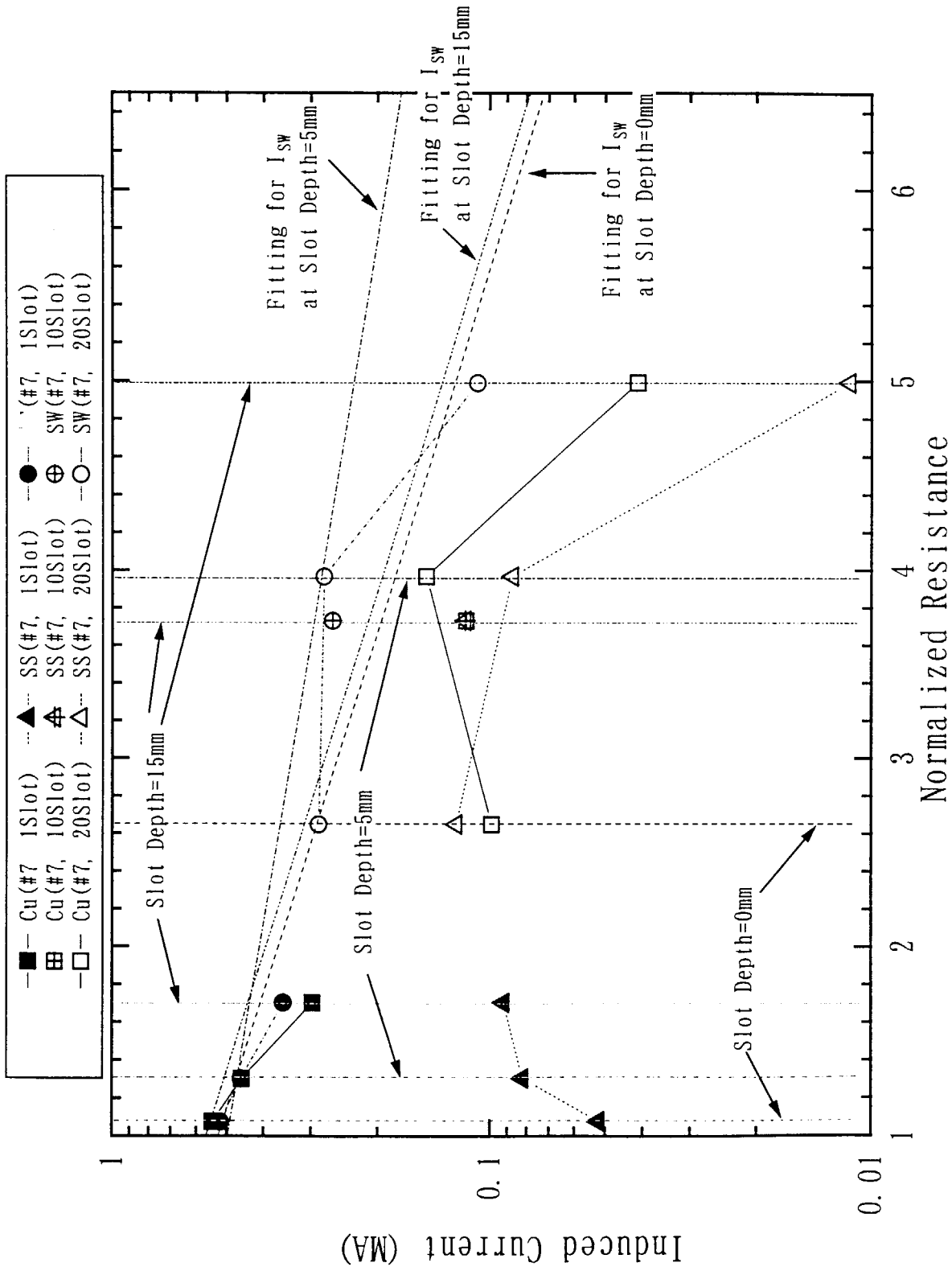


Fig. 3.2.1-1 Induced Current vs Normalized Resistance in Case of Type I (#7,  $t_{SS}=20\text{mm}$ )

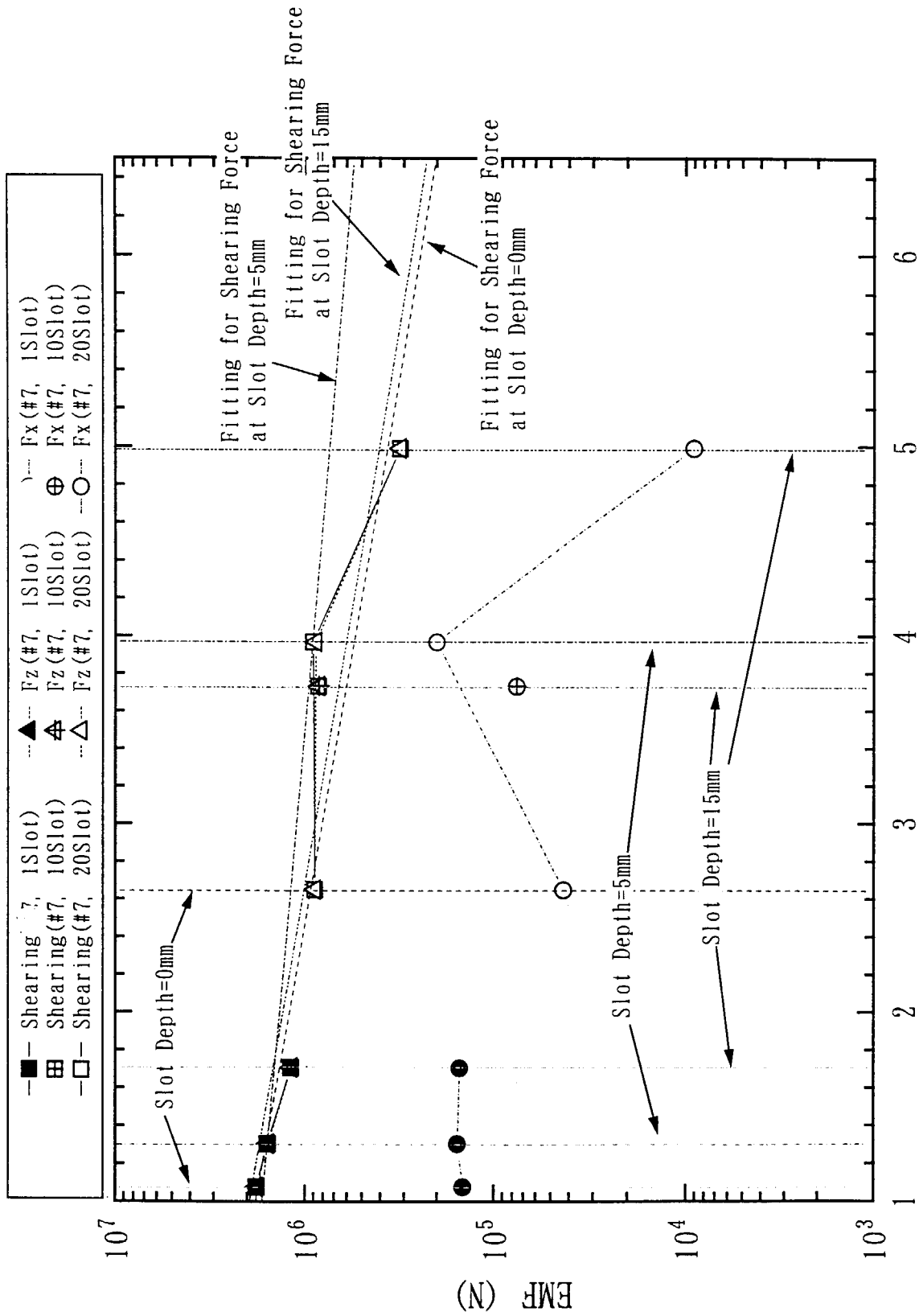


Fig. 3.2.1-2 EMF vs Normalized Resistance in Case of Type I (#7,  $t_{ss}=20\text{mm}$ )

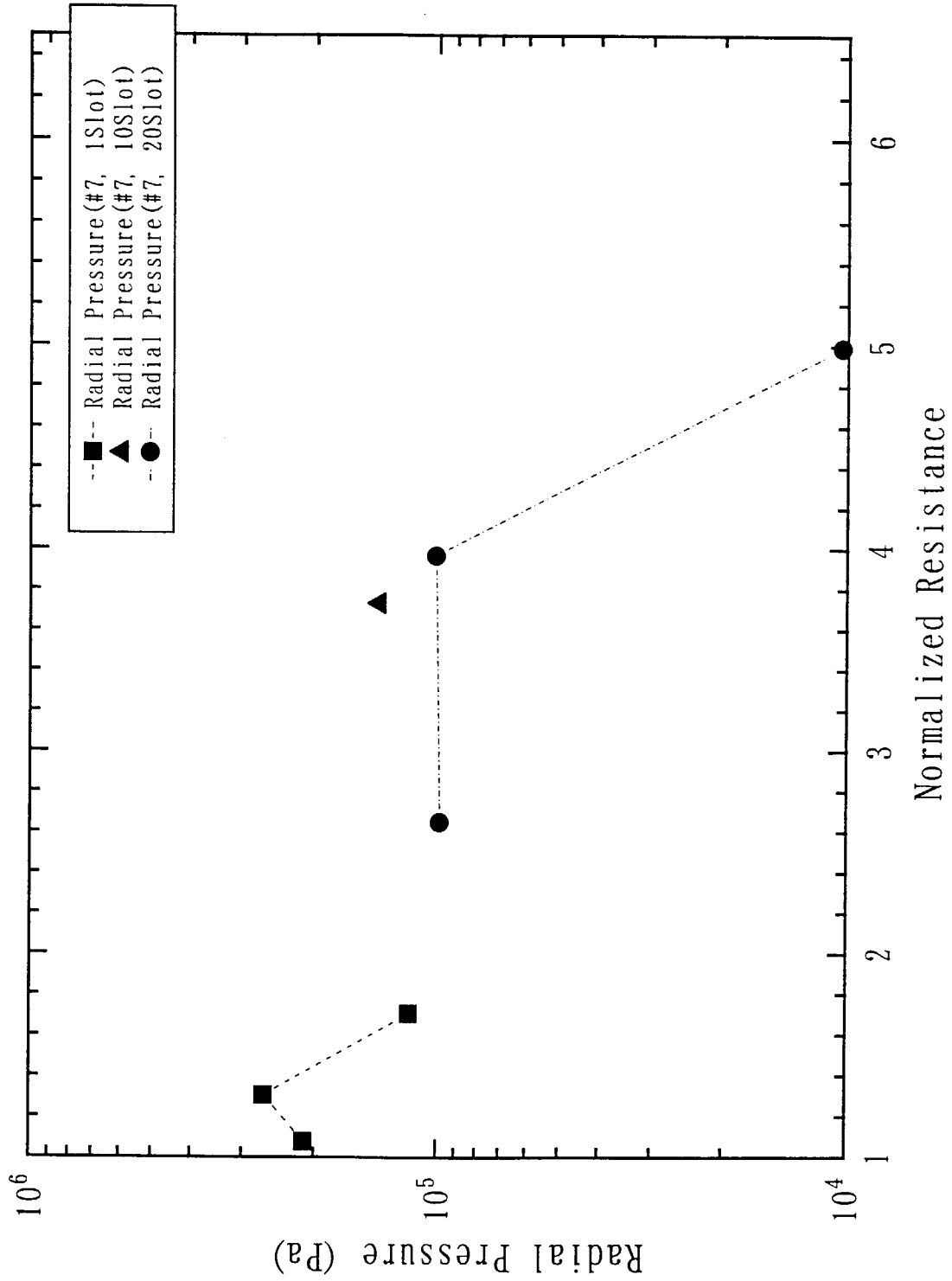


Fig. 3.2.1-3 Radial Pressure vs Normalized Resistance in Case of Type I  
 (#7,  $t_{SS}=20\text{mm}$ )

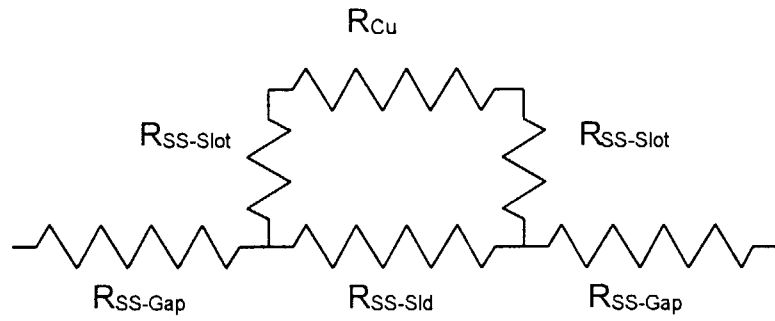


Fig. 3.2.1-4 Equivalent Circuit for Slot Resistance

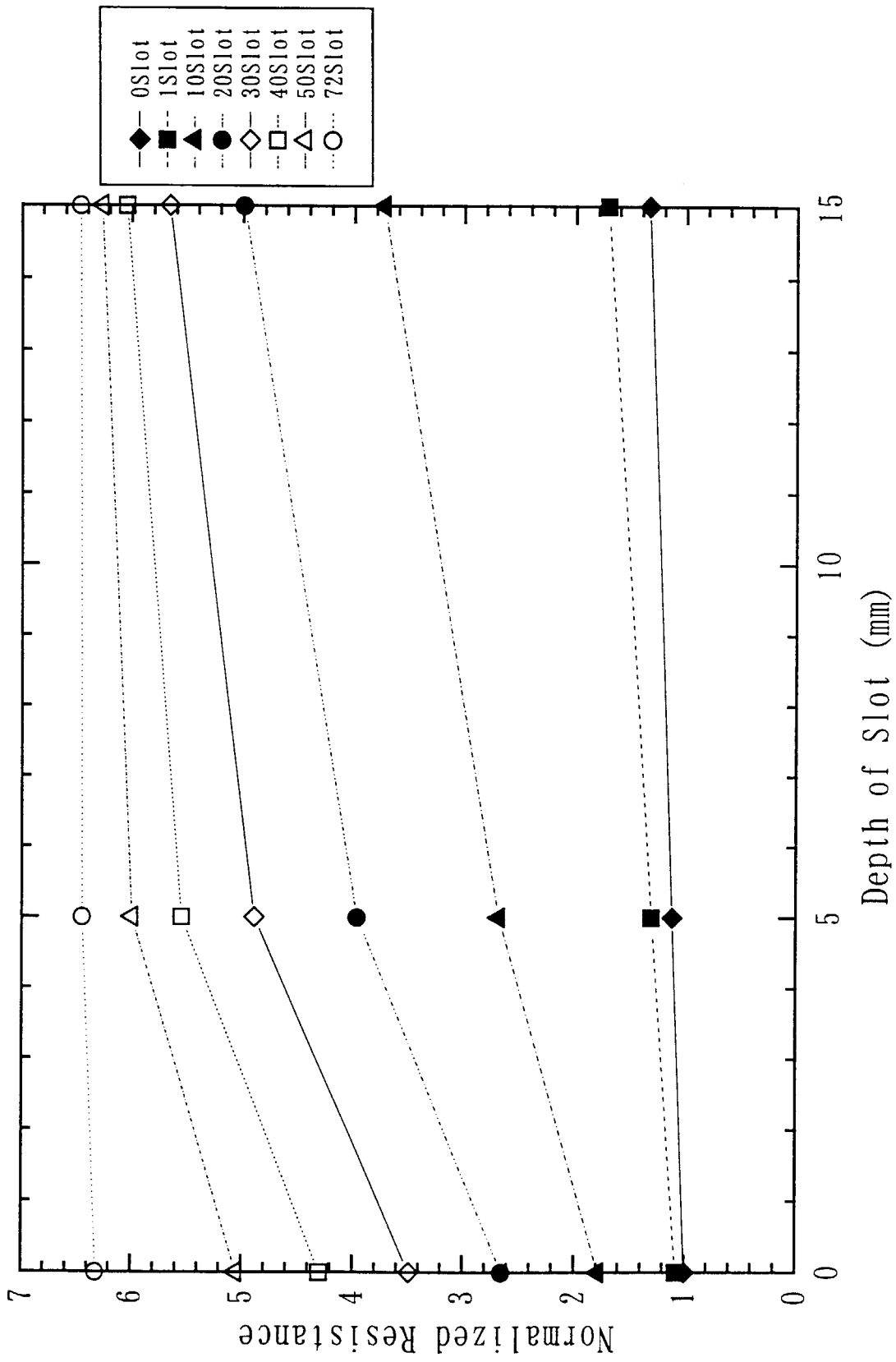


Fig. 3.2.1-5 Normalized Resistance vs Slot Depth in Case of Type I (  $t_{SS}=20\text{mm}$  )

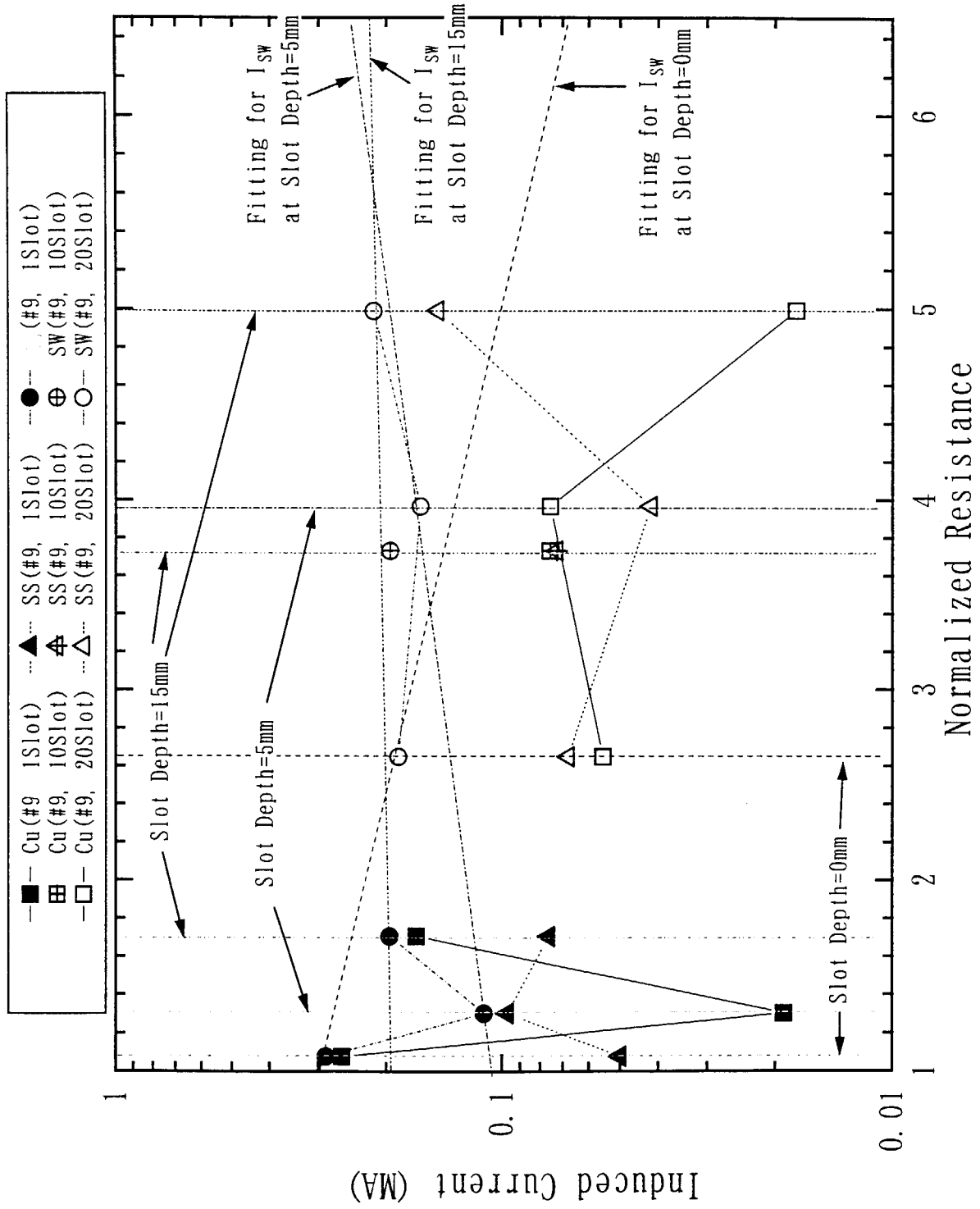


Fig. 3.2.1-6 Induced Current vs Normalized Resistance in Case of Type I (#9,  $t_{SS}=20\text{mm}$ )



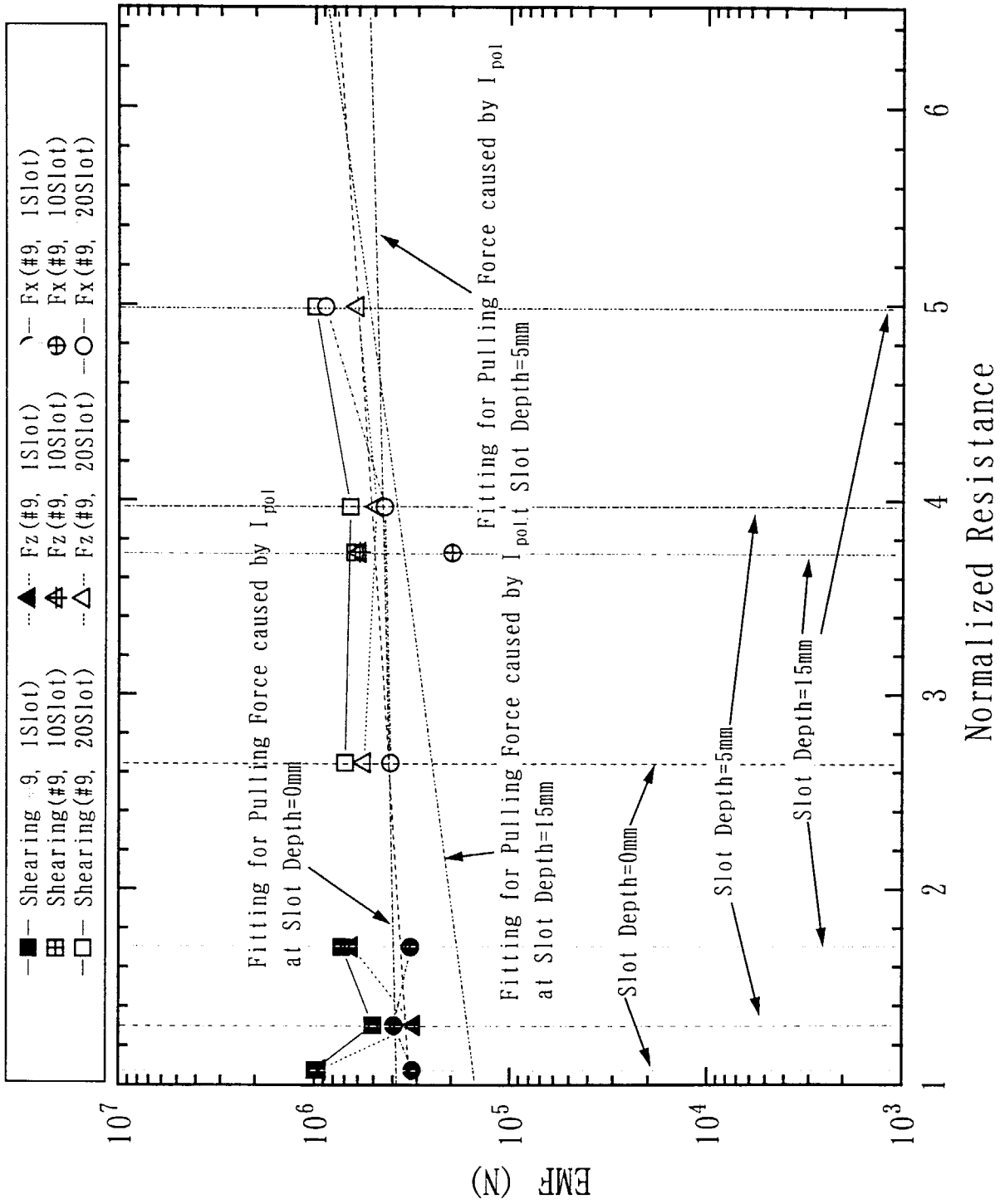


Fig. 3.2.1-7 EMF vs Normalized Resistance in Case of Type I (#9,  $t_{ss}=20\text{mm}$ )

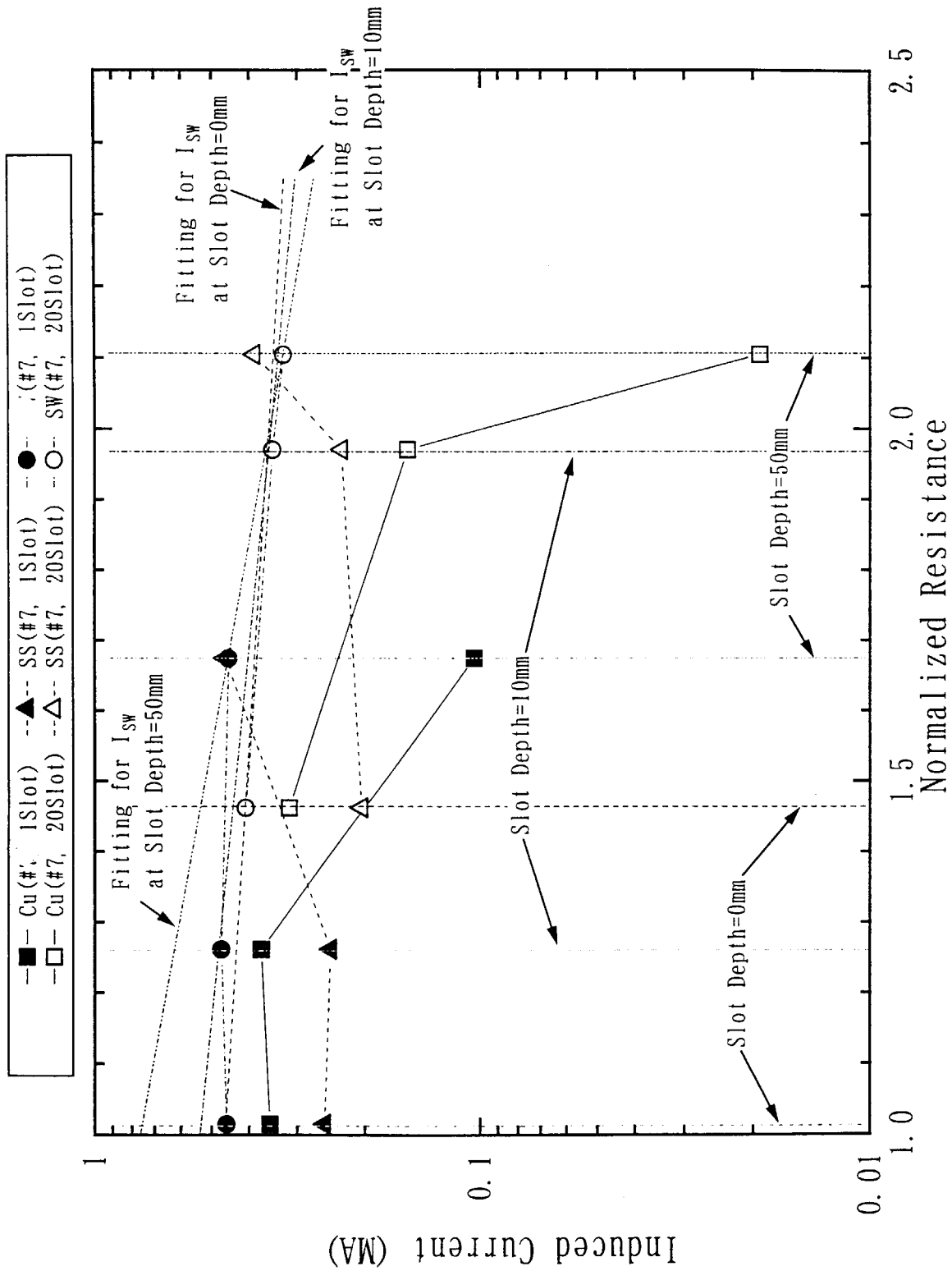


Fig. 3. 2. 2-1 Induced Current vs Normalized Resistance in Case of Type II (#7,  $t_{SS}=100\text{mm}$ )

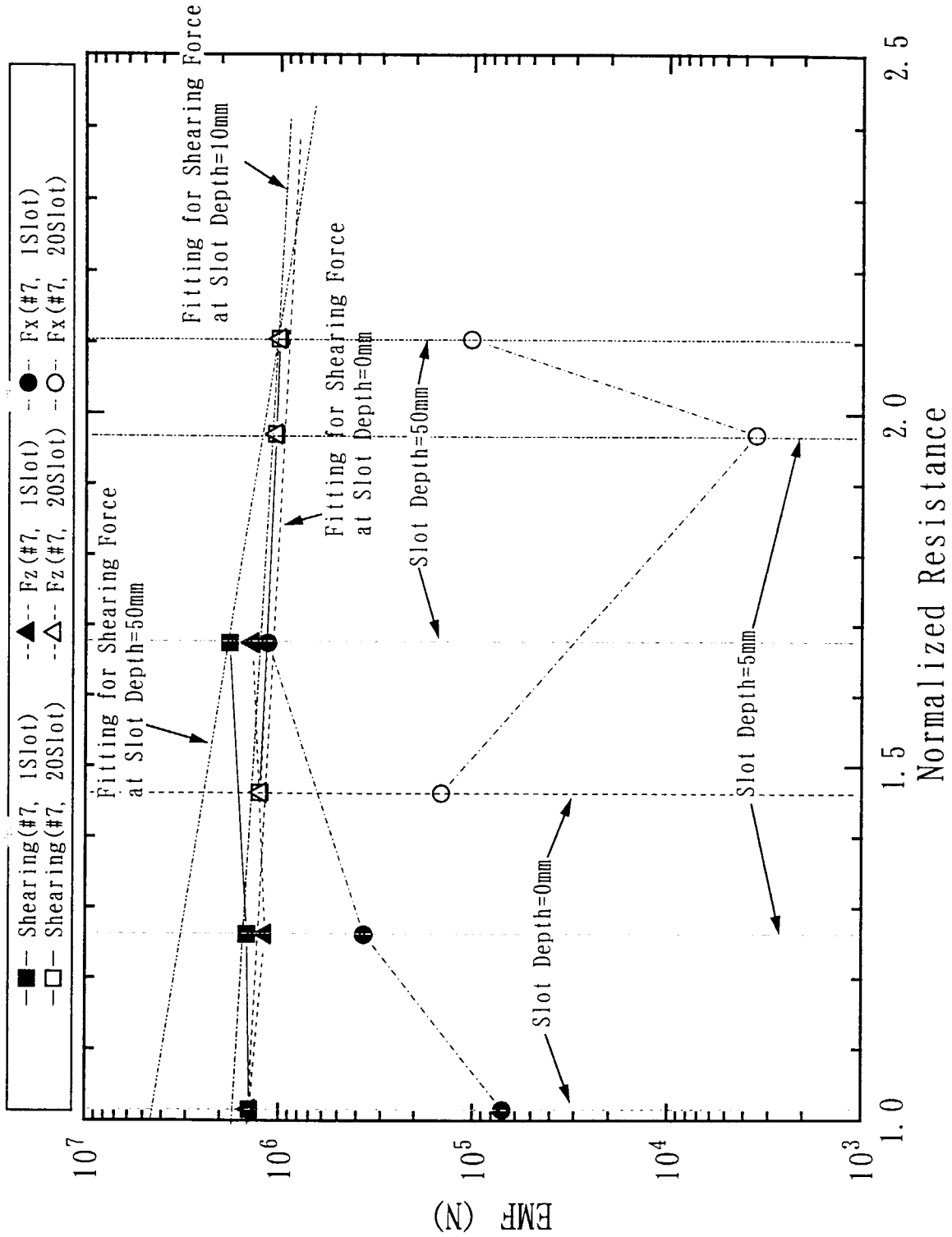


Fig. 3.2.2-2 EMF vs Normalized Resistance in Case of Type II (#7,  $t_{SS}=100\text{mm}$ )

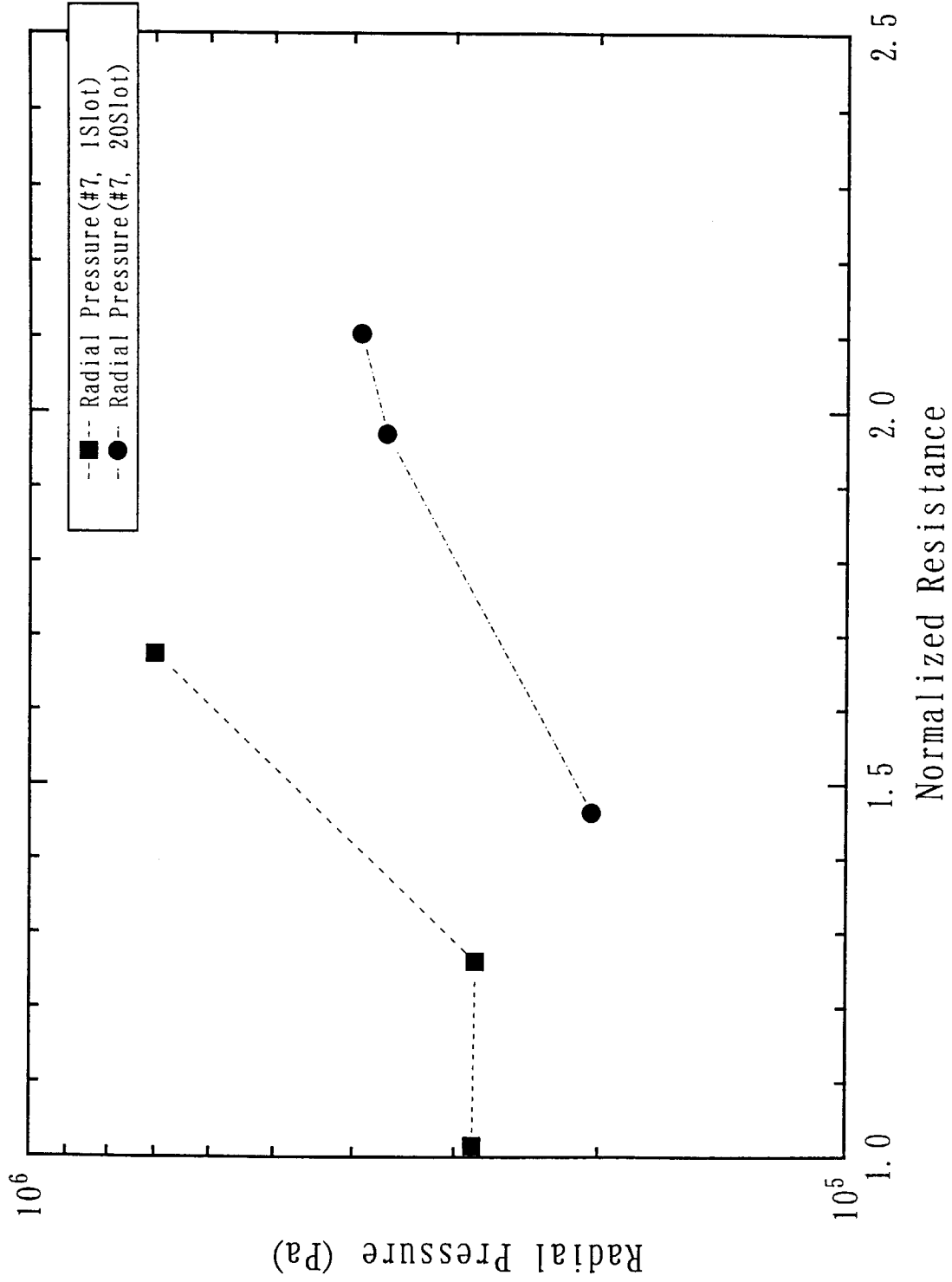


Fig. 3. 2. 2-3 Radial Pressure vs Normalized Resistance in Case of Type II  
(#7,  $t_{ss}=100\text{mm}$ )

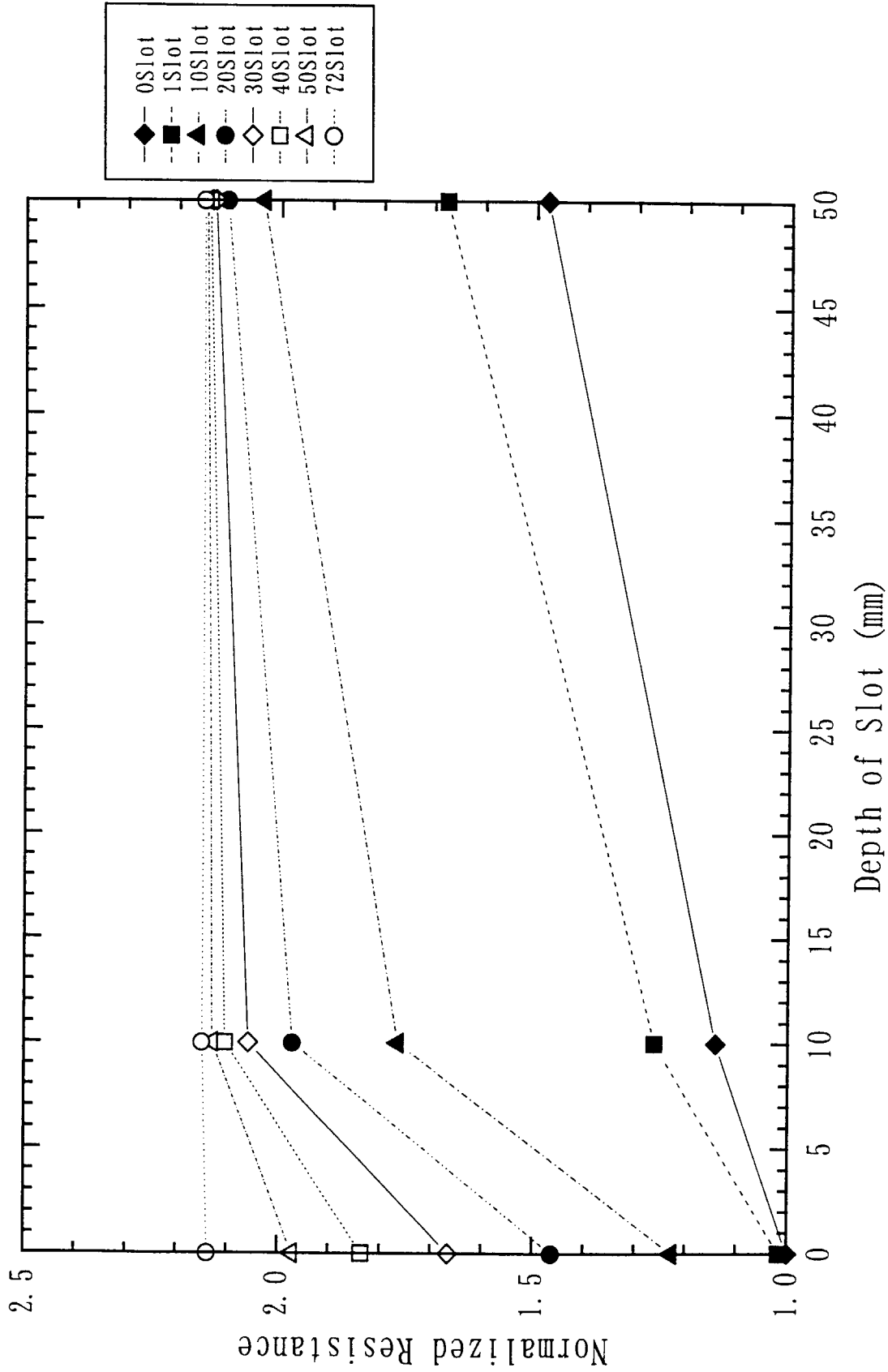


Fig. 3. 2. 2-4 Normalized Resistance vs Slot Depth in Case of Type II (  $t_{SS}=100\text{mm}$  )

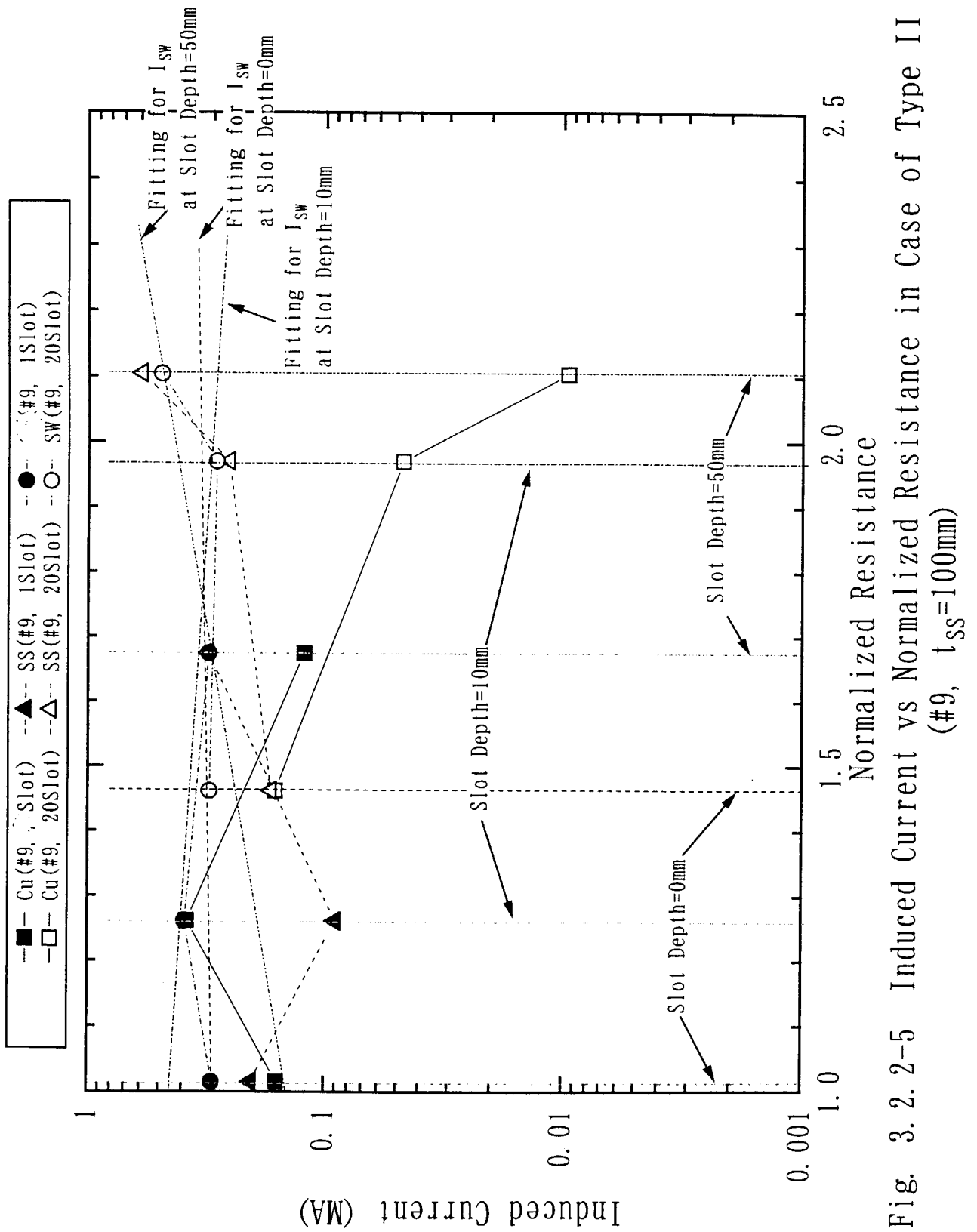


Fig. 3.2.2-5 Induced Current vs Normalized Resistance in Case of Type II (#9,  $t_{ss}=100\text{mm}$ )

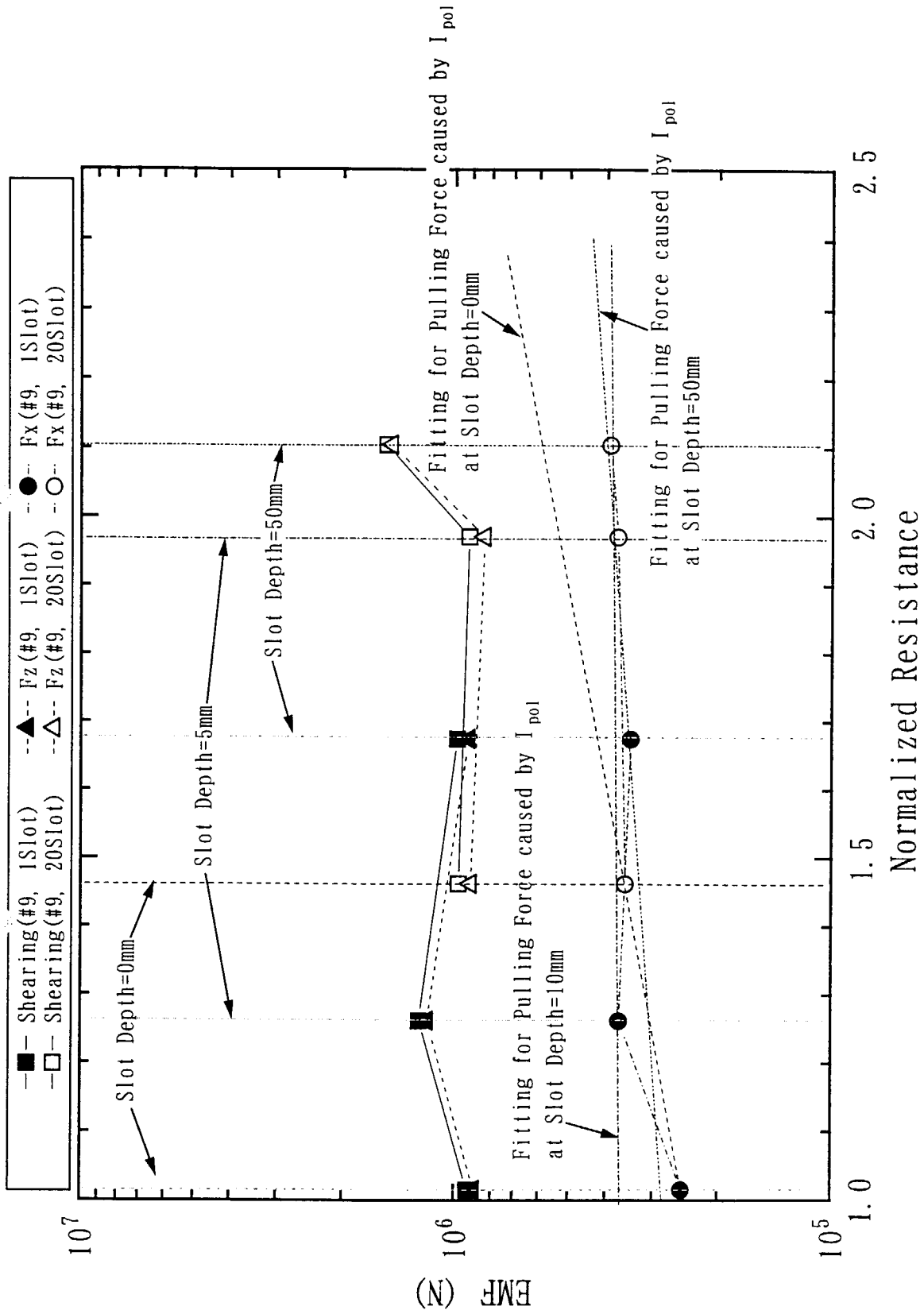


Fig. 3. 2-6 EMF vs Normalized Resistance in Case of Type II (#9,  $t_{SS}=100\text{mm}$ )

### 3.3 Conclusions

To verify the effect of slotting between the first wall cooling channels for electro-magnetic force reduction, electro-magnetic analysis had been carried out with parameters of the number of slot and the slot depth. Two analytical models are applied to the calculations using Box-Shell element. One has the element thickness of 20 mm on the plasma-side shield block (called Type I) which corresponds to the distance from FW to the first row of cooling tube. The other has the element thickness of 100 mm (called Type II) which corresponds to the skin depth for the 50 ms plasma disruption.

As a result, the following conclusions were obtained.

- a.) In both case of Type I and Type II, slotting on the first wall become effective for the #7 module, but it is not effective for the #9 module.
- b. Realistic solution is number of slot of 10 ~20 with the depth of 2 mm for both case of Type I and II.
- c. For the case of Type I, the reduction of electro-magnetic force is more than 50%, but that is 20~30% for Type II. In actually, considering the current distribution inside the shield block, the electro-magnetic force reduction by slotting seems to be that of Type II.



## 4. Module Fabrication Procedure

### 4.1 Fabrication Procedures

The 11th shield blanket module, shown in figure 4.1-1, is investigated because of smallest curvature on the module surface. The flowchart of fabrication process for the shield blanket module is shown in figure 4.1-2

#### 4.1.1 Fabrication of First Walls

In the first wall of the shield blanket, the cooling pipes of stainless steel(SS) are located inside the copper of the heat sink. The first wall is fabricated by connecting two copper plates and SS pipes. Grooves for setting the cooling pipes are machined on copper plates, and the SS pipes are set on the grooves. Ends of the first wall module (top and bottom of the module) have SS plates in order to connect the shield block. These components are bonded by hot isostatic pressing (HIP).

The 11th module have two curvatures in the toroidal and the poloidal direction. To shape the curvature in the toroidal direction, the first wall is divided into several parts in toroidal direction. The curvature in the poloidal direction is shaped by bending of the first wall parts (copper plates and SS tubes). Around of the front access hole, grooves and pipes should be curved to avoid the hole. Front access holes are drilled after HIP bonding. The fabrication procedures of the first wall are shown in figure 4.1-3~4.1-7.

#### 4.1.2 Fabrication of Shielding Blocks

A shielding block is fabricated by SS forged or rolled material. The 11th shielding module have 3-D curved surface and curved cooling channels around front access holes. It is difficult to shape the curvature by bending and drilling process only. The shielding block is divided into 5 parts.(see figure 4.1-8) for machining.

The fabrication process of shielding block is similar to that of first wall. The divided shield block is machined for cooling channel grooves. The groove depth in the parts of A~C change to shape the curvature in the poloidal direction. The curvatures in the parts of A~C are shaped in the toroidal direction by bending and in the poloidal direction by machining, respectively.

Pipes for the cooling channel are bent in the toroidal curvature. The toroidal curvature in the part of D is shaped by machining. After the shaping, the grooves for the cooling channel in the middle part are machined and the cooling channels in the back side are made by drilling. After assembly of cooling pipes and the shield blocks, they are bonded by HIP process. The fabrication procedures of a shield block are shown in figure 4.1-9~4.1-14.

#### **4.1.3 HIP processing**

HIP bonding is applied for bonding the first wall to the shield block at same time. The assembly of all the module components before HIP processing is shown in figure 4.1-15. As the preparation of HIP process, the interface between SS plates and shield block/cooling pipes at upper and lower ends of the first wall are welded to seal, respectively. The interface between shield blocks, and the interface between cooling pipes and blocks are also welded to seal. The other interfaces are sealed by welding of canning. After that sealing, the module is bonded by HIP process. The conditions of HIP should be tested by previous R&Ds.

#### **4.1.4 Machining after HIP bonding**

After HIP process, the canning is removed, and cooling headers and external shape are formed by machining. Holes for the flexible joint are machined after Be armor bonding. The covers for headers are welded after machining. The detailed process are shown in figure 4.1-16, 4.1-17.

#### **4.1.5 Bonding of Be Armors**

Finally, Be Armor is bonded by HIP on the first wall surface. After preparation for HIP process, Be tiles are arranged to fit the curvature of the first wall surface, and the canning material is welded. After HIP process, the canning material is removed, and machined the holes for flexible joint.

The detailed procedure is shown in figure 4.1-18.

### **4.2 Problems for Module Fabrication**

It is possible to apply the procedure to any module basically. However, R&D is necessary to fabricate the all shield blanket module. Issues are listed as

follows:

1) Bending process of cooling pipes around front access hole

The allowable bending curvature of circular pipe is about 3 times larger than that of pipe diameter. But the curvature by current design is less than that limit. The deformation of pipe cross section due to bending should be checked, and also the investigation of bending process is required.

2) Shaping of interface of shield block parts for HIP bonding

The shaping of shield block parts with curvature should be examined to match the interfaces in the poloidal direction.

3) Multi-layered HIP bonding process of shield block

The assembling of shielding parts, seal welding of the bonding interfaces before HIP process, and inspection method for bonded interfaces after HIP process should be examined.

4) Molding method of canning material

Canning plate should be fit to 3-D forms of modules. Forming method for 3-D curved canning plate should be examined.

5) Be bonding method

Selection of interlayer material, HIP bonding condition, fixture tools of Be tiles on the module surface should be examined.

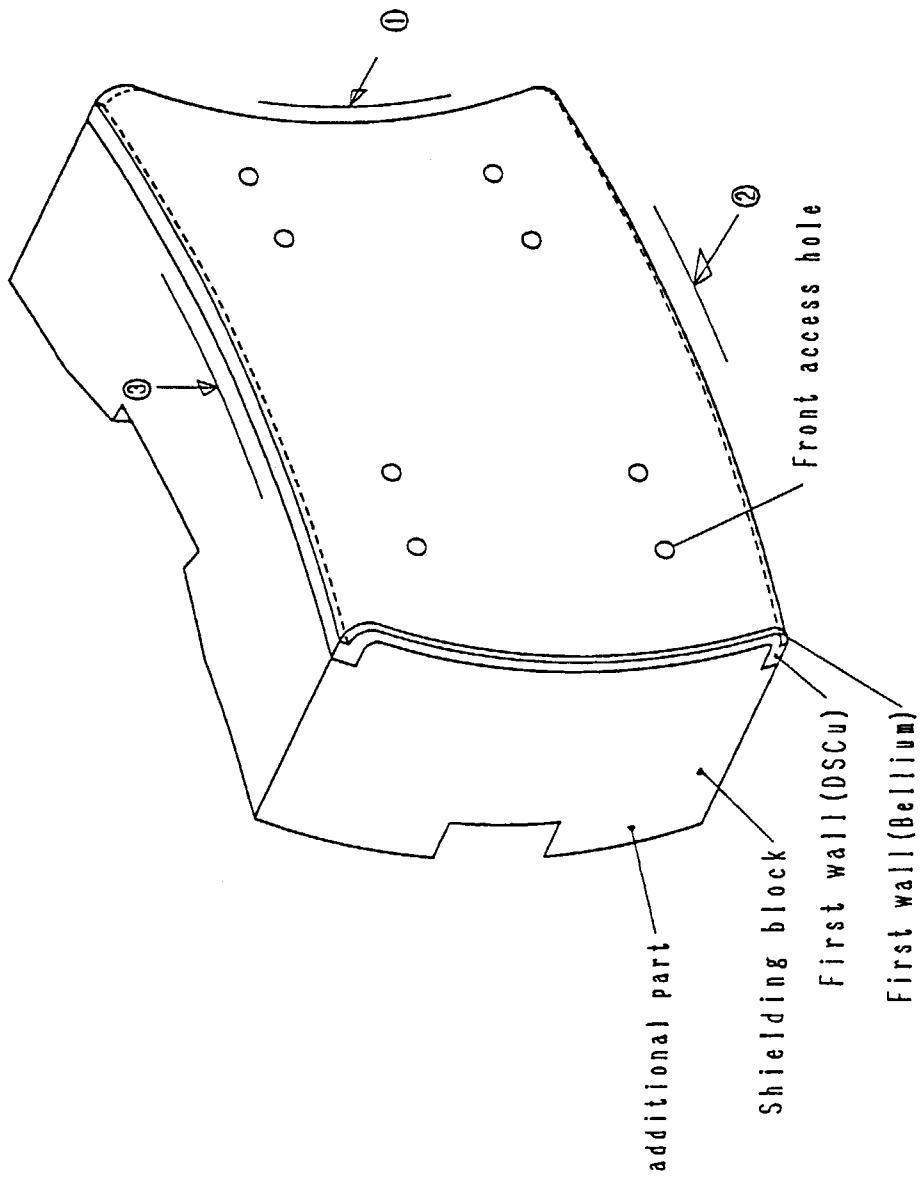


Fig. 4.1-1 Blanket module No.11

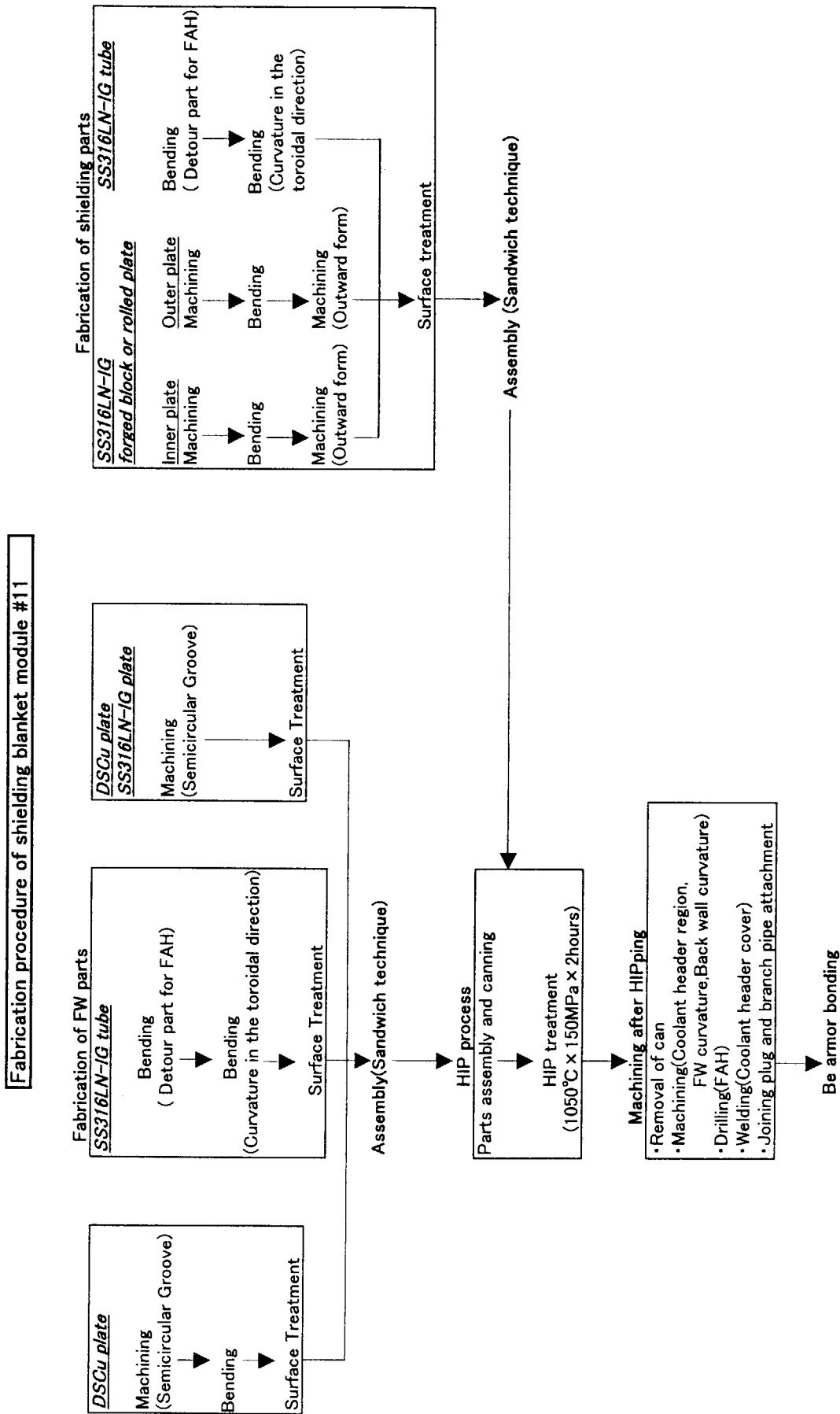


Fig.4.1-2 Fabrication procedure of shielding blanket module

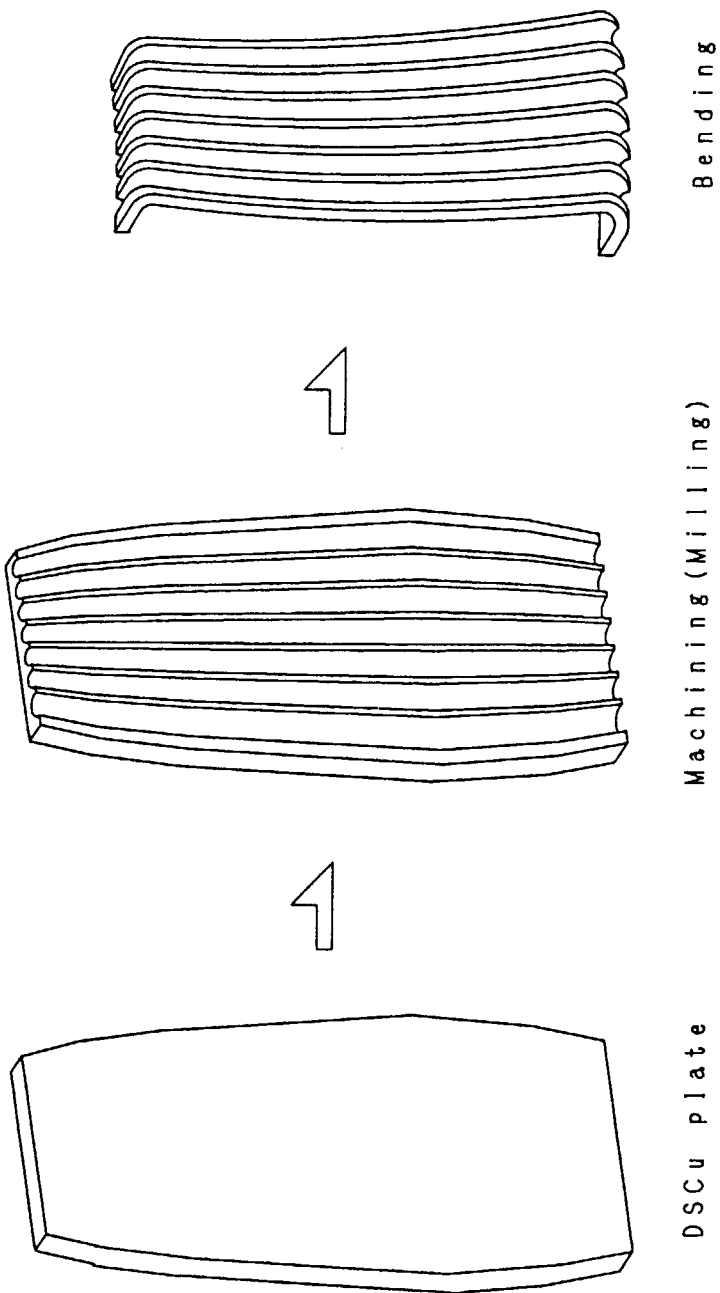
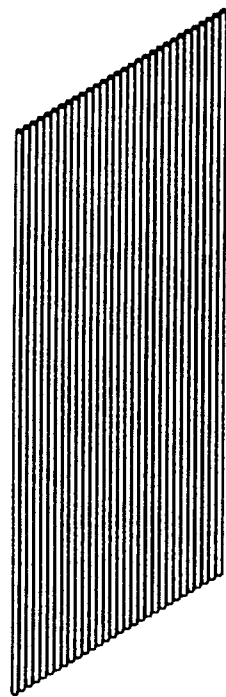
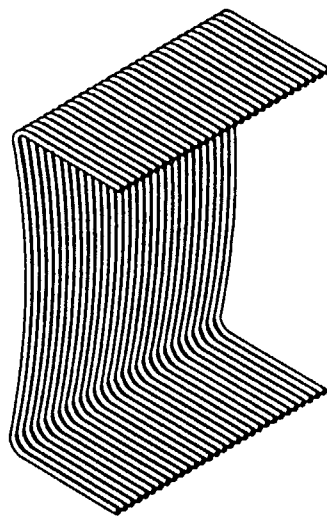
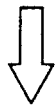


Fig. 4.1-3 Fabrication of DS-Cu inner plate for FW (without front access hole)



Machining



Bending

Fig. 4.1-4 Fabrication of coolant channels for FW  
(without front access hole)

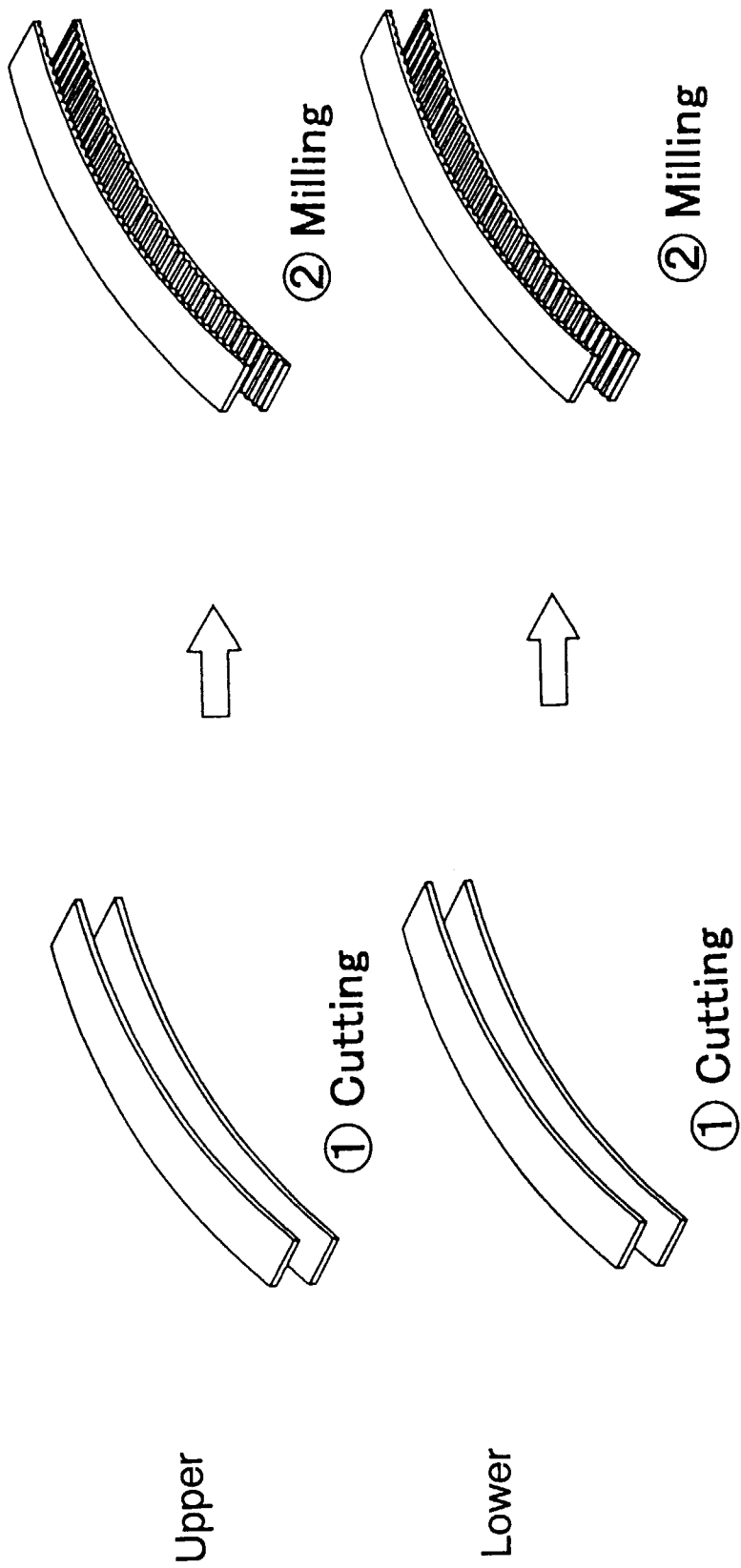


Fig. 4.1-5 Top and bottom plate fabrication procedure



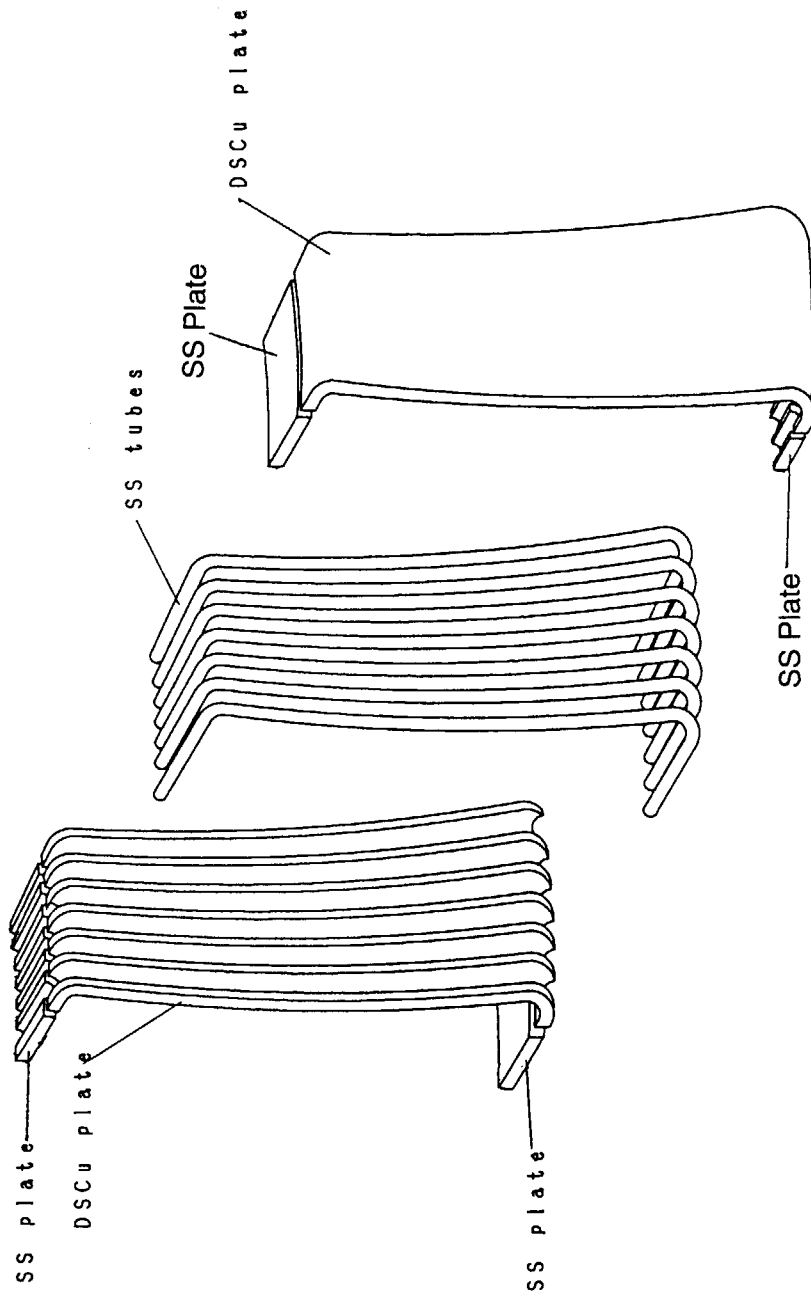


Fig. 4.1-6 Assembly of FW (without front access hole)

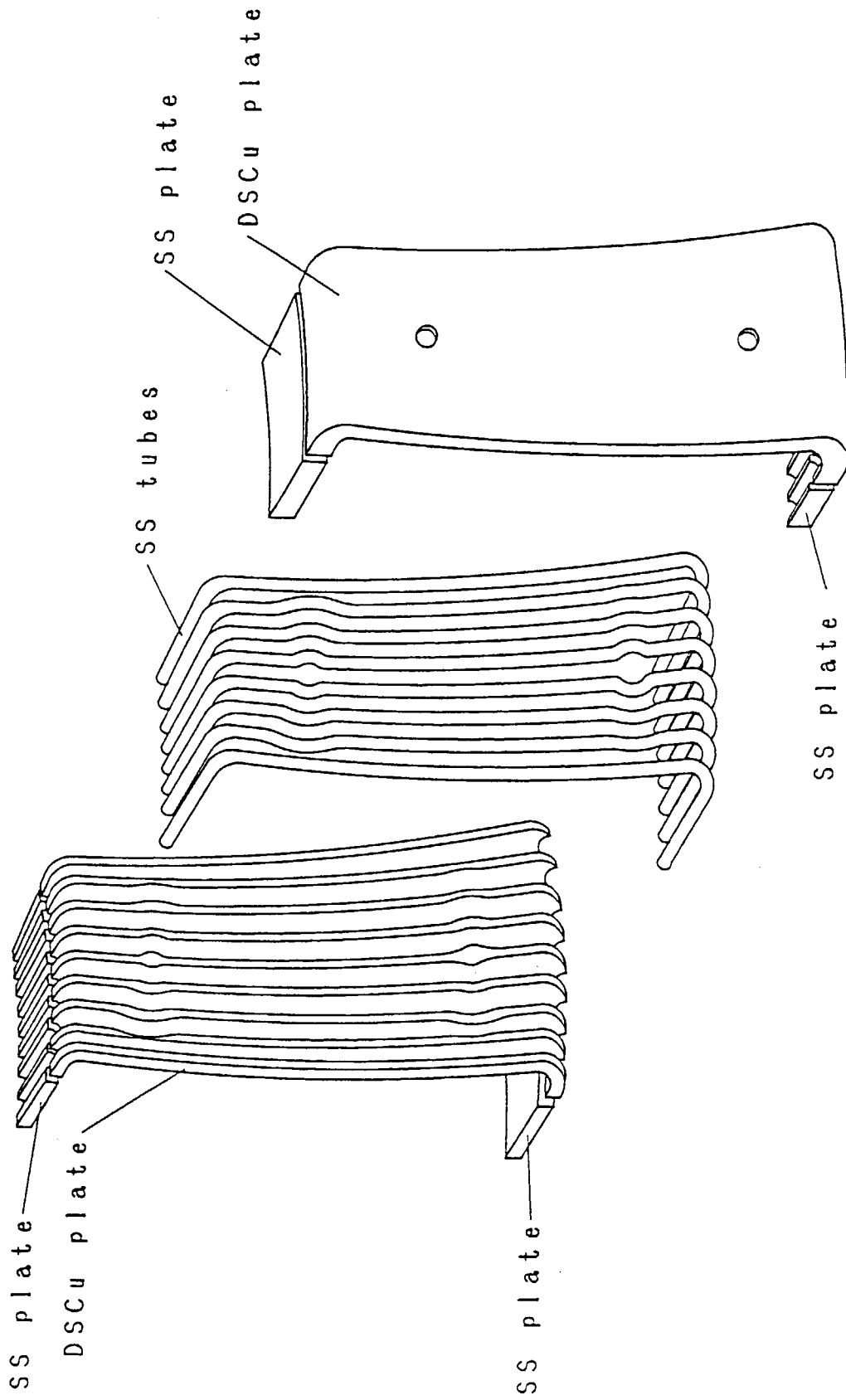


Fig. 4.1-7 Assembly of FW (with front access hole)

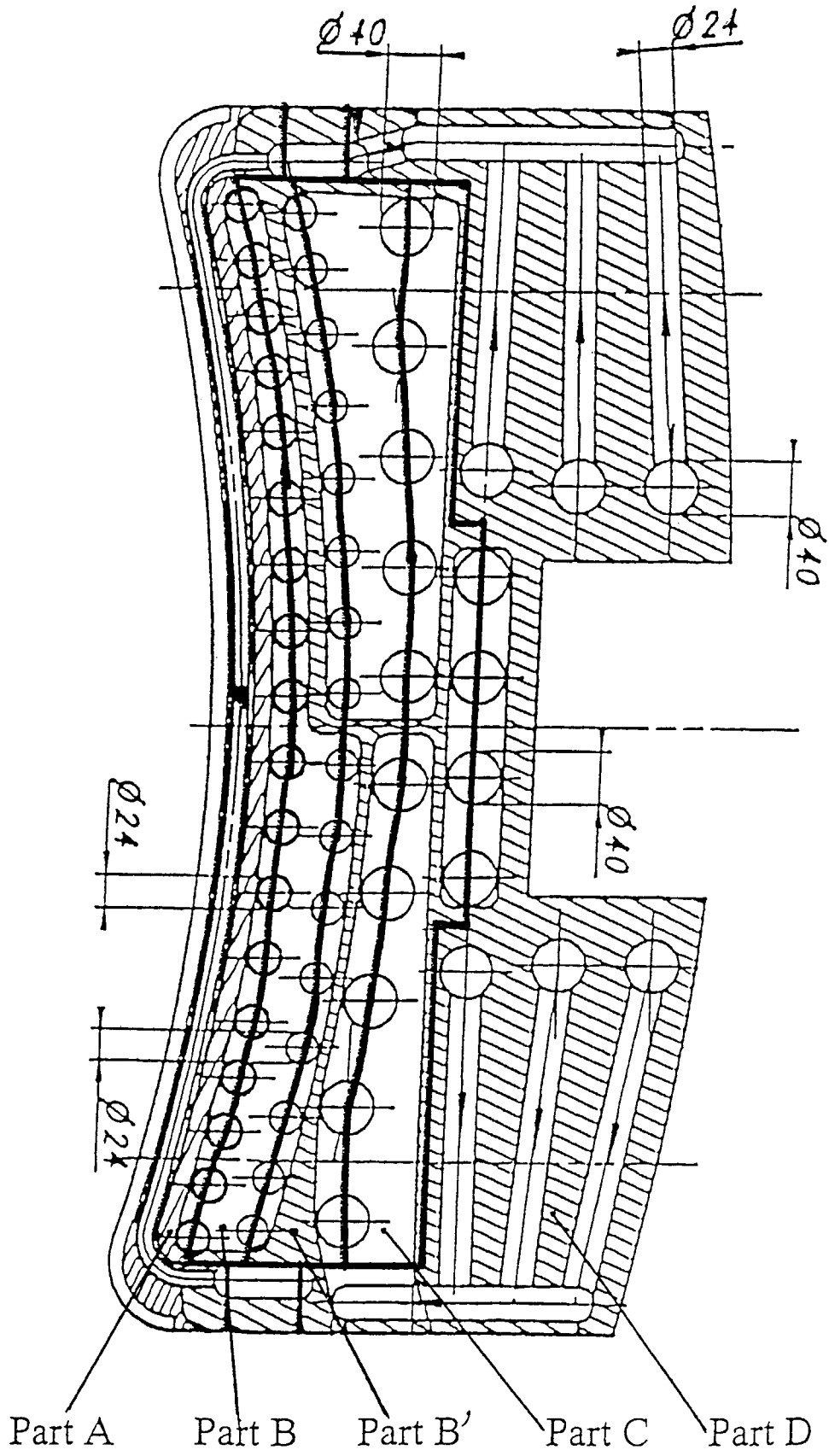


Fig. 4.1-8 Partition pattern of shield block  
(Left header side view)

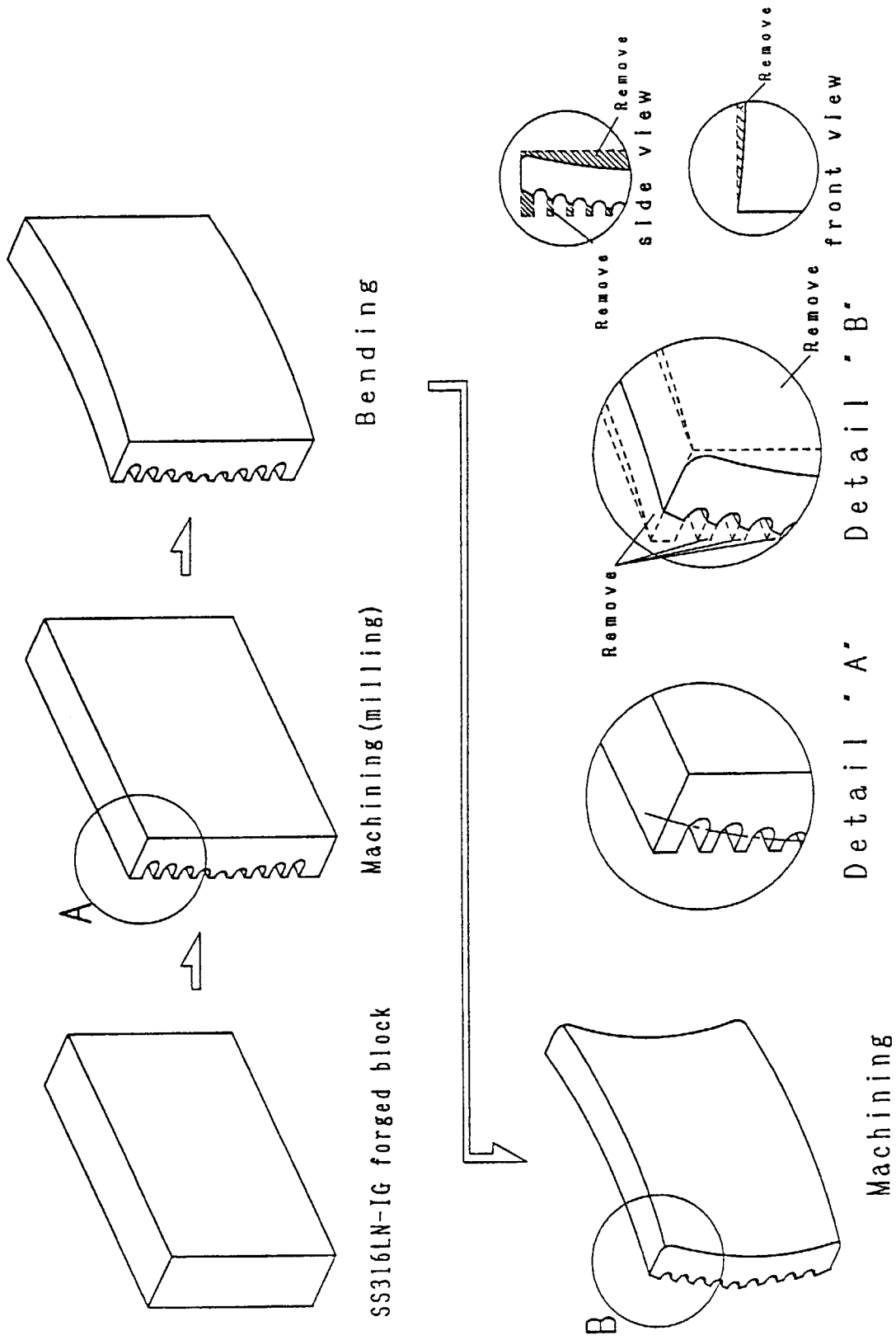


Fig. 4.1-9 Fabrication of shield block (A part)

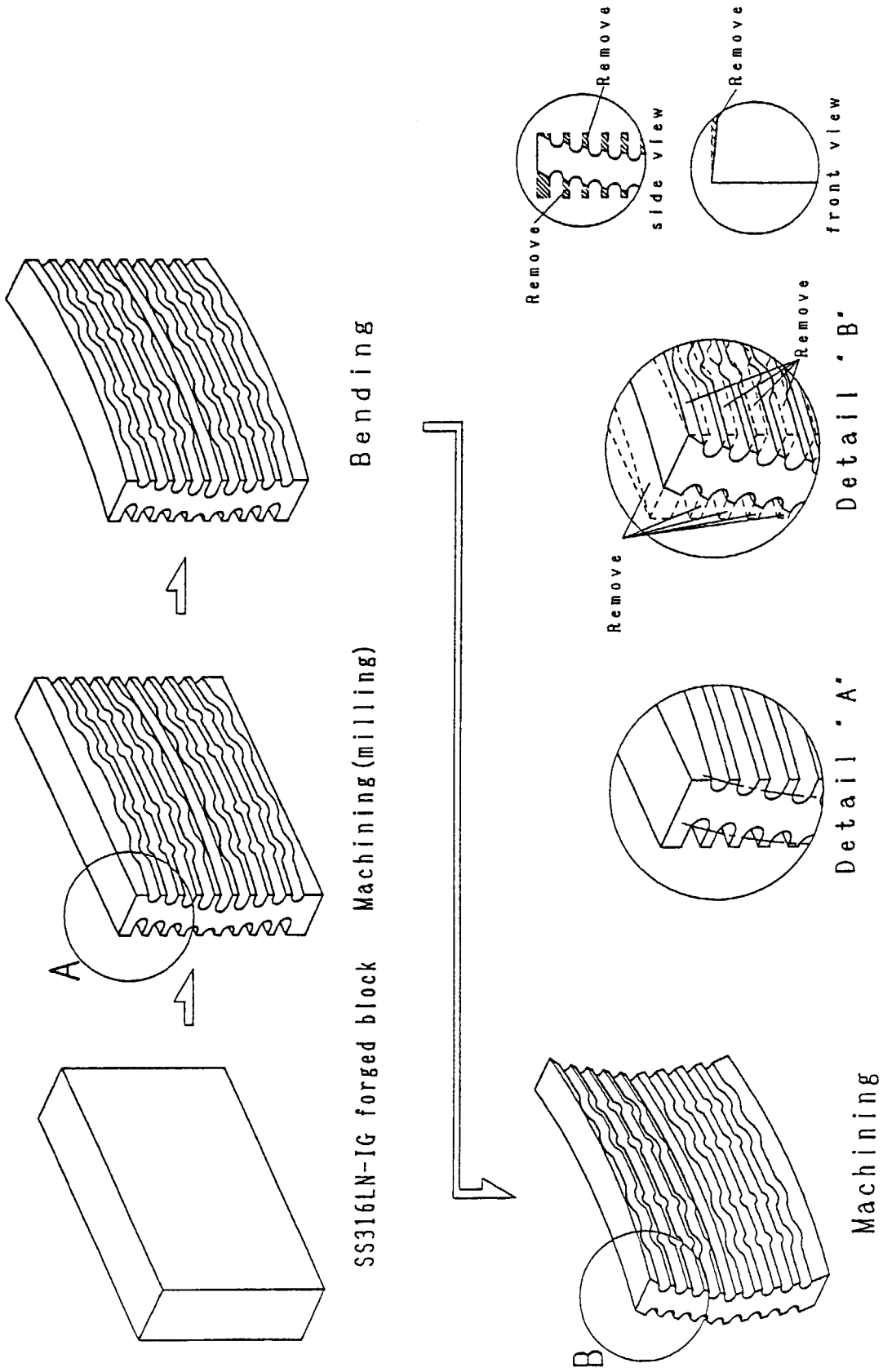


Fig. 4.1-10 Fabrication of shield block (B, B' part)

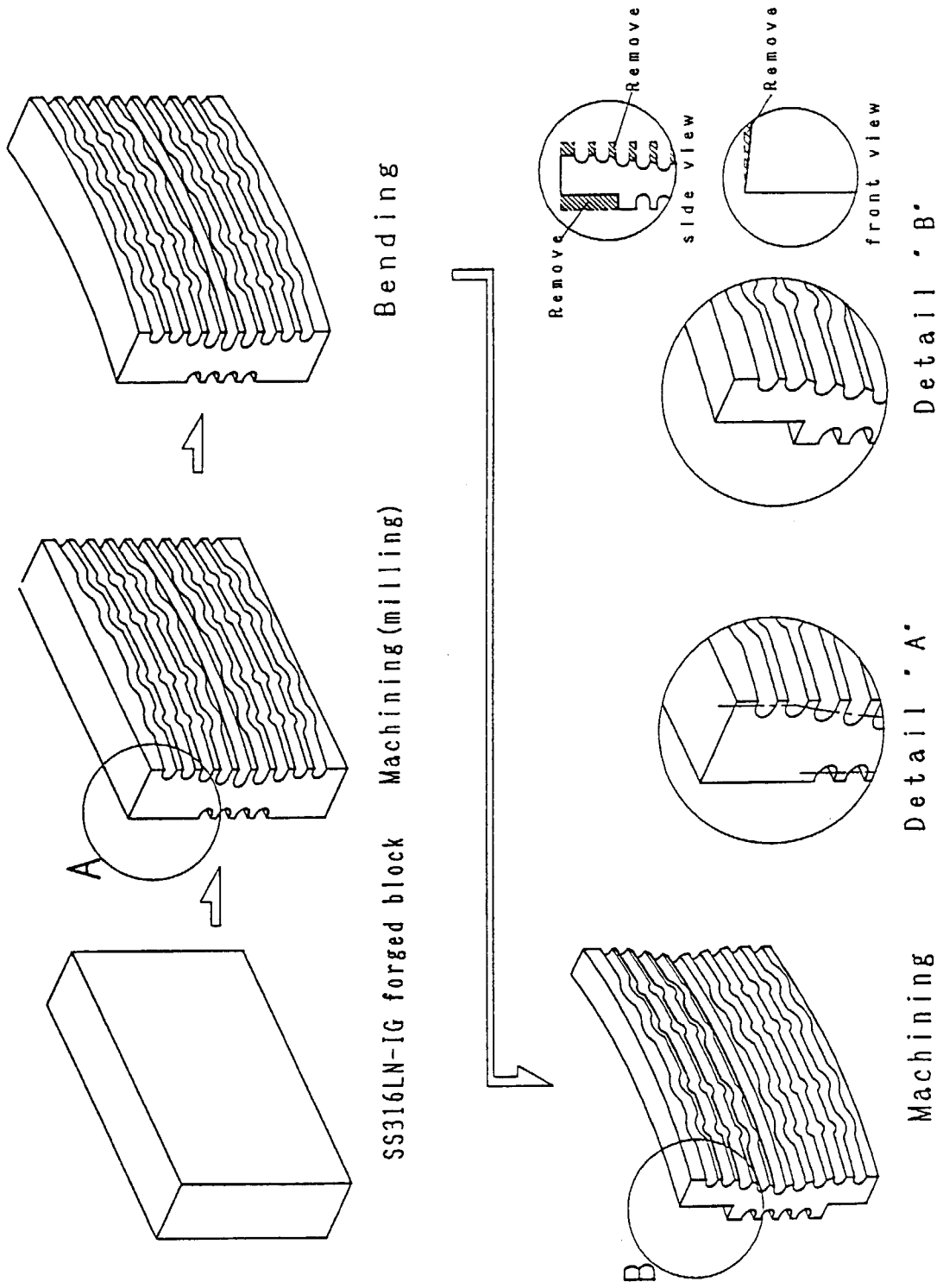


Fig. 4.1-11 Fabrication of shield block (C part)

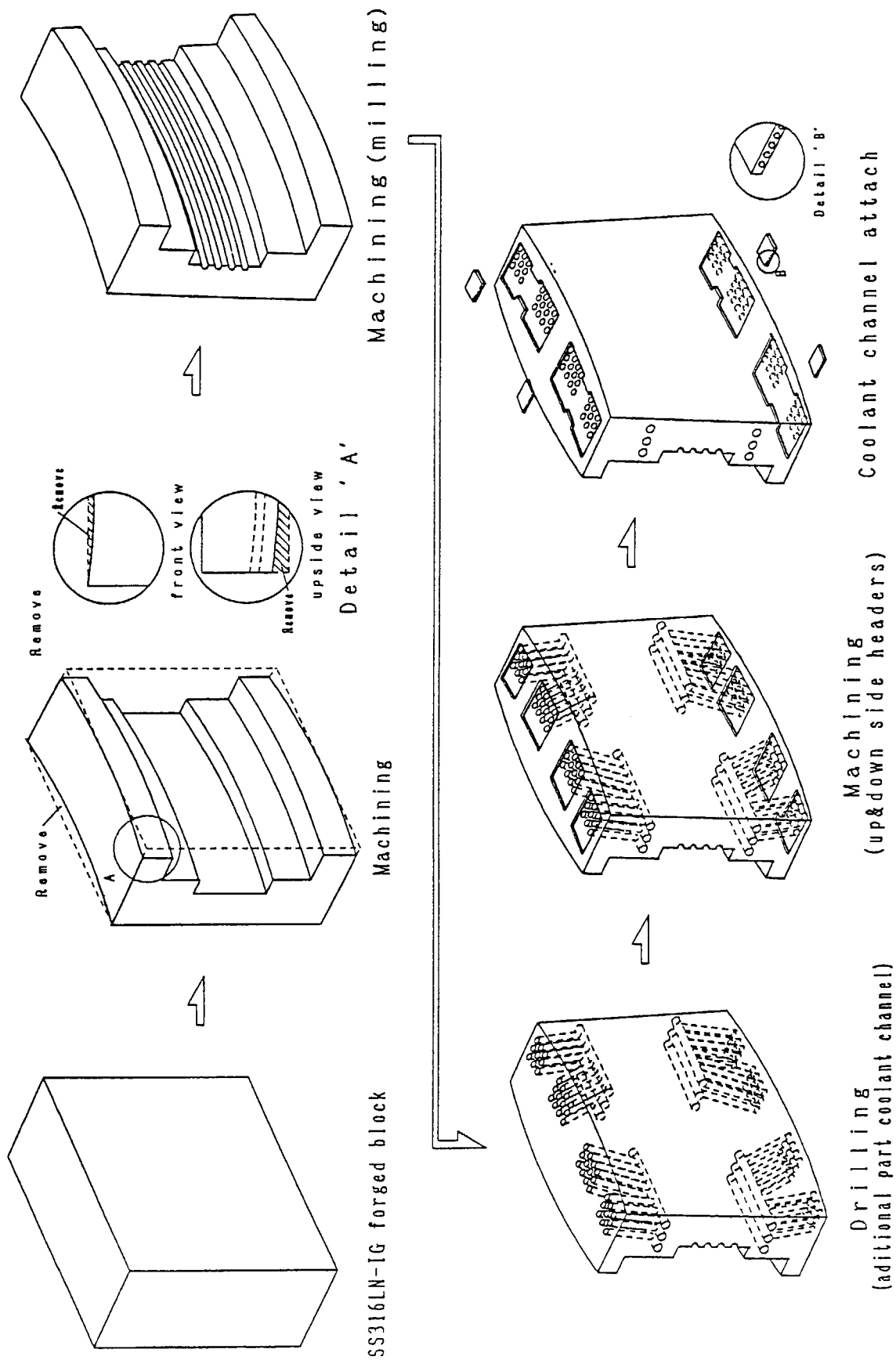


Fig. 4.1-12 Fabrication of shield block (D part)

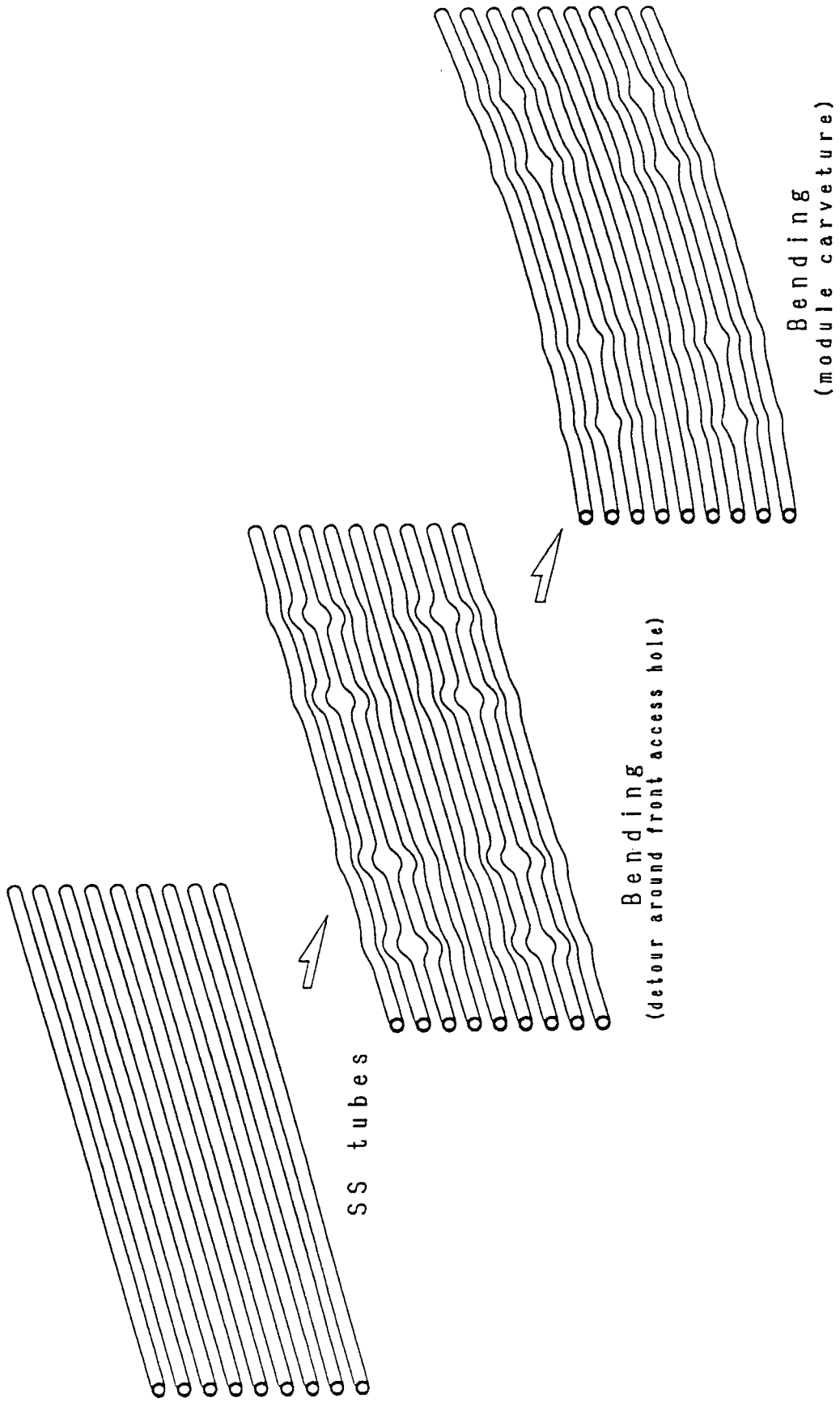


Fig. 4.1-13 Fabrication of coolant channel tubes for shield block



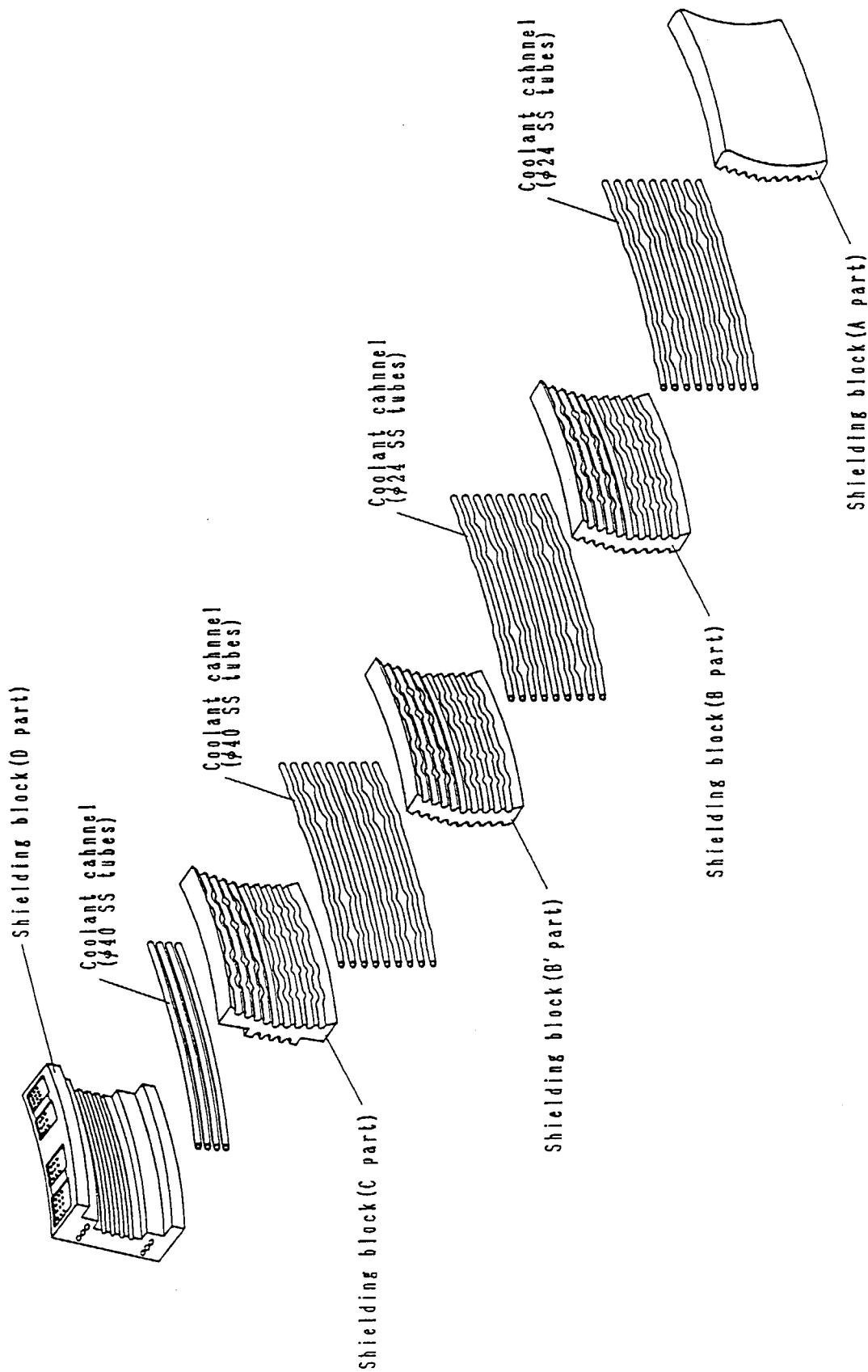


Fig. 4.1-14 Assembly of shield block

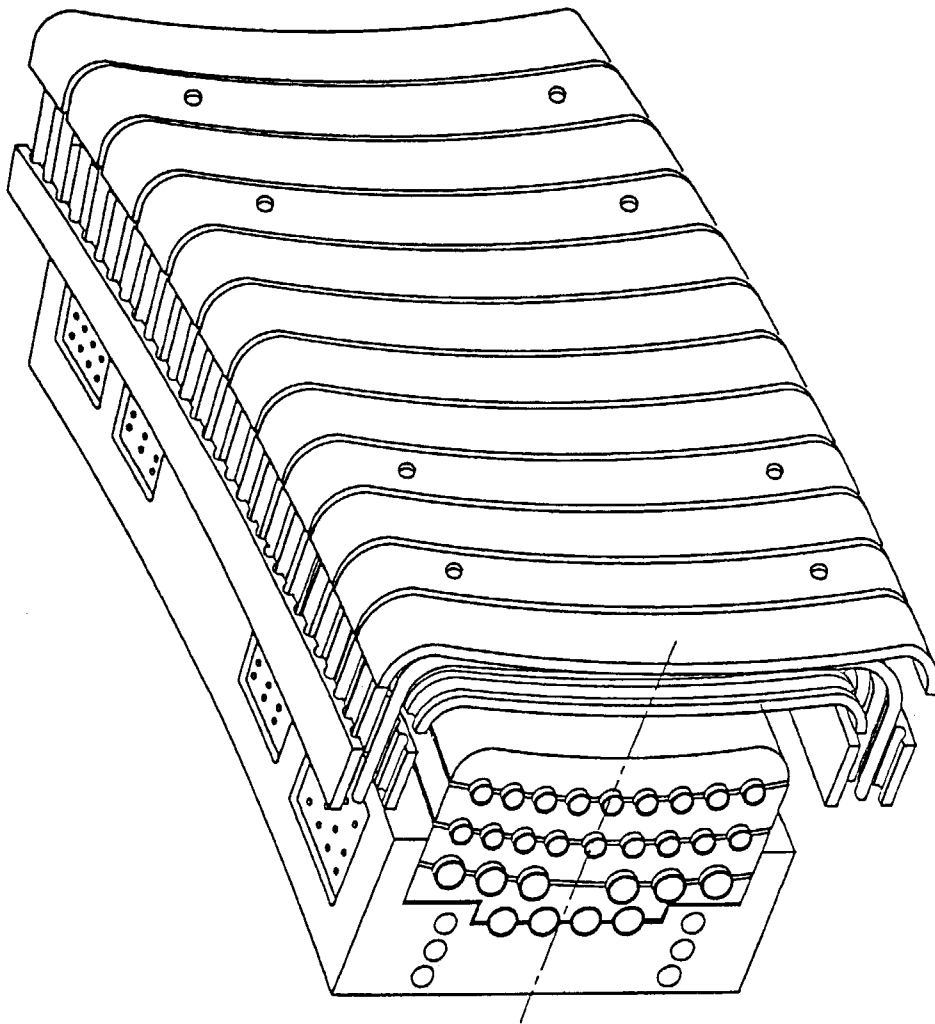


Fig. 4.1-15 Assembly of shield blanket module No.11

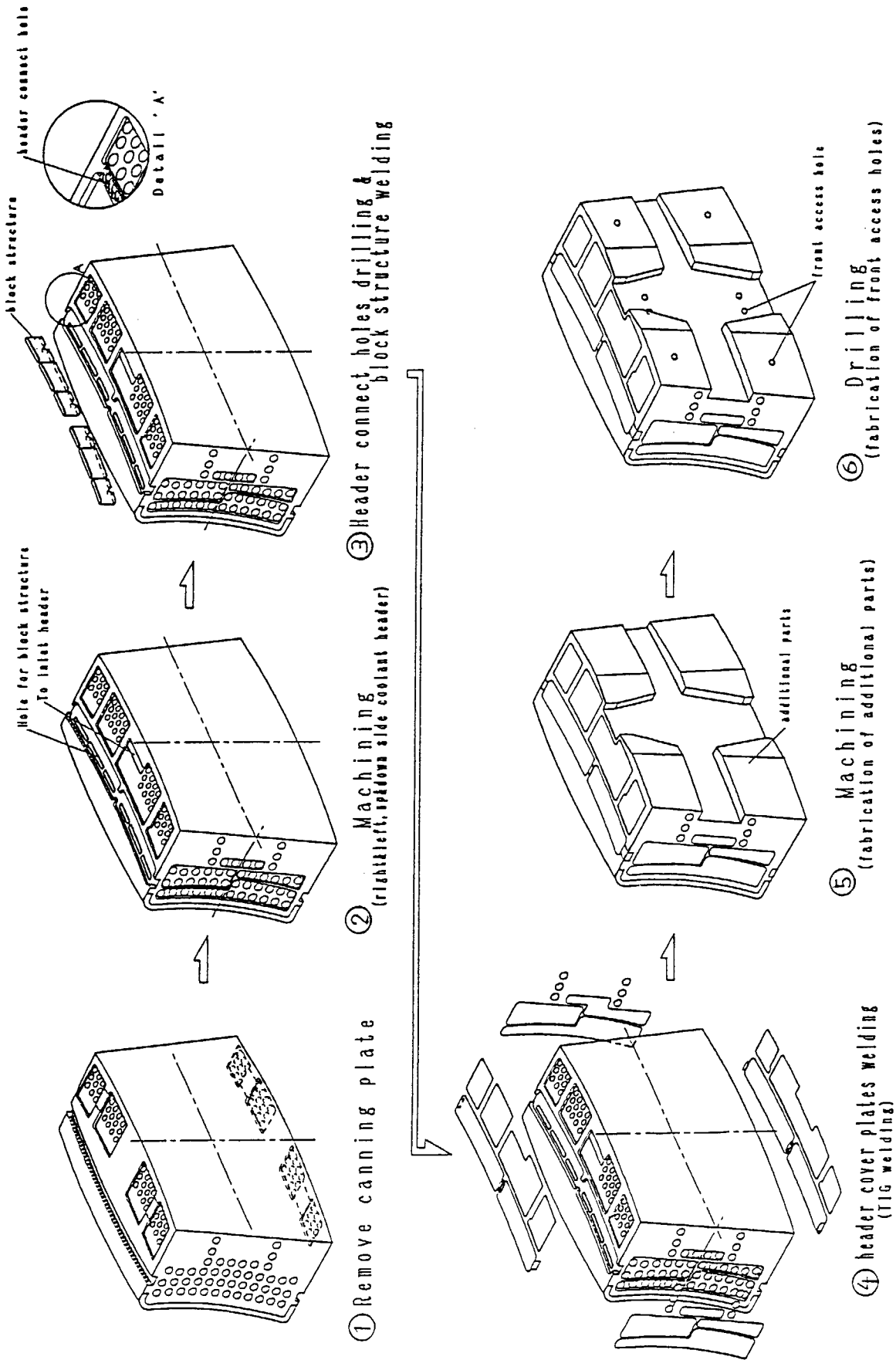


Fig. 4.1-16 Fabrication procedure (After HIP process)

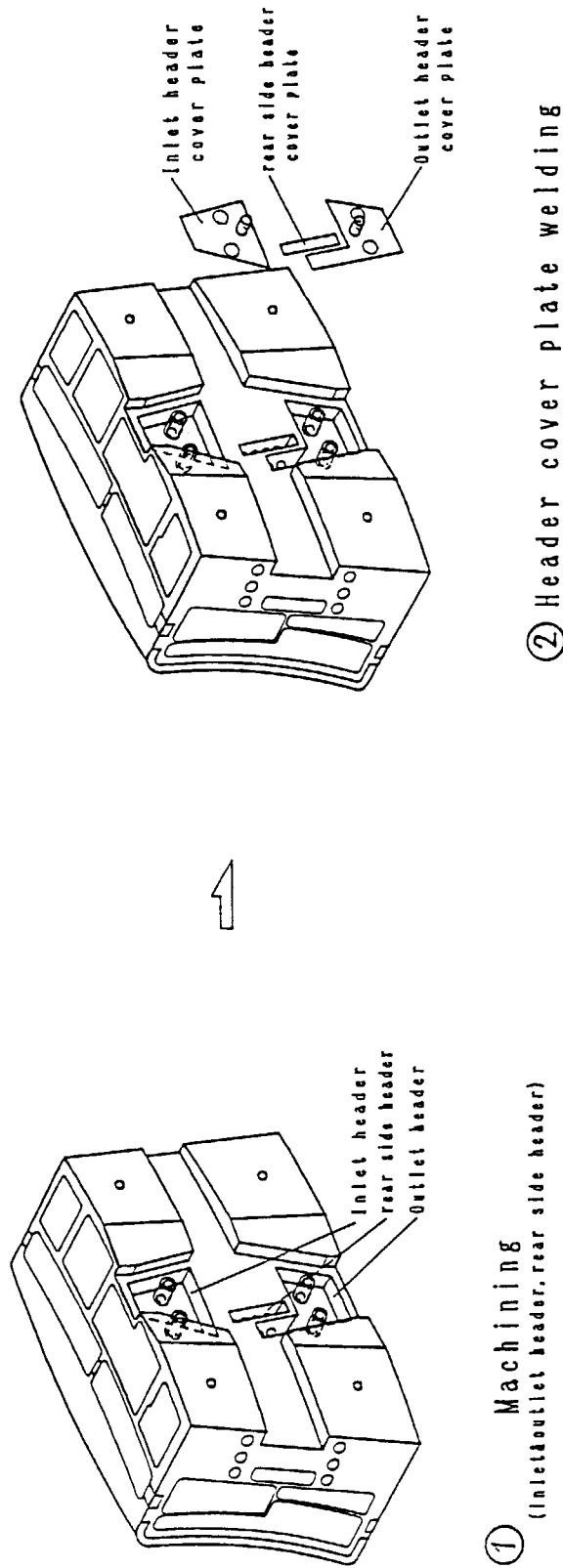


Fig. 4.1-17 Fabrication of coolant headers

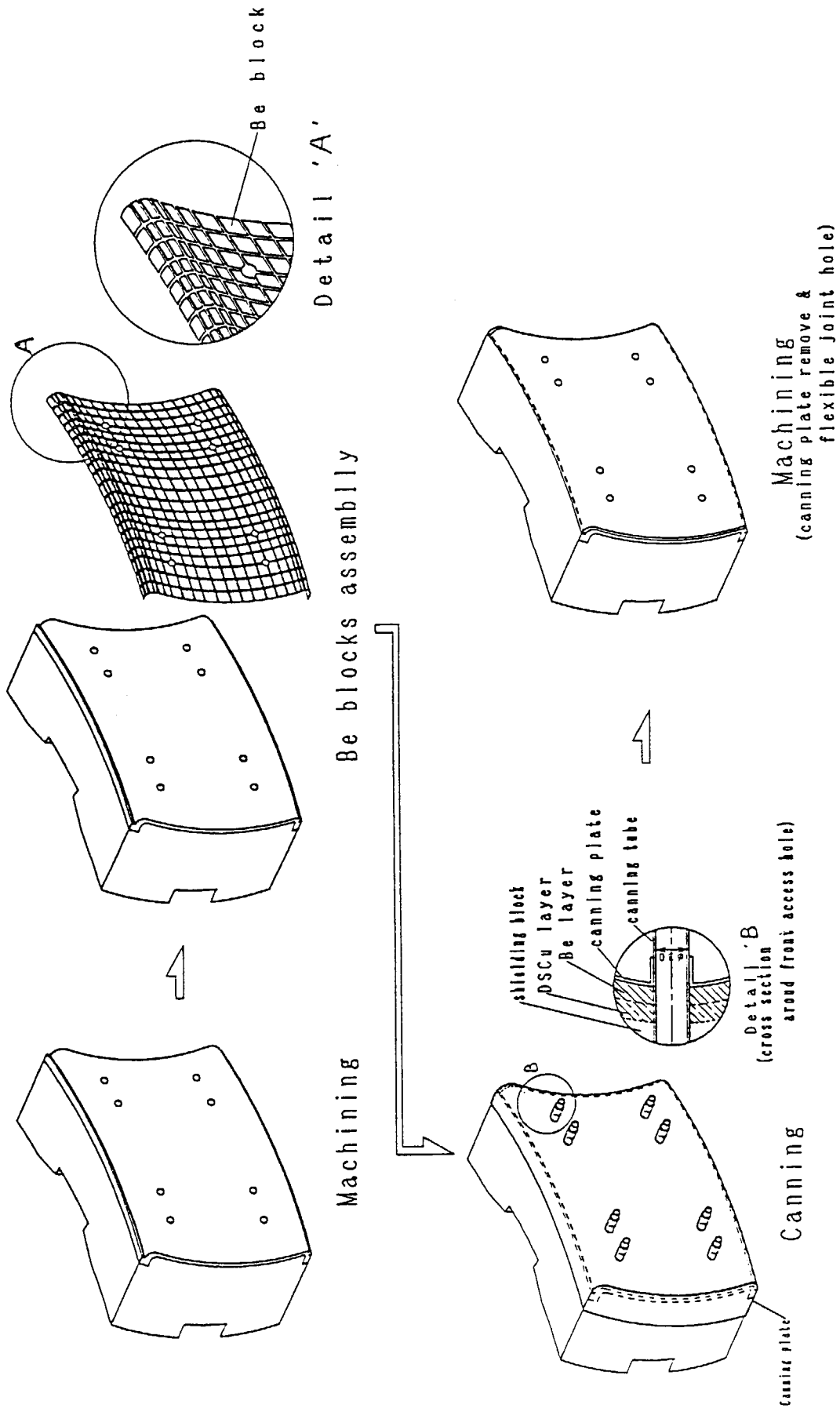


Fig. 4.1-18 Fabrication of Beryllium layer

## 5. Back Plate Fabrication Procedure

### 5.1 Design Concept

The back plate is a toroidally continuous stainless steel structure with a "horse shoe" poloidal shape[5.1]. The modules are connected to the back plate by flexible connectors to transmit the mechanical loads on the modules, hydraulic connectors for supplying cooling water, and electrical straps to ensure the continuity of the electrical current path between the modules and back plate. The mechanical connection make the modules demountable for maintenance using remote handling tools and techniques.

The features of back plate are as follows :

- 1)Thickness of inner wall : 50 mm
- 2)Thickness of outer wall : 70 mm
- 3)Thickness of the cooling rib : 40 mm
- 4)The toroidal pitch of ribs : about 500 mm
- 5) Back plate has flexible housing, center pin and cooling pipes connecting bush for the attachment of flexible support.
- 6)The cooling ribs separate inlet and outlet coolant flow.
- 7)The flexible housings and internal pegs support electromagnetic force and water pressure.
- 8)The sufficient internal pegs are added considering the stress distribution.
- 9)Additional ribs are also provided around port for reinforcement.

Fig. 5.1 shows the back plate structure including these features. The TIG welding is used between outer wall and rib. The inner wall and ribs are welded using through wall electron beam welding. After drilling holes for flexible housing, the flexible housing is attached and welded by TIG welding. These welding structures are also used in ITER vacuum vessel. However, the incomplete welding structures may still remain and need more investigation.

The welding concept for connecting the rib to the inner wall is illustrated in Fig. 5.2. There are 6 option processes being considered. The option 1 is the e-beam welding in which the procurement of H shaped steel is difficult. The option 2 is the through wall e-beam welding (TWEB) which needs less machining time and is the most efficient welding method. The option 3 is the e-beam welding in which the ribs need for positioning steps and need more machining time. The option 4 is TIG full penetrating welding which needs more welding time than the option 3 welding. The option 5 is the TIG full penetrating welding which may be possible to weld completely by butt welding. However it needs precise positioning between outer wall and rib, and that will be more disadvantageous. The option 6 is full penetrating TIG welding which will need machining process for rib structures. The TWEB

welding seems to be the most appropriate welding method on the joint of cooling rib and inner wall.

## 5.2 Fabrication Procedure

The fabrication steps associated with welding are illustrated in Fig. 5.3. The fabrication of the back plate begins with the receipt of plate stock and forging. All the components of the back plate are constructed by 316 LN stainless steel.

The following fabrication procedure is under consideration.

- 1) Cut the plate into the appropriate size.  
The inner and outer wall are cut in the appropriated size. The rough cut plate shall have allowances for geometry changes due to cutting and bending operations.
- 2) Bend the plate into the required shapes.  
Each plate is individually hot pressed into its final 3-D geometry illustrated in Fig. 5. 4. In case of 2-D shape, the plate is formed by rolling machine.
- 3) Machine for the module attachment.  
The plates are machined into the appropriate geometry and measured for dimensional information map.
- 4) Weld cooling ribs.  
The cooling ribs are welded to outer walls by TIG welding completely. Non destructive test(NDT) around welded region is performed. The ultrasonic test (UT) and penetrant test (PT) will be available.
- 5) Weld the inner wall and cooling rib.  
The inner wall and cooling rib are welded. The through wall electron beam(TWEB) welding is under consideration. The concept is illustrated in Fig. 5. 5.
- 6) Perform non destructive test(NDT) around welded region.  
The inner wall and cooling rib shall be welded completely. The ultrasonic test (UT) or penetrant test (PT) is available.
- 7) Weld the connecting components to the inner wall.  
The components are welded by TIG welding. The TWEB welding of outer wall to channel plate and TIG welding flexible housing to inner and outer wall are illustrated in Fig. 5. 6.
- 8) Perform non destructive test(NDT) around welded region.

The inner wall and connecting components shall be welded completely. The ultrasonic test (UT) or penetrant test (PT) is available. The back plate segments are completed by the mentioned procedure.

9) Assembly and welding for back plate sector.

The back plate sector consist of three segments. The resultant segments shall be assembled and welded each other to fabricate back plate sector. The plate segments are mounted in welding fixtures illustrated in Fig. 5.7, adjusted to the correct alignment and welded using an automated welding system. The Narrow Gap TIG welding process are under consideration at this time.

10) Perform non destructive test(NDT) around welded region.

The segment boundary shall be welded completely. The ultrasonic test (UT) is available. The back plate assembly are measured for dimensional information map. The back plate assemblies are completed by the mentioned procedure.

11) Weld the inboard and outboard structure to the assembly.

The cooling header, inboard structure, lower inboard structure, outboard structure and lower outboard structure are welded to the back plate assemblies for fabricating back plate sectors. These structures are welded by TIG welding.

12) Heat treatment.

The residual stress of back plate sectors shall be removed using annealing heat treatment after all welding process finished. The annealing heat treatment conditions are as follows:

Temperature :  $880-900 \pm 15$  °C

holding time : 3 hour

cooling condition : Air coolant

The temperature control should be more careful in annealing heat treatment. Intercrystalline corrosion will be observed when the stainless steel back plate is kept at the temperature region of 500 - 850 °C for a long time. The stainless steel also make unstable internal metallic structure when they are heated up to the temperature of 930 °C for a long time.

13) Perform non destructive test(NDT) around welded region.

The assembly and the structures shall be welded completely. The back plate sectors are measured for dimensional information map. The ultrasonic test (UT) or penetrant test (PT) is available.

14) Machine back plate side edge for field joint.

The back plate sectors are dressed for field joint welding. All edges of each back plate sector to be welded are prepared by machining. The machining is illustrated in Fig. 5. 8.

15) Machine flexible housing



The rough machined back plate housing are machined detailed for flexible support attachment. The resultant back plate sectors are measured for dimensional information map.

16) Pressure test (PT) and leak test are performed.

The resultant back plate sectors are tested for pressure test and leak test. The back plate sectors are completed by the mentioned procedure.

### 5.3 Annealing Process to Remove Residual Stress

The residual stress of back plate sectors shall be removed using annealing heat treatment after all welding process finished. The annealing heat treatment conditions are as follows:

Temperature :  $880-900 \pm 15$  °C

holding time : 3 hour

cooling condition : Air coolant

The temperature condition should be controlled more precisely in annealing heat treatment. The inappropriate heat treatment cause trouble as follows:

1) Intercrystalline corrosion

The surplus carbon over the solution limit precipitate in the steel grain boundary when the annealing temperature is risen up from 500 °C to 850 °C (especially, the temperature from 600 °C to 700 °C is terrible ) for more than 3 hours. The chromium carbide is formed around the grain boundary and the intercrystalline corrosion is caused by the chromium deficiency inside the grain.

2) Formation of unstable metallic structure

The carbon is resolved in the grain when the steel is held at 930 °C for more than 3 hours. The unstable metallic structure is formed by the carbon resolving.

Therefore, the heating time, temperature and cooling rate should be controlled strictly in the annealing process to remove the back plate residual stress. The large scale annealing and cooling reactor should be prepared for back plate fabrication.

### 5.4 Prevention of Welding Deformation

The tolerance control in general has been recognized as a key issue in back plate manufacturing. The splice plate welding is the most important process in the back plate manufacturing flow. Many jigs are used for the prevention of splice plate welding deformation. The stay is used for welding deformation prevention in back plate sector connecting boundary and shown in Fig. 5.9. The fixing jigs, wedge shaped jigs and adjusting liners are also used for welding and shown in Fig. 5.10. The adjusting liners fix the position of welding surface. These jigs are removed after a temporary welding distance piece is inserted. The distant piece is used for the welding shrink prevention.

## 5.5 Estimation of Welding Deformation

The splice plate welding test has been performed in order to estimate welding deformation. The test pieces geometry of splice plate are shown in Fig. 5.11. The welding lines of (1)-(8) are double U groove. The groove angles and root faces of (1)-(6) are 4 degree x 2 and 2.5 mm, respectively. The groove angle and root faces of (7)-(8) are 15 degree x 2 and 2 mm, respectively. The measuring points of test piece are shown in Fig. 5.12. The changes of position for p1-p9 are measured. The number of welding layer is 9 and 7 fixing jigs are used.

Test result is shown in Fig. 5.13. The shrink deformation of splice plate are measured in the case of soft, hard and no fixations. These result shows that the back plate shrink deformation is estimated to be less than 8 mm in toroidal direction and the angular deformation by welding is estimated to be less than 3 degree.

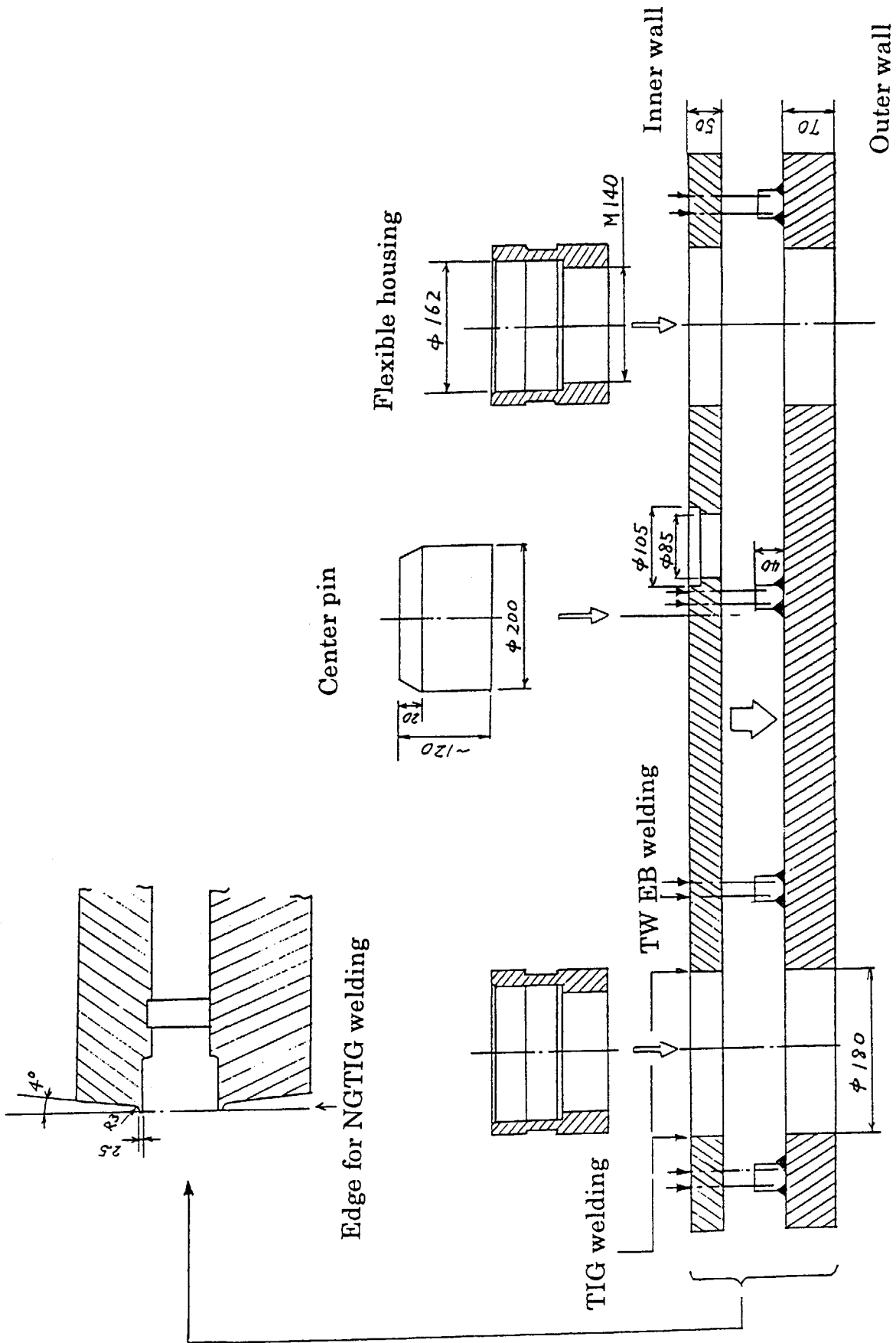


Fig. 5.1 Fundamental structure of blanket back plate.

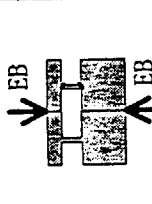
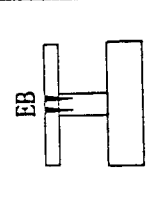
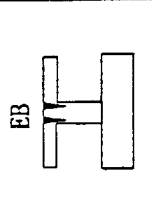
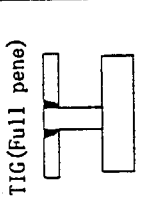
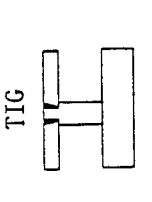
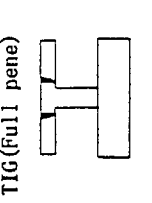
Option No.	Option 1	Option 2	Option 3	Option 4	Option 5	Option 6
Structure						
Procurement	1 (almost Impossible)	5	5	5	5	3
Weldability	5	5	5	3	4	3
Machinability	5	5	4	3	3	3
Cost	1	5	4	2	3	2
Reliability	4	4	4	5	4	5
Total	16	24	22	18	19	16

Fig. 5.2 Manufacturing method of double wall back plate.

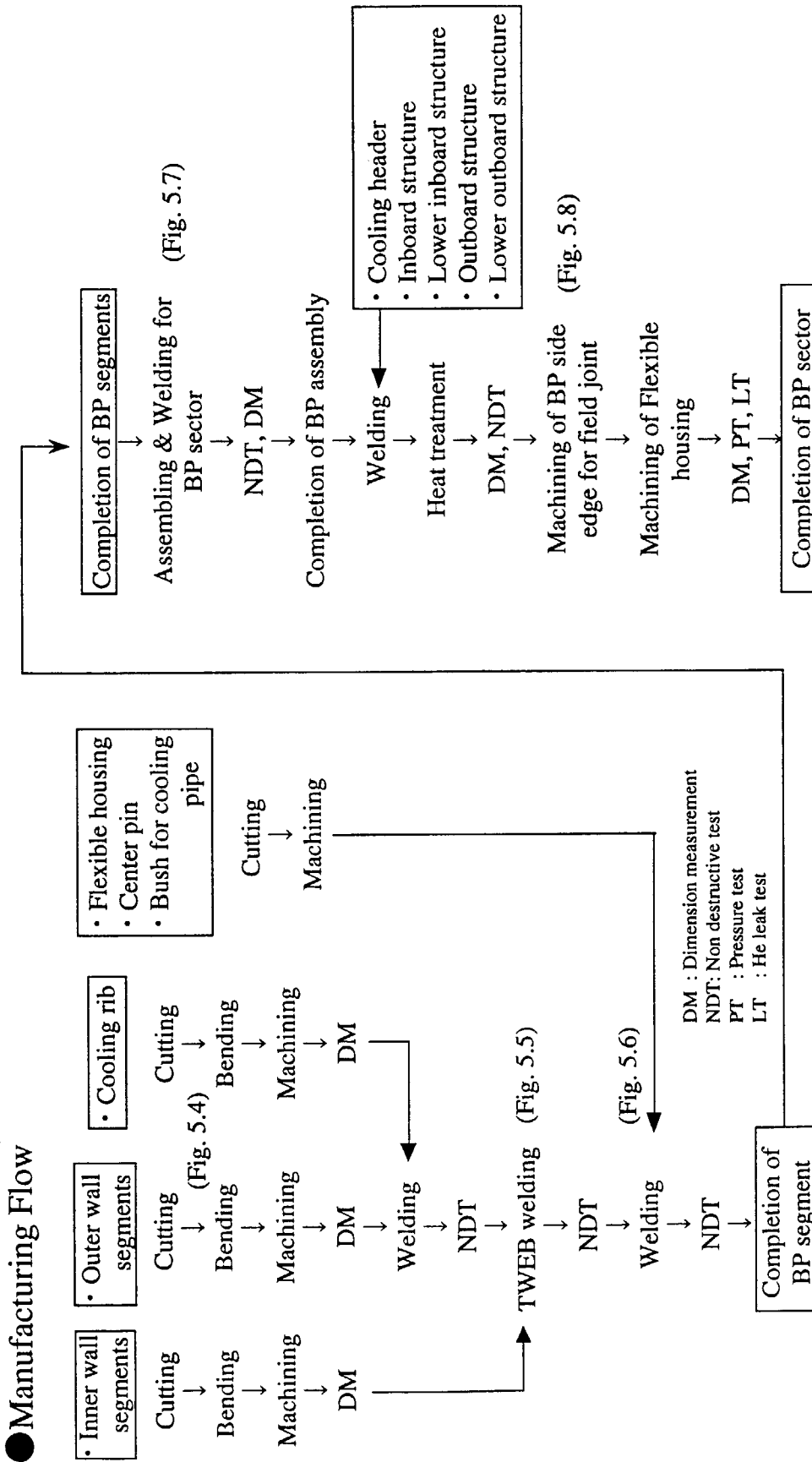


Fig. 5.3 Manufacturing flow of back plate sector

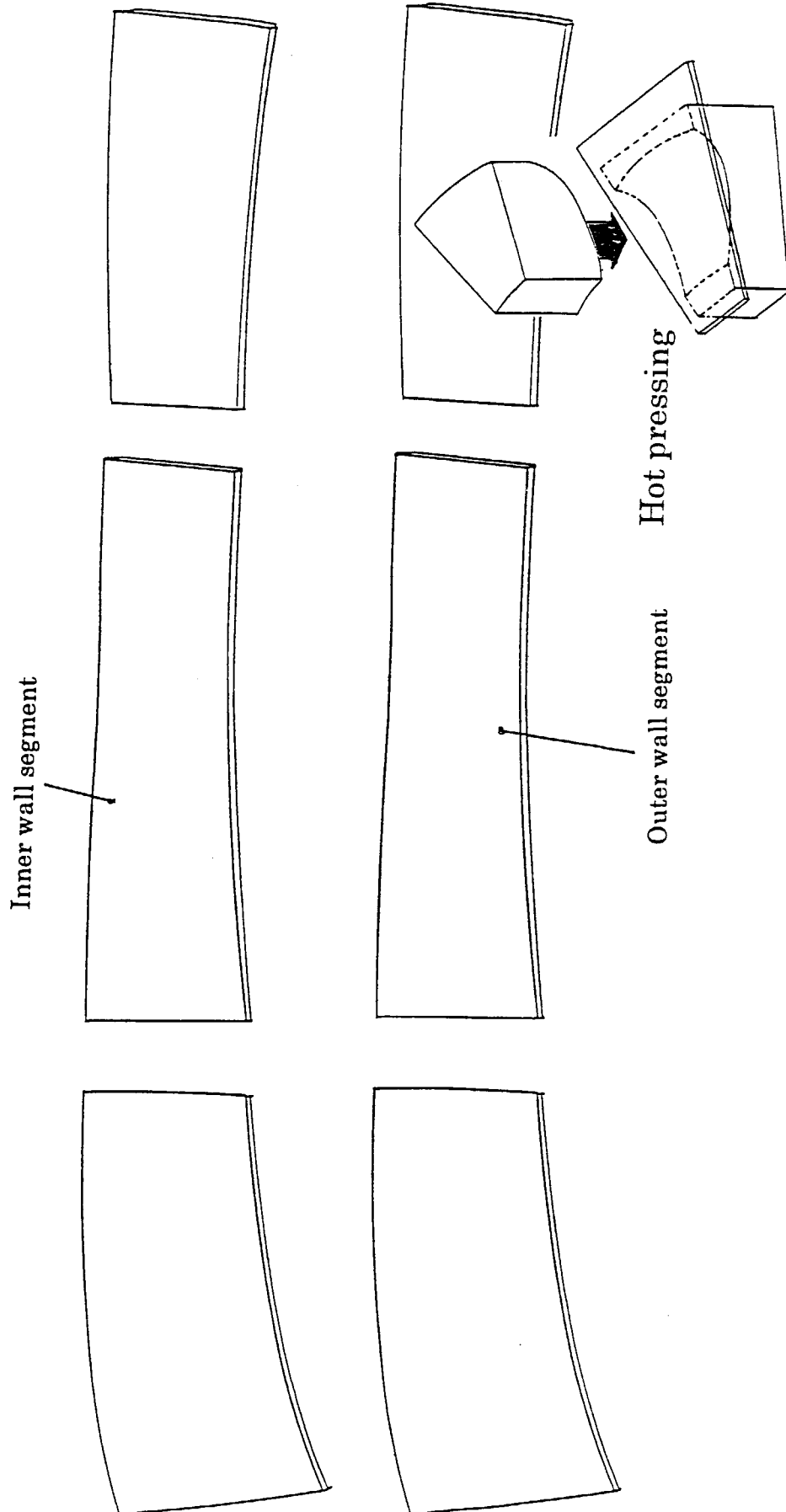


Fig. 5.4 Cutting and bending of SS plates.

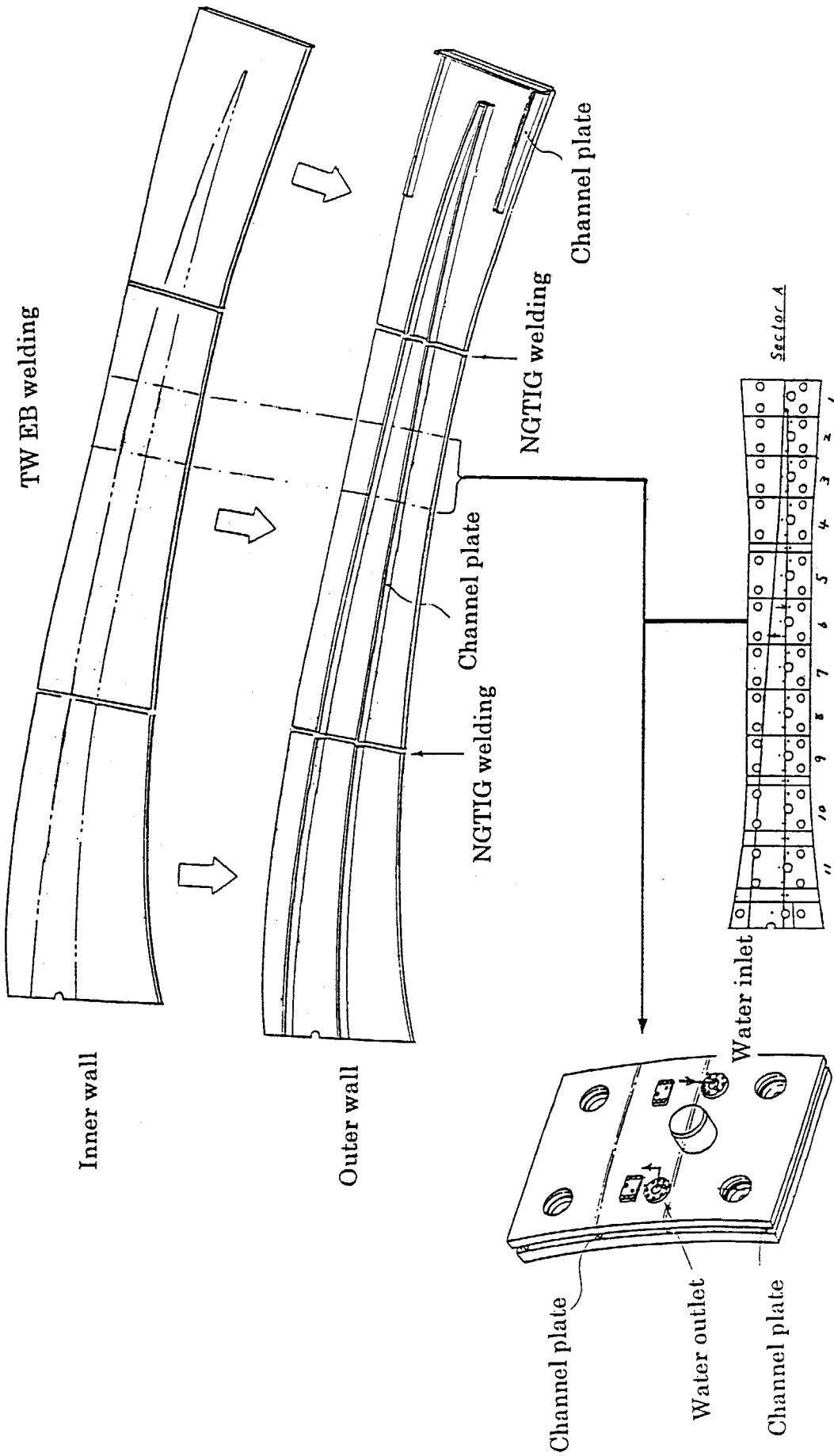


Fig. 5.5 Fundamental structure of inboard blanket back plate.

Back Plate for No.6 Module

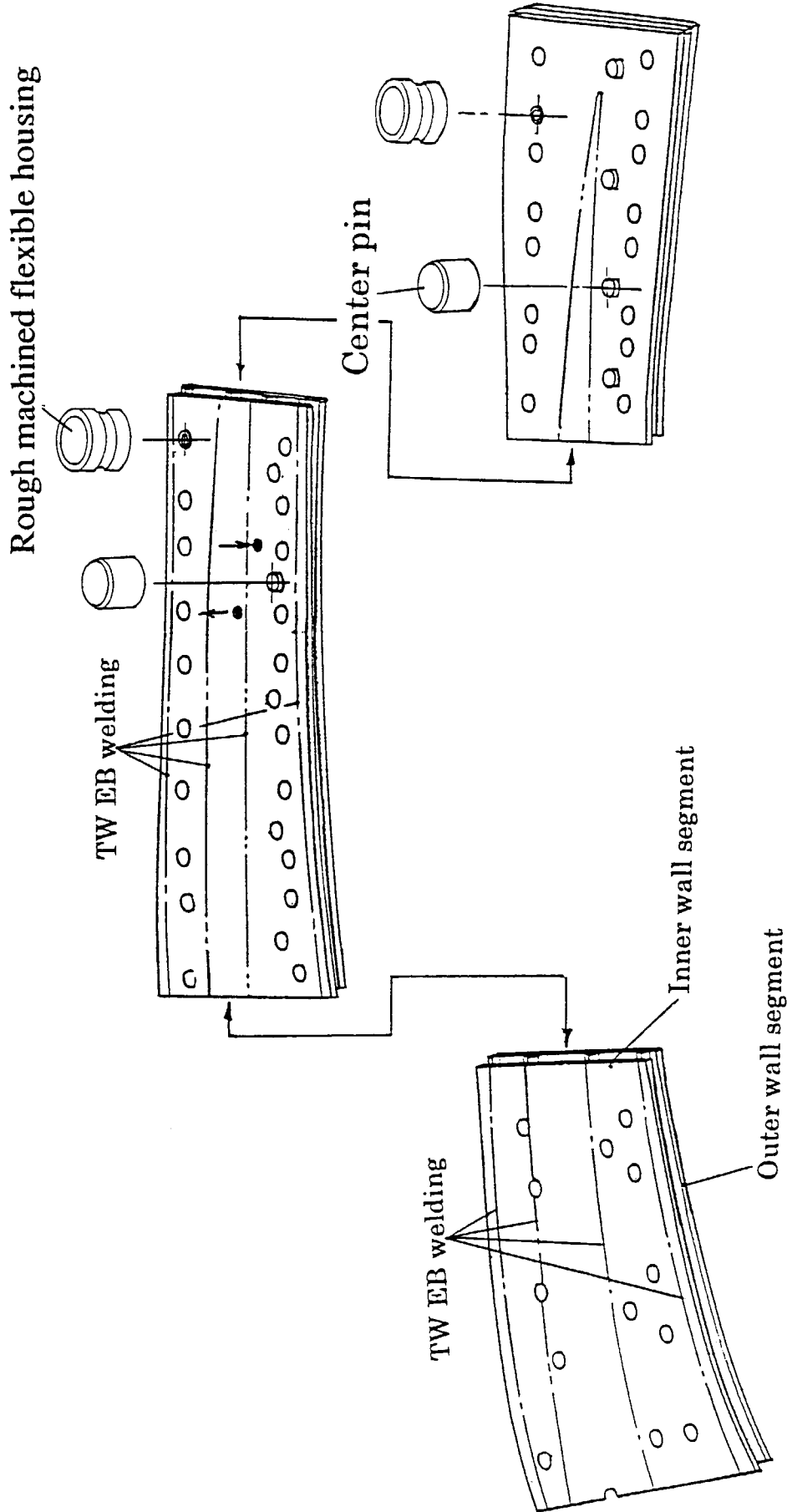


Fig. 5.6 TW EB welding of outer wall to channel plate and  
TIG welding flexible housing to inner and outer wall.



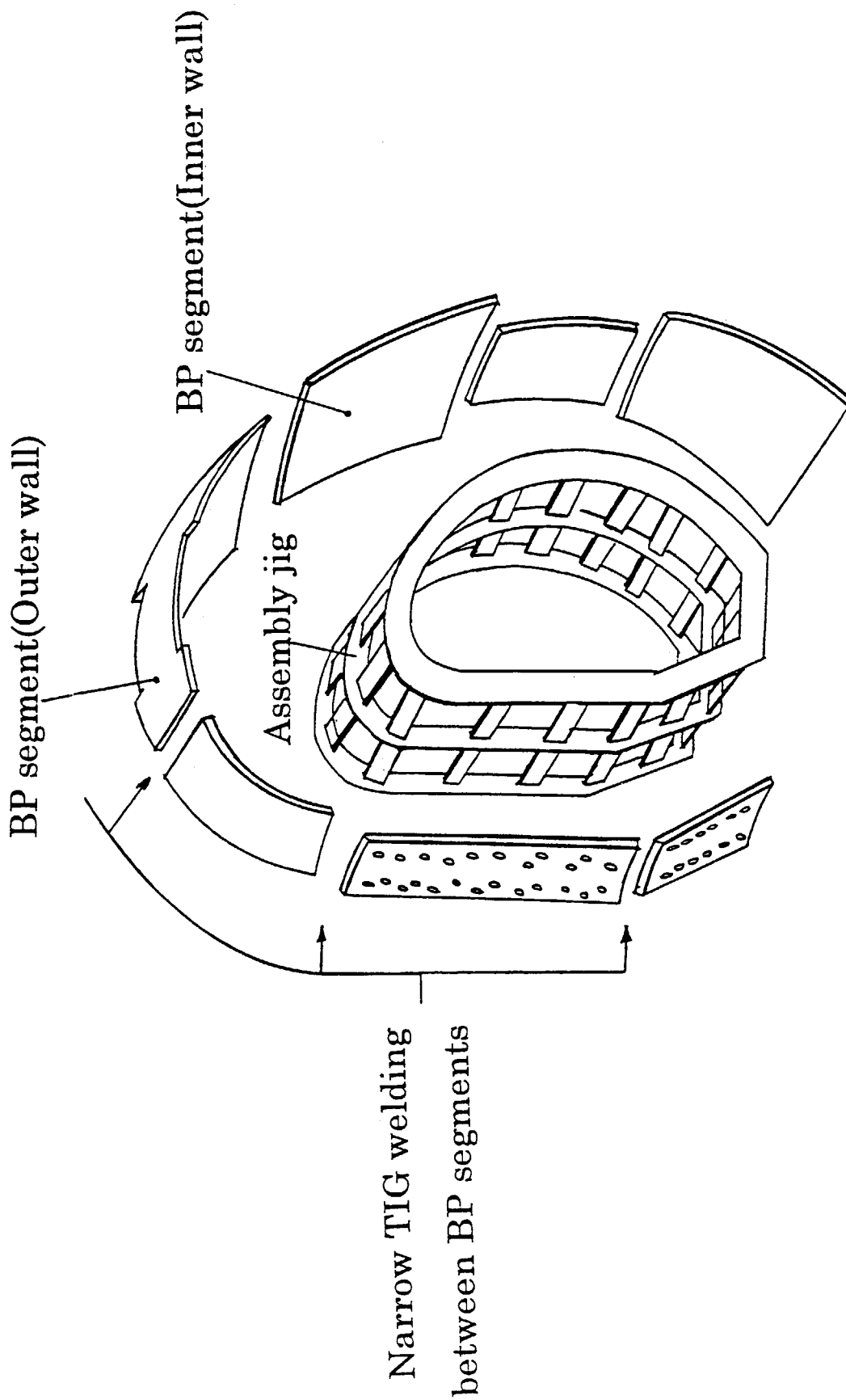


Fig. 5.7 Back plate segment assembly.

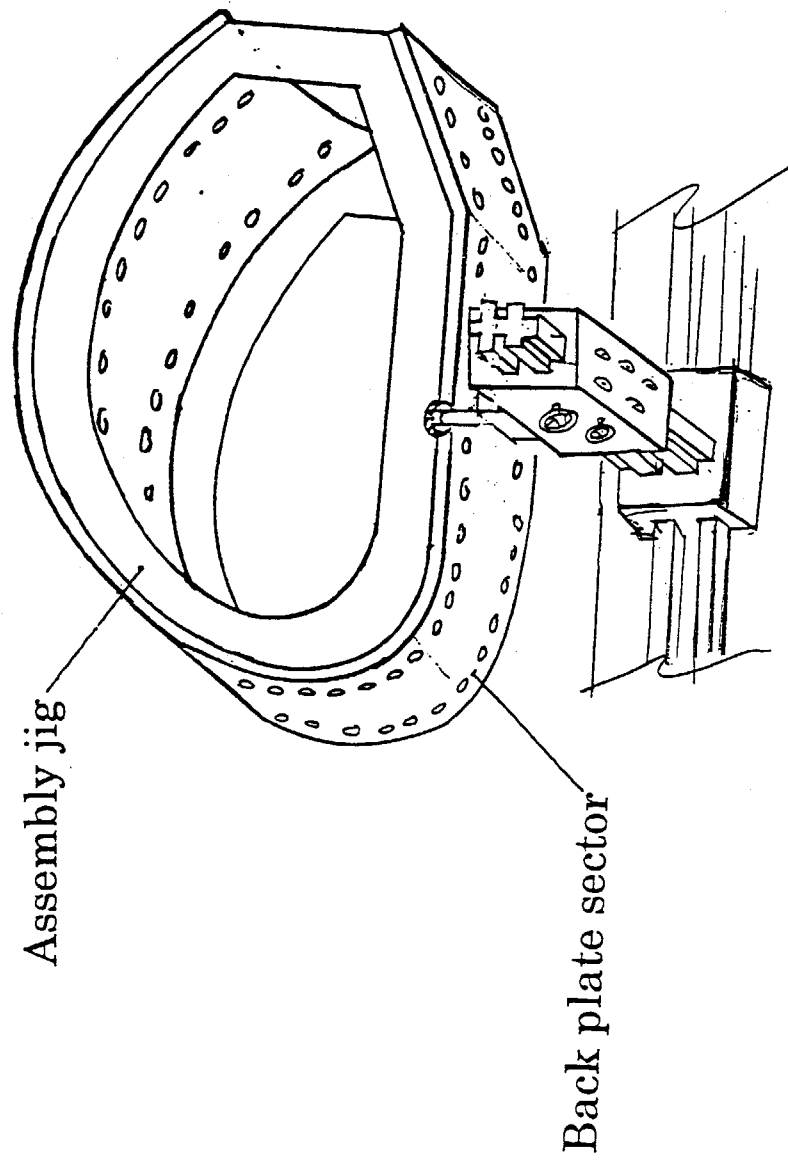


Fig. 5.8 Machining of back plate edges.

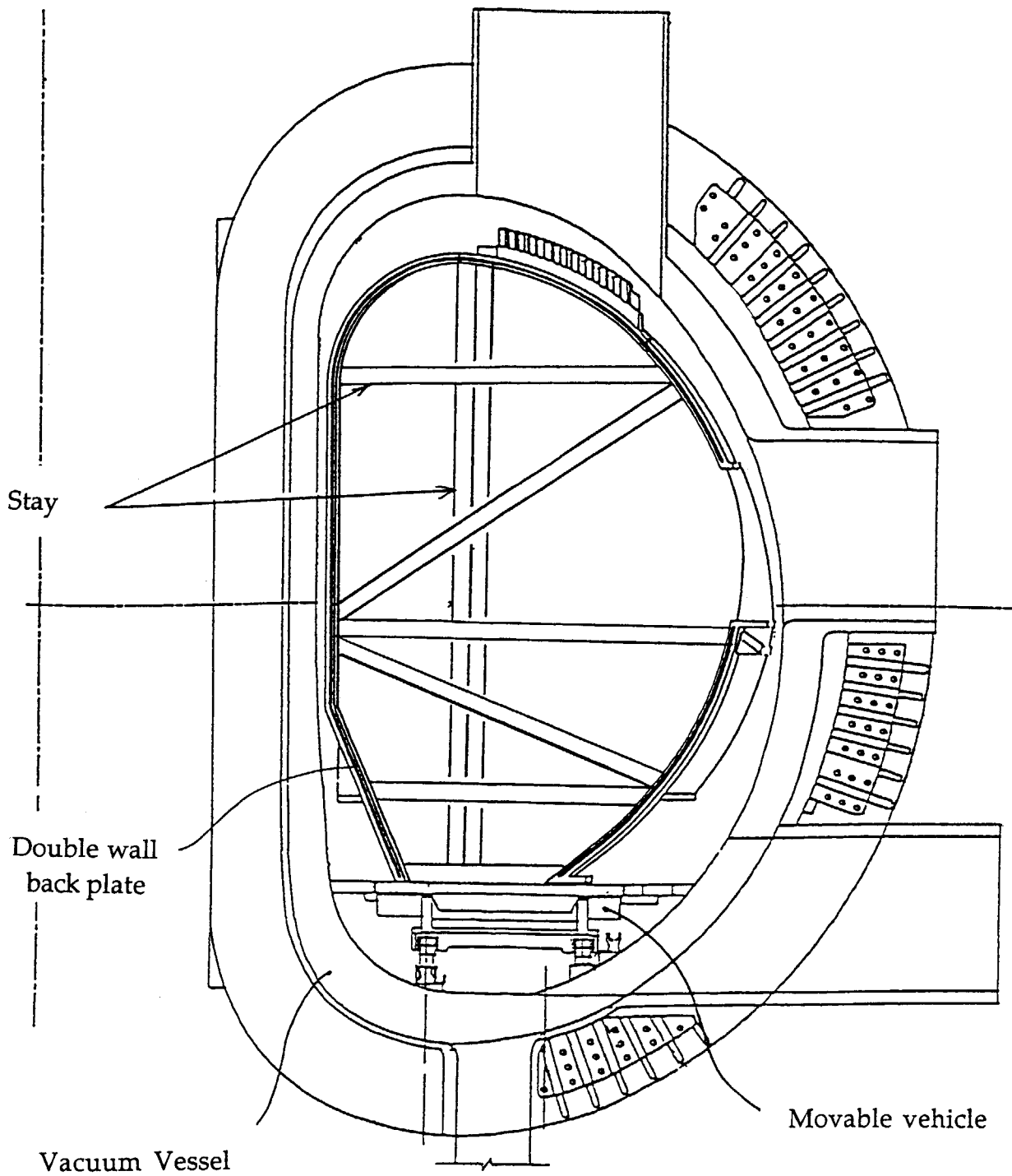
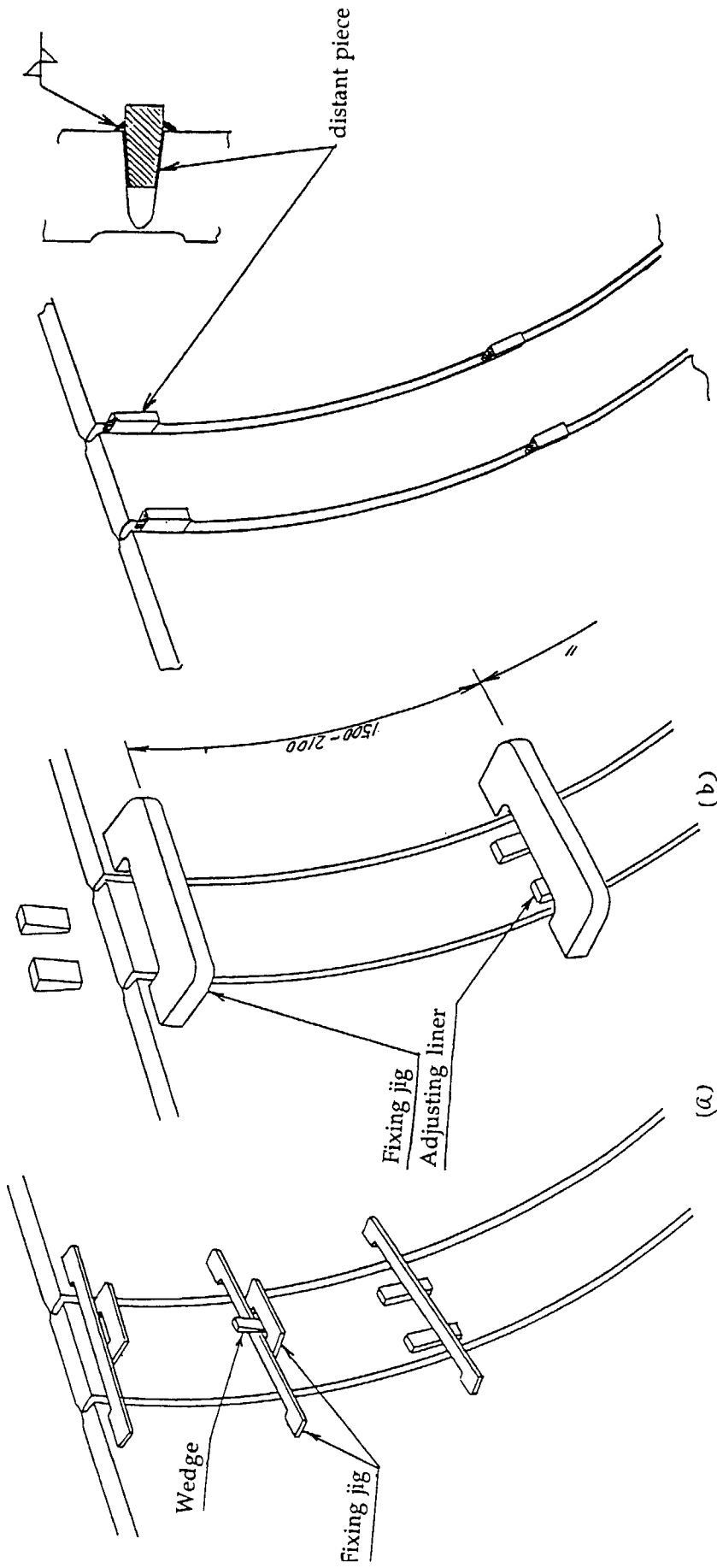


Fig. 5.9 Back plate fixing tool "Stay" for welding deformation prevention.



Insertion of deformation prevention pieces.

Splice plate positioning method.

Fig. 5.10 Welding jigs for deformation prevention.

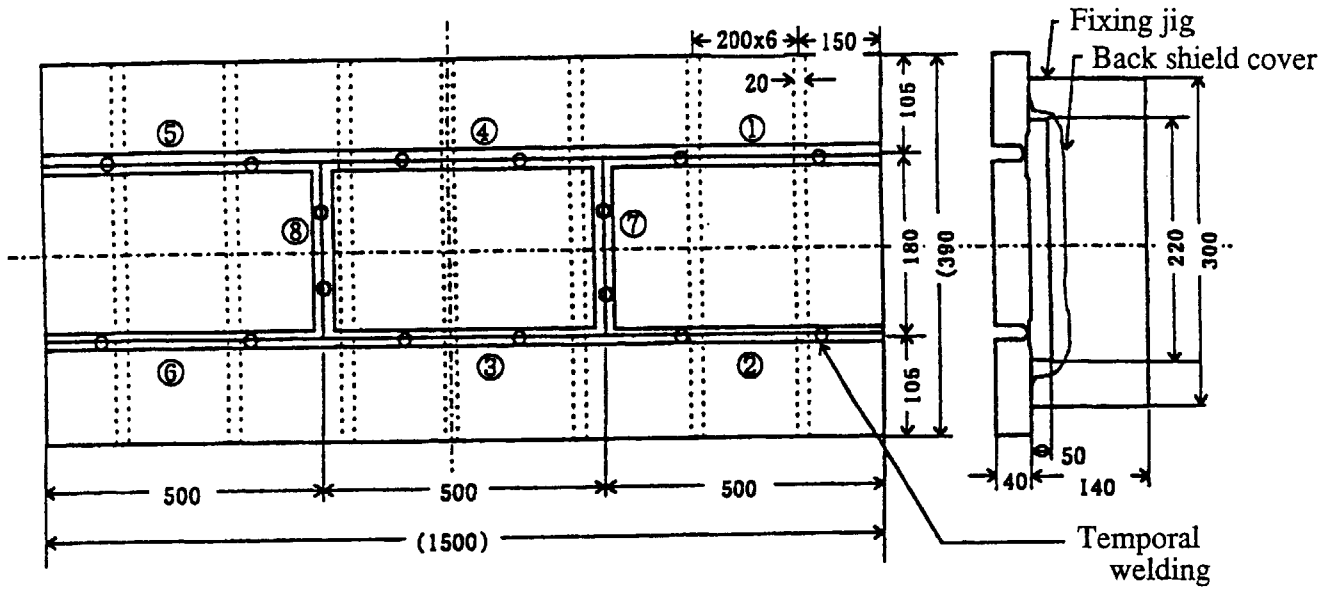


Fig 5.11 The test piece of plice plate for welding

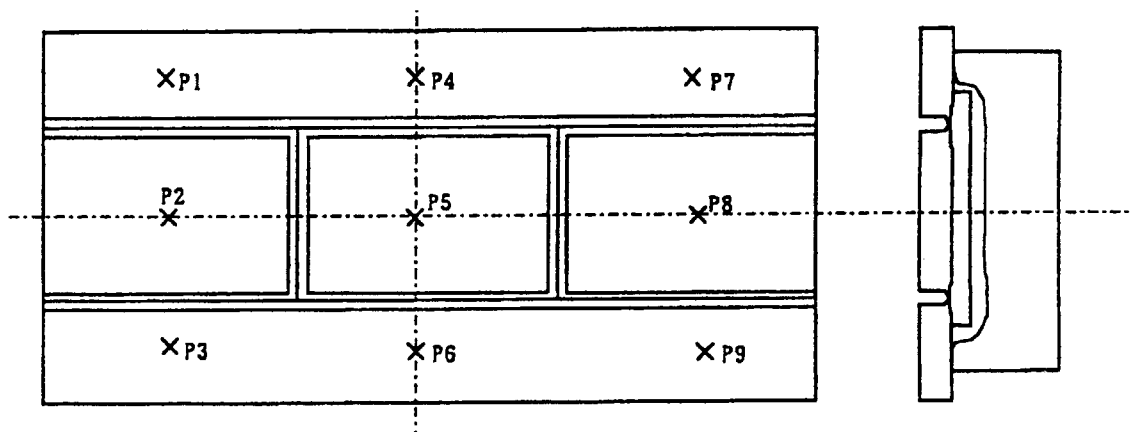


Fig. 5.12 The measuring point of test piece

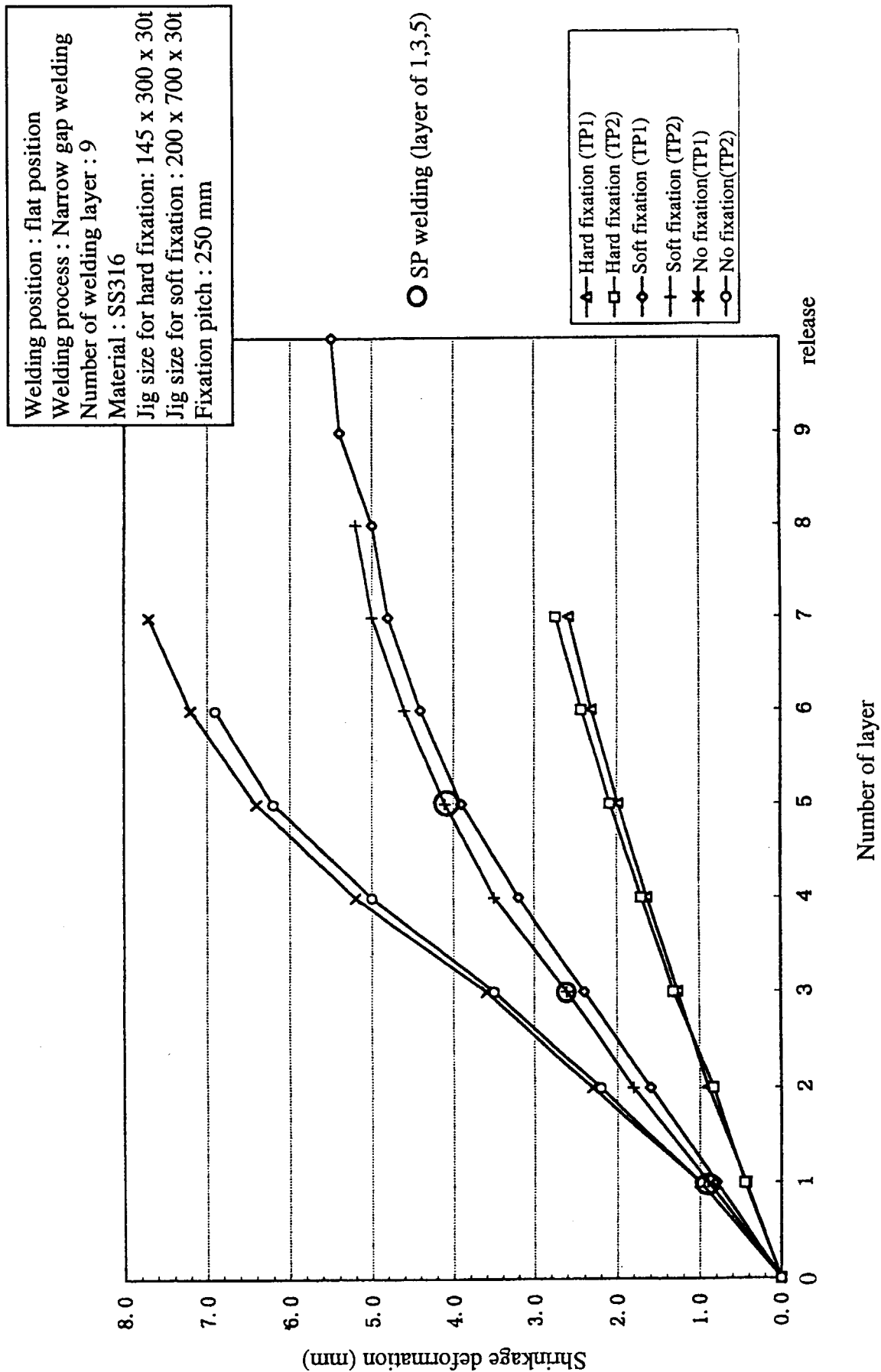


Fig. 5.13 The shrinkage deformation of back plate test piece

## 6. Port Limiter Design

### 6.1 Support Structure

#### 6.1.1 Design Requirement

Port limiter is located in the equatorial ports for improved maintainability. Support and alignment system should provide a supporting structure for the limiter under the EM impulse loads as well as under the steady weight load. The presented design is based on the following key restrictions, requirements, assumptions.

- Supporting of the limiter under EM loads summarized in Table 6.1[6.1]
- Alignment shown in Table 6.2[6.1]
- Cooling for nuclear heat
- Shielding
- Reliability of the support structure

#### 6.1.2 Conceptual Design

The alignment system have an adjustable geometry in order to provide support at the required location and orientation of the limiter front surface. The support system should be set in a shield plug to support the limiter closely. Table 6.4 shows the comparison of the support system. Worm and gear system is selected to drive and lock the alignment structure because it is possible to make the system compact .

The scheme of the support structure is shown in Fig.6.1. The support system has the following adjustable functions.

- Radial translation is provided by the sliding between inner and outer shafts connecting the center of the limiter.
- Rotations about vertical and horizontal axes are provided by the rotation at the sphere support of the outer shaft.

The adjustable mechanism for each direction is as follows;

- The inner shaft is driven in the radial direction by ball screw attached at the edge of the inner shaft.
- Rotations about vertical and horizontal axes are driven by combination of turning-arm and inner-bushing rotation. Fig. 6.2 shows the alignment mechanism for the rotation. The square area a-b-c-d are supposed to movable area. The point M and N are the center of the turning arm and the inner bushing. The initial point O moves to the point P along the curve R1. Then the point P moves to the point E along the curve R2. The point O can be moved to any point in the area a-b-c-d. The turning arm and the inner bushing are driven by worm and worm gear.

Table 6.3 shows the design parameters of the support structure. The Fig.6.3 shows the schematic design of support and alignment system. The support mechanism for EM loads is as follows;

- Poloidal moment of 900kNm is supported by the sphere support and the edge of outer shaft.
- Radial torque of 220kNm is transmitted to the outer shaft through the square cross section of the inner shaft. The outer shaft is supported by the eccentricity of the outer shaft at the sphere support.
- Radial pressure is supported by the sphere support through the ball screw at the edge of inner support.

The vacuum seal between a driving rod of the air motor and the plasma chamber can be made by bellows, shown in Fig.6.4. The driving mechanism is supported at the flange of shield plug. Though the driving rod should be lengthened, the vacuum seal mechanism itself has been usually used for vacuum seal of rotation rod.



Table 6.1 Main Alignment Requirement

Degree of Freedom	Amount of Movement	Accuracy
Translation		
Radial	$\pm 20\text{mm}$	$\pm 0.5\text{mm}$
Toroidal	Not Required	Not Required
Vertical	Not Required	Not Required
Rotation about center of limiter		
Vertical Axis	$\pm 0.725^\circ$	$\pm 0.07^\circ$
Horizontal Axis	$\pm 0.45^\circ$	$\pm 0.04^\circ$
Radial Axis	Not Required	Not Required

Table 6.2 Electro-magnetic and Weight Load

Type of the Load	Value
EM Loads	
Poloidal Moment	900kNm
Radial Torque	220kNm
Radial Pressure	0.2MPa
Weight Loads	
Weight of the Limiter	137.28kN

Table 6.3 Design Parameters of Support Structure

(1) Limiter support shaft			
• Inner shaft diameter	290 mm		
• Shaft length	2500 mm		
• Shaft Weight	43 kN		
(Inner shaft 16.3 kN, Outer shaft 26.3 kN)			
(2) Diameter of sphere support	700 mm		
(3) Adjustable support structure			
• Inner shaft			
Driving mechanism	Ball and Screw		
Driving force	Air motor		
	Torque	1.4 Nm	
	Rotation speed	900 rpm	
All gear ratio	1/19800		
Driving velocity	0.015 mm/sec		
Amount of movement	30 mm		
• Turning arm			
Driving mechanism	Worm and gear		
Driving force	Air motor		
	Torque	1.4 Nm	
	Rotation speed	900 rpm	
All gear ratio	1/26400		
Driving velocity	0.204 mm/sec		
Amount of movement	$\pm 13$ degrees		
• Inner bush			
Driving mechanism	Worm and gear		
Driving force	Air motor		
	Torque	1.4 Nm	
	Rotation speed	900 rpm	
All gear ratio	1/26400		
Driving velocity	0.204 mm/sec		
Amount of movement	$\pm 10$ degrees		

Table 6.4 Comparison of Port Limiter Driving System

System	Support		Driving Force		Monitor		Comment
	Point	Mechanism	Point	Device	Point	Device	
Hydraulic Cylinder	Shielding Plug	Pins and Rods	Shielding Plug	Cylinder/Link	Cryostat	Oil Servo	A lot of Space and Stopper Required
Rack&Pinion	Shielding Plug	Sphere Surface	Cryostat	Motor/ Rack& Pinion	Cryostat	Encoder/Potentiometer	Large Mechanism
Ball Screw	Shielding Plug	Pins and Rods	Cryostat	Motor/ Screw	Cryostat	Encoder/Potentiometer	Large Mechanism
Air Motor	Shielding Plug	Sphere Surface	Shielding Plug	Air Motor/ Worm gear	Shielding Plug	Potentiometer	Compact
JCT Design	Shielding Plug	Eccentric Bushings	Shielding Plug	Hydraulic Motor & Cylinder	-----	-----	JCT Design

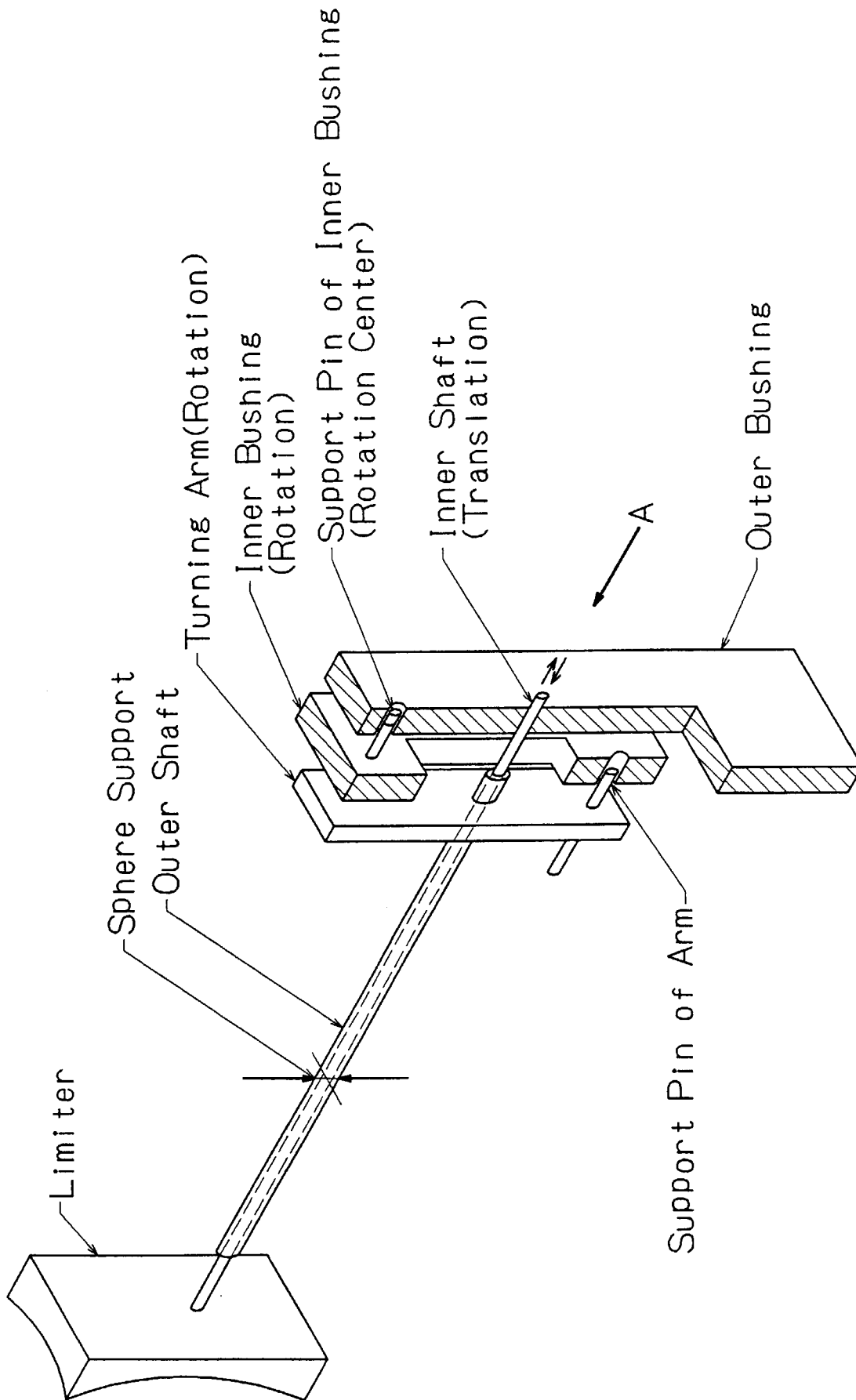


Fig. 6.1 Scheme of Limiter Support Structure

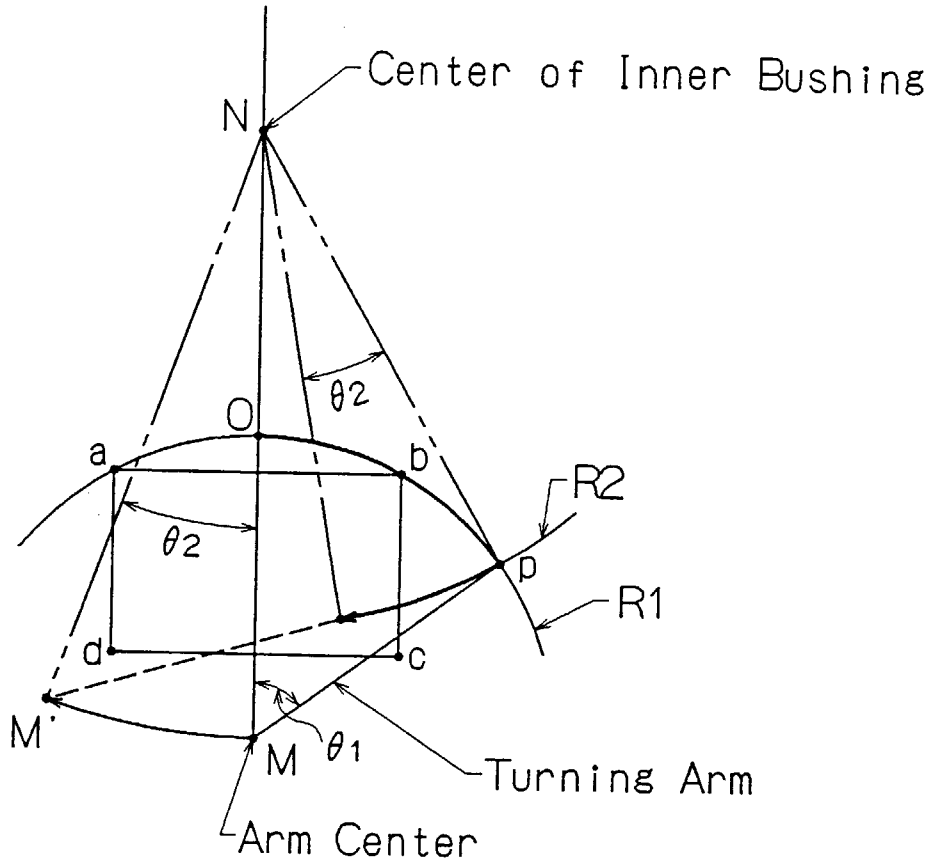


Fig. 6.2 Scheme of Positioning

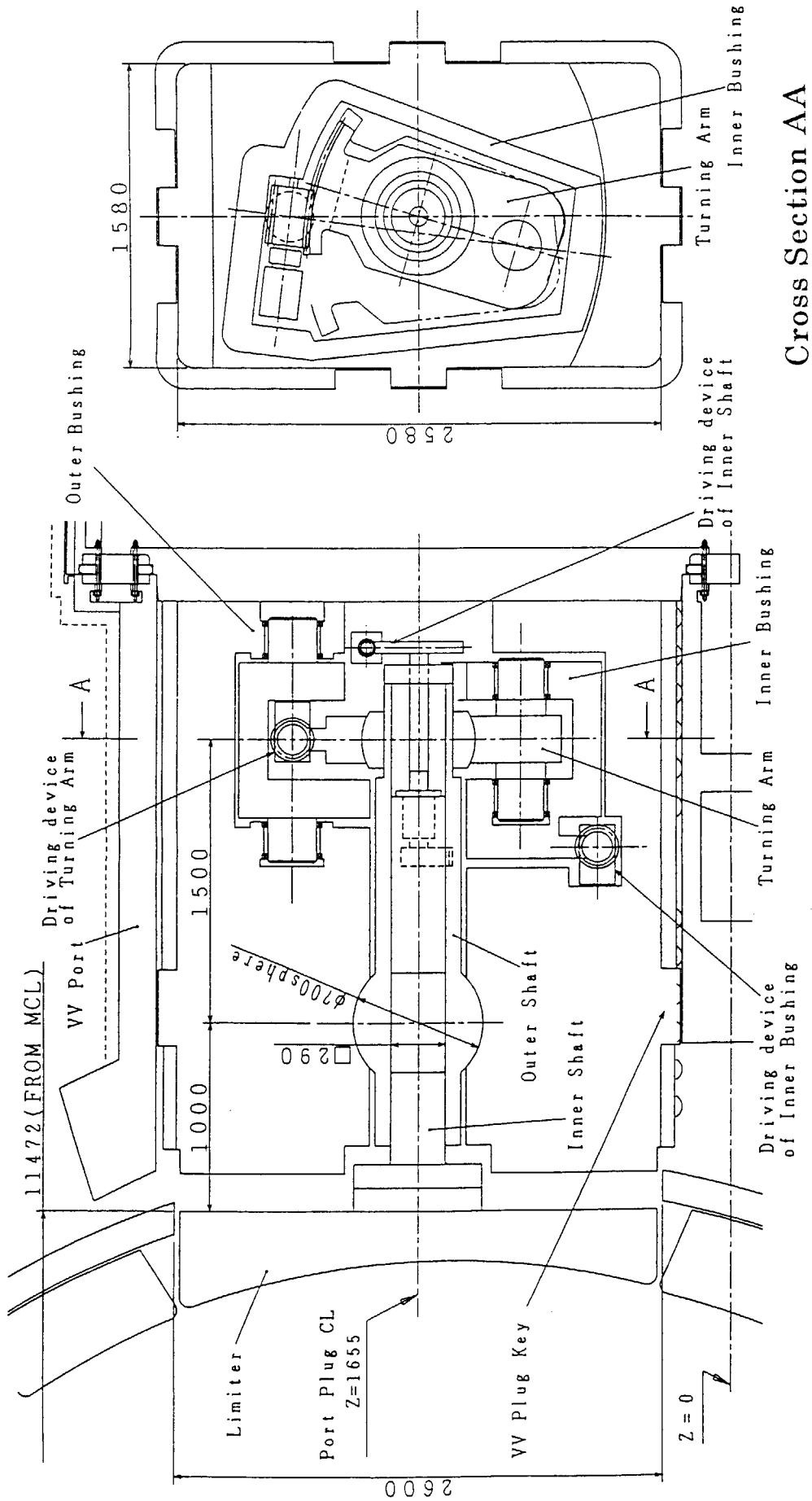


Fig. 6.3 Scheme of Limiter Support Structure

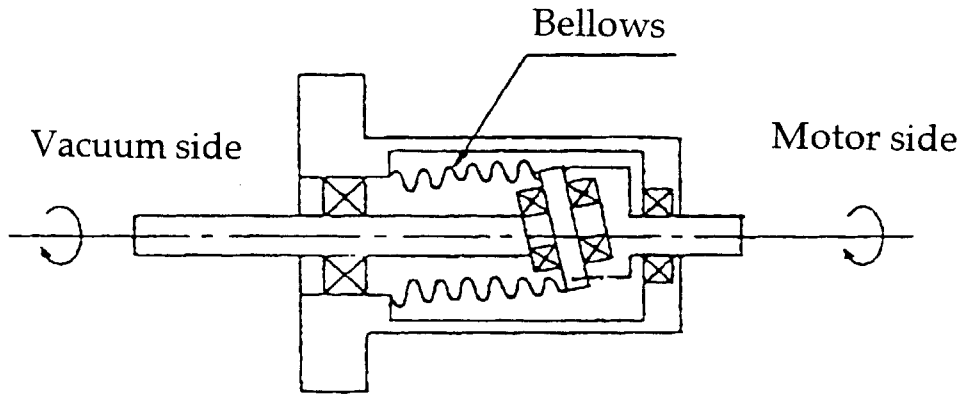


Fig.6.4 Concept for vacuum seal of rotation rod

## 6.2 Fabrication

In the reference design, the port limiter are an assembly of 43 mm thick vertical plates welded together at the rear section. Alternative port limiter designs have been proposed here from the view point of fabrication.

### 6.2.1 Reference Design

Vertical plate of the port limiter is formed by HIPing two stainless plates with an included cooling tube inserted into a serpentine cooling path, shown in Figs. 6.2.1 and 6.2.2. The FW is also added by HIPing the water cooled copper and ~4 mm thick Be layers. The electron beam (EB) welded rear section forms a continuous hard backing and the ~1 mm gap between vertical plates is insulated by alumina coating to prevent arcing.

The following points may be proposed to improve the fabrication.

- Alternative low-cost forming of vertical plate
- Easy FW assembly to the vertical plate.
- Easy forming of a serpentine cooling path
- Easy vertical plate assembly to the rear section.

### 6.2.2 Alternative Design

#### 6.2.2.1 Mechanical Joint of FW

Mechanical joint between FW and a vertical plate is an alternative structure shown in Fig. 6.2.2.1 and 3. Two FW units with Be tiles are connected to a vertical plate by brazed pins or bolts.

Merit of the alternative design is that the bonding between armor tiles and heat sink is easier than that of the reference design because of easy handling of small FW units. The bonding reliability will be higher and the cost of the fabrication will be lower. A concern is the heat removal of nuclear heating for pins or bolts. To improve the thermal conductivity between pins or bolts and vertical plate, pins or bolts can be brazed to the vertical plate. Brazing materials should be selected from the view point of the melting point of 350 - 500 °C. Removal methods of pins from the vertical plate are a thermal method to re-heat pins and a mechanical method to debond the joint.



Thermal conductivity at brazed pin joint and optimum brazing material should be examined.

#### 6.2.2.2 Mechanical Joint of Vertical Plate

The cross sections of vertical plate in the alternative design are shown in Figs. 6.2.2-2 and 4. Bending radius of stainless steel (SS) cooling pipes is large enough to bend easily. Coolant collectors welded by EB are installed at the rear side of the vertical plate. Each vertical plate is joined together by bolts to assemble and disassemble easily. It is also easy for the bolt joint to insulate between the vertical plates. Only screw area of bolt is brazed to increase thermal conductivity between bolts and the vertical plate.  $\text{Al}_2\text{O}_3$  is coated on non-screw area of bolt to insulate between adjacent vertical plates.  $\text{AlN}$  spacer is used between the bolt and vertical plate because of the characteristic of insulation and good thermal conductivity as shown in Fig. 6.2.2-5.

### 6.2.3 Fabrication method and process

#### 6.2.3.1 Fabrication of heat sink

Two types of fabrication method and process are described as follows.

Type A for heat sink fabrication is shown in Fig. 6.2.3-1. Grooves for DsCu cooling tubes are machined in a plat heat sink plate. Two heat sink plates are HIPed with cooling tubes inserted between plates and SS pipes are bonded at their DsCu pipe edges. Sixteen grooves can be manufactured in DsCu plates, size of which is  $3000 \text{ mm}^L \times 15 \text{ mm}^t \times 800 \text{ mm}^W$  due to production ability. After HIPing, the heat sink plate is cut to 50 mm width pieces. The heat sink pieces are bent and machined to final shape.

The other fabrication method, Type B, is shown in Fig. 6.2.3-2. A groove with final shape is machined in a DsCu plate, the size of which is  $2600 \text{ mm}^L \times 290 \text{ mm}^W \times 15 \text{ mm}^t$ . A cooling pipe with built-in swirl tape is bent to final shape and joined SS pipes to the edges. The pipe is inserted between the plates and HIPed. The HIPed plates are machined to the final shape.

The final shape by Type B can be more accurate than that by type A But Type B needs high accurate machining to insert curved swirl pipes in the heat sink, therefore its cost will be higher. As an alternative method of type A, a straight cooling tube with the width of 50 mm can be HIPed not to cut the

HIPed plate. Type A is considered to be a reference fabrication method of the heat sink because of cost.

Brazing and HIP bonding can be used as bonding methods between cooling tubes and heat sink plates. Fabrication cost of brazing will be lower than that of HIP to allow large tolerance between bonded surfaces. These fabrication methods are composed in following table.

	HIP	Brazing
Cost	No Good	Better
Fabricability	Good	Good
Bonding strength	Better	Good
Quality assurance	Good	Good

#### 6.2.3.2 Fabrication of vertical plate

A limiter module of 2560 mm<sup>H</sup> x 740 mm<sup>W</sup> x 44 mm<sup>t</sup> has thirty-six SS vertical plates. The vertical plate is a bonded structure by HIPed or brazing to install cooling pipes inside the plate. EB welding or mechanical joint using bolts are applied to assemble the vertical plates and the rear section.

The reference fabrication method to join the vertical plates is HIP shown in Fig.6.2.3.3. The vertical plate is machined precisely, and serpentine bent tubes are placed in the grooves. Bonding interface of HIP may be pressure boundary of coolant in coolant headers

Another fabrication method is brazing which can allow larger tolerance between cooling tubes and grooved plate than that of HIP. Fabrication process using mechanical joint with the rear shield is shown in Fig. 6.2.3-4. Only the screw area of bolts is brazed to cool the nuclear heating of the bolts. Shear force due to electro-magnetic forces can be withstand by the protrude structure of vertical plate shown in Fig.6.2.2.5.

Low-cost fabrication method of vertical plate is casting. Casting needs neither precise machining nor bonding of serpentine cooling tubes. Fabrication methods are compared in the following table.

	HIP	Brazing	Casting
Cost	High	Low	Lower
Fabricability	Good	Better	Much better
Strength of bonding surface	Better	Good	No bonding surface
Quality assurance, inspection	Good	Good	No data

### 6.2.3.3 Limiter Module

Total fabrication process of port limiter modules is described here and shown in Fig. 6.2.3.6.

- 1) Heat sinks and vertical plates are fabricated by above mentioned method. SS pipes are welded to both edges of a DsCu cooling pipe in a heat sink. Other parts, beryllium tiles, and pins or bolts are manufactured and insulation coating is performed except screw parts of bolts.
- 2) Beryllium tiles are bonded on the heat sink.
- 3) Insulation coating in vertical plate surfaces is performed. Insulation material is Al<sub>2</sub>O<sub>3</sub>.
- 4) FWs are jointed to a vertical plate by bolts.
- 5) After joining of SS pipes at the cooling tube edge, coolant collectors are welded.
- 6) Vertical plates are piled up and assembled by bolts.
- 7) Welding between manifold and cooling pipes is performed.
- 8) Screws of pins and bolts in a limiter module are brazed at the same time in vacuum
- 9) Surface of FW is machined in final curvature.

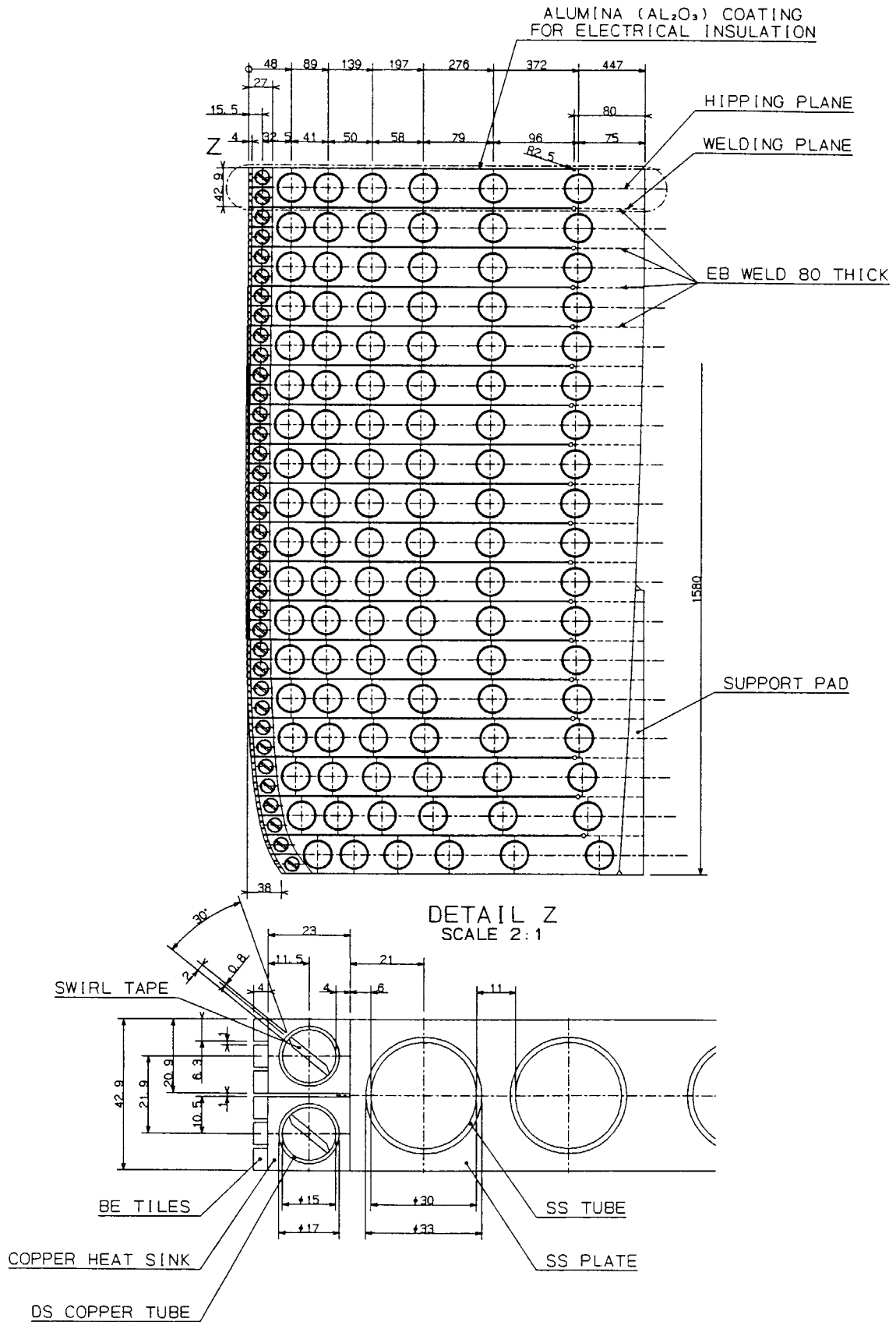


Fig. 6.2.1 Port Limiter Module (JCT Design)



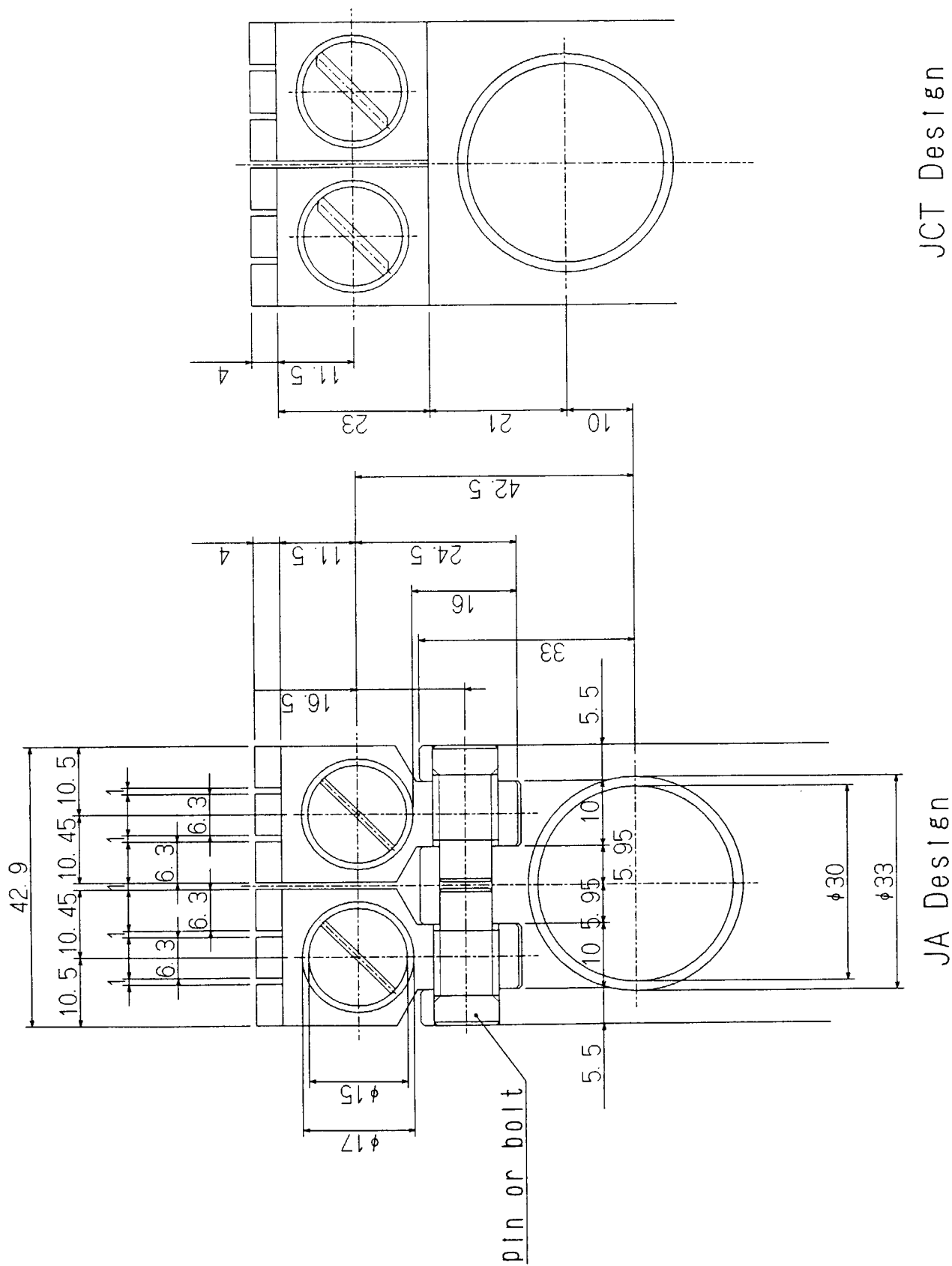


Fig. 6.2.2.1 First Wall in Port Limiter Module

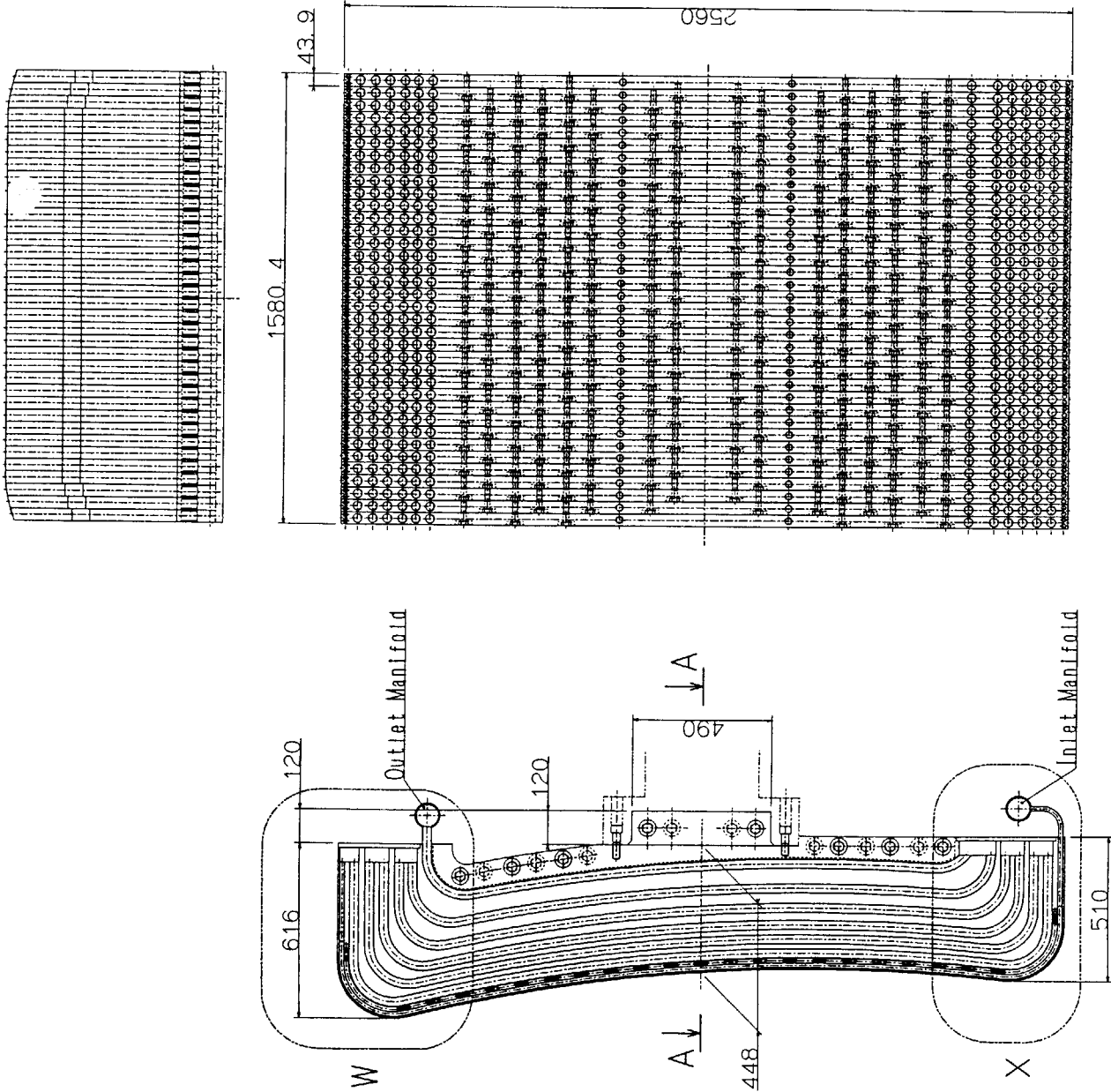


Fig. 6.2.2.2 Port Limiter Module





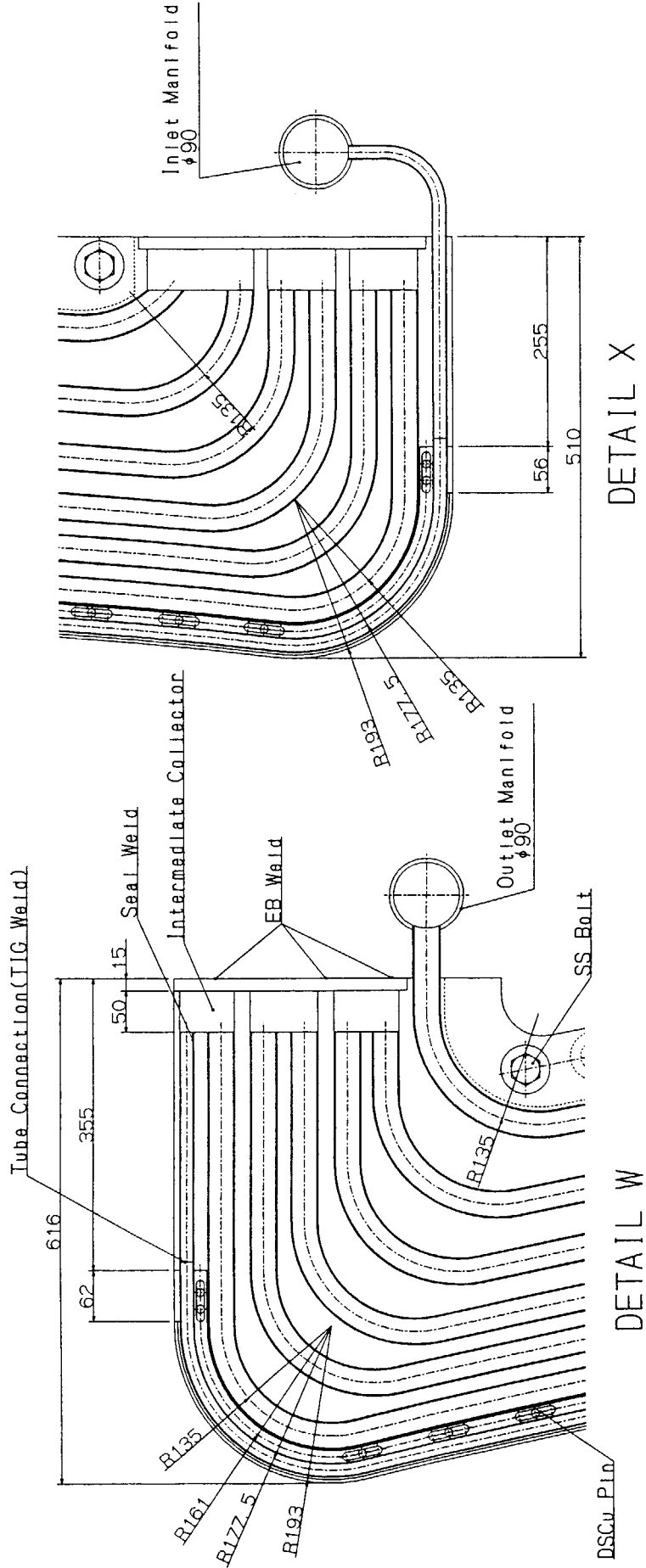


Fig. 6.2.2.4 Detail Design of Limiter Module

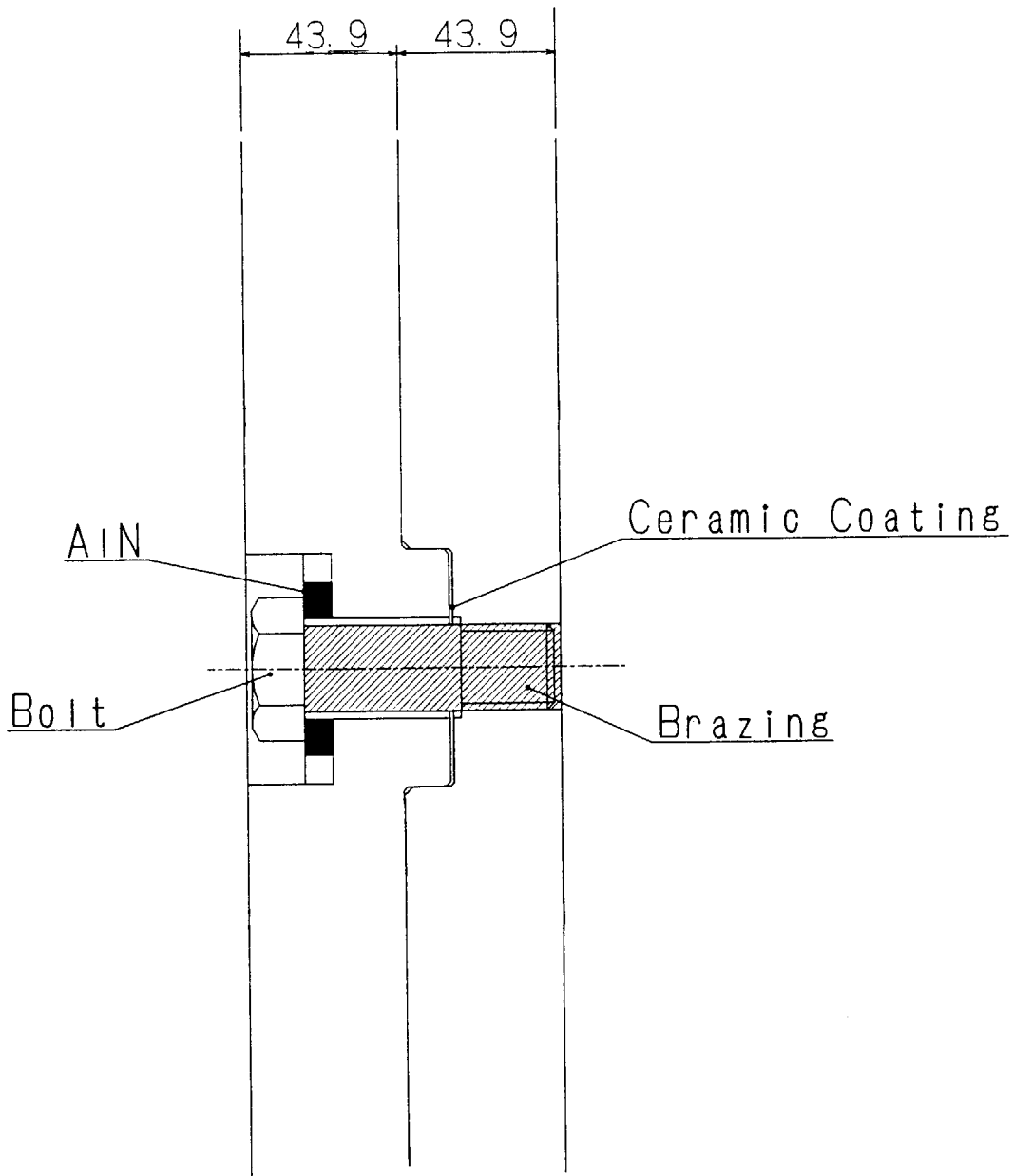


Fig. 6.2.2.5 Bolt Joint in Shield Plate

⑥ final machining

⑤ bending

④ cut out pipes from a HIPed plate

③ canning and HIP

② Insert cooling pipes between two plates bonding SS pipes to both edges of DSCu pipe

① machining grooves

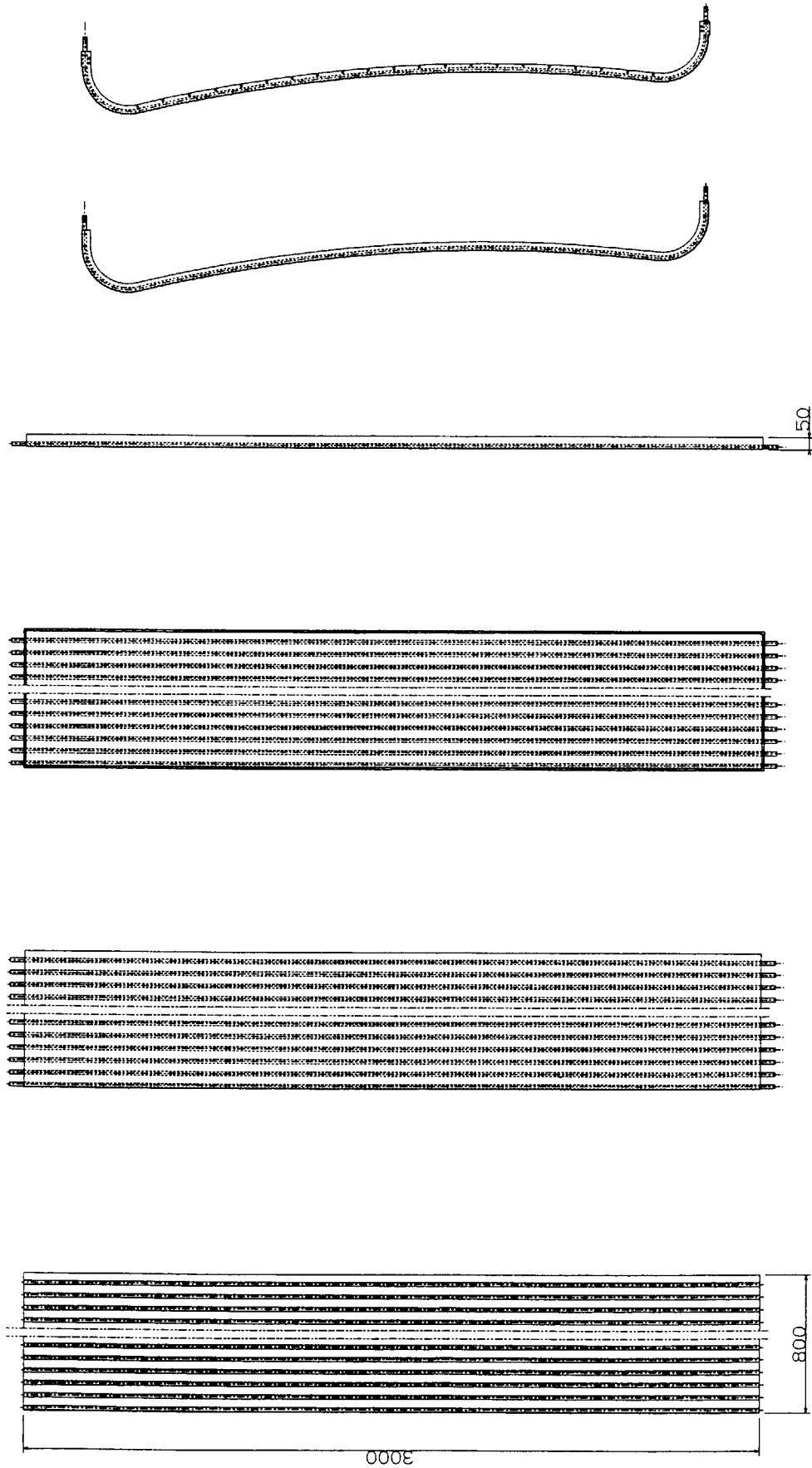


Fig. 6.2.3.1 Fabrication Process of Heat Sink (Type A)

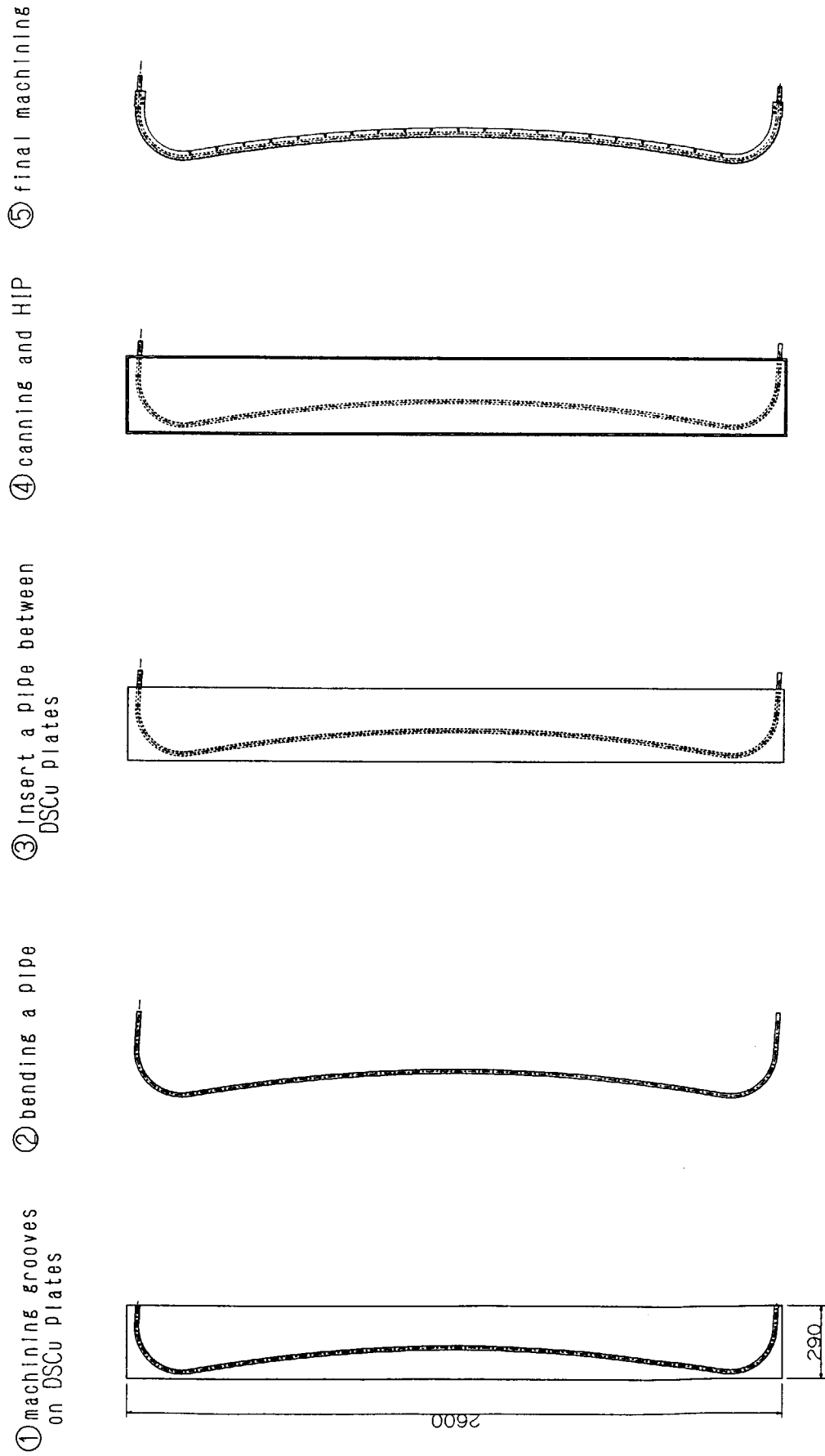
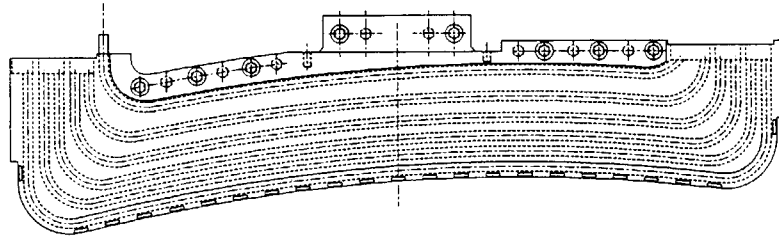
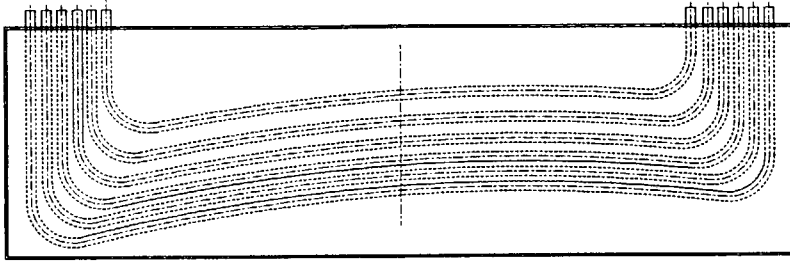


Fig. 6.2.3.2 Fabrication Process of Heat Sink (Type B)

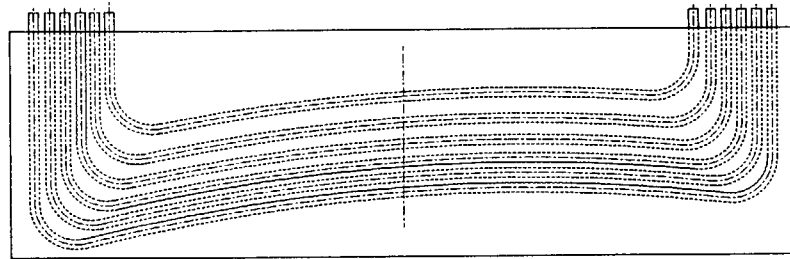
⑤ final machining



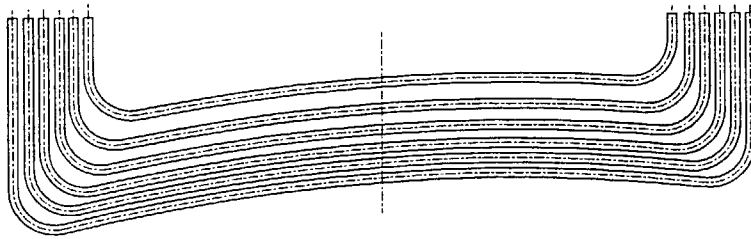
④ canning and HIP



③ Insert pipes between two plates



② bending pipes



① machining grooves on SS plates

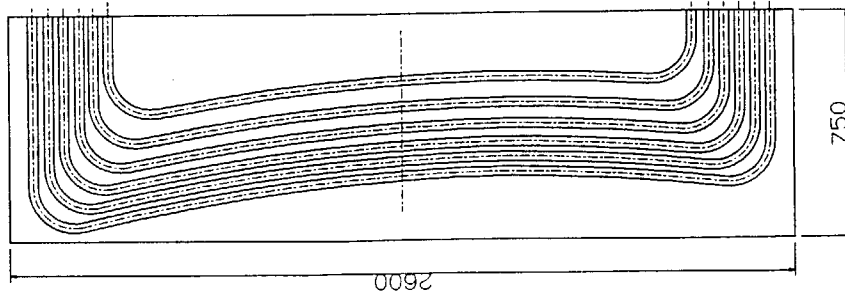


Fig. 6.2.3.3 Fabrication Process of Shield Plate (HIP)

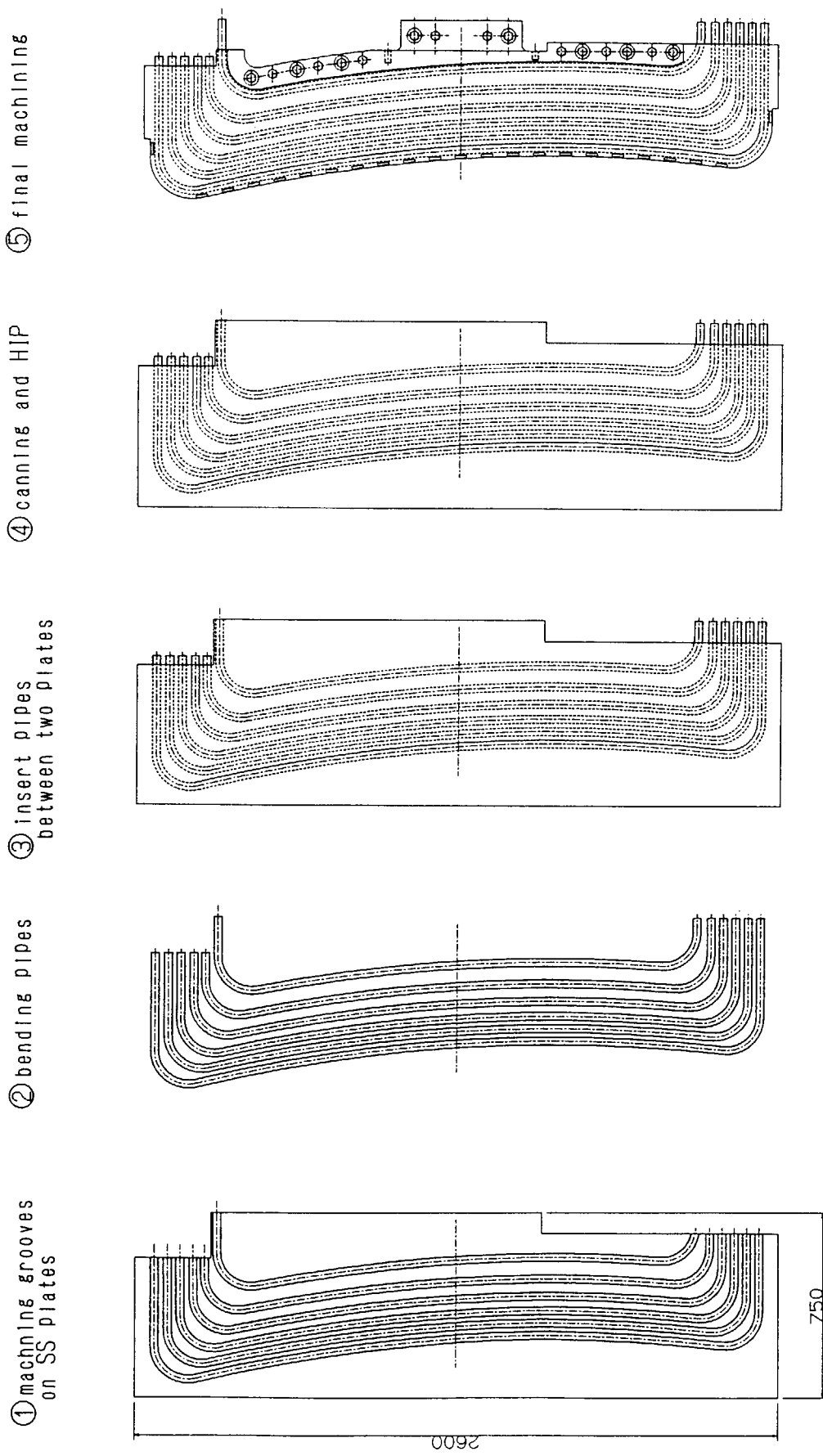


Fig. 6.2.3.4 Fabrication Process of Shield Plate (Brazing & Bolt)

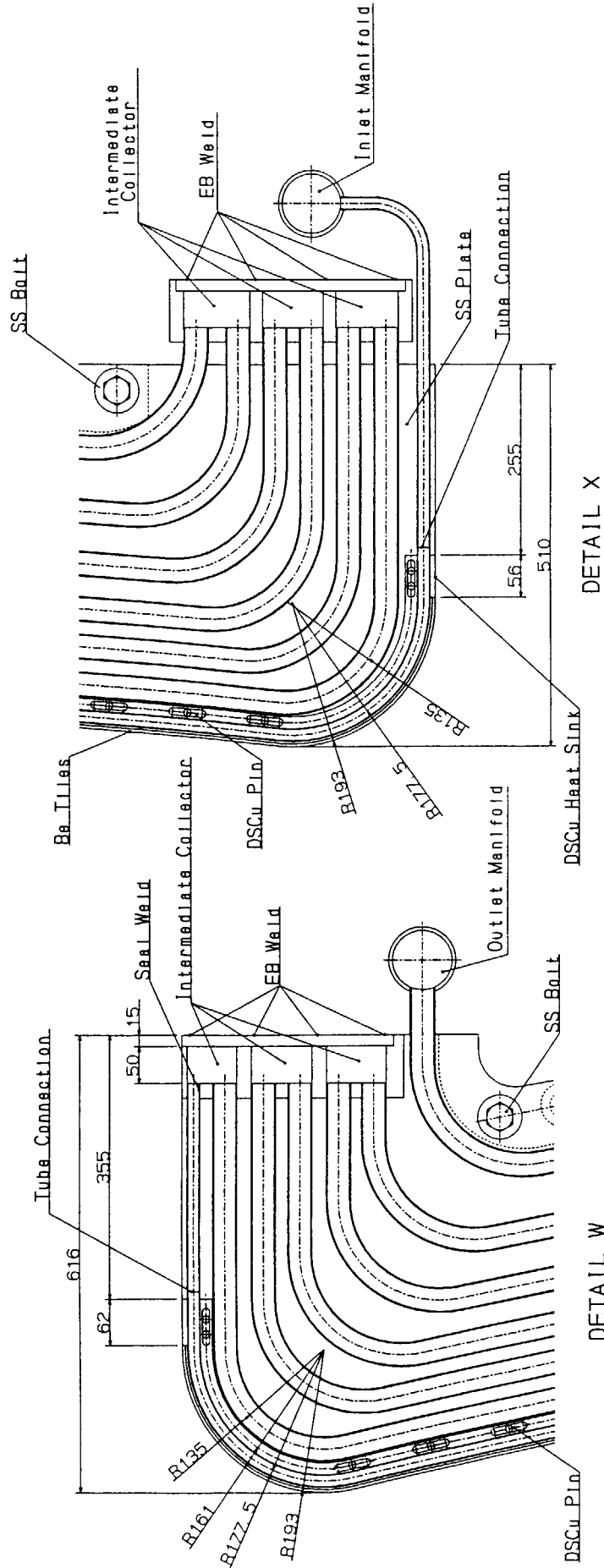


Fig. 6.2.3.5 Detail Design of Limiter Module (Brazing & Bolt)

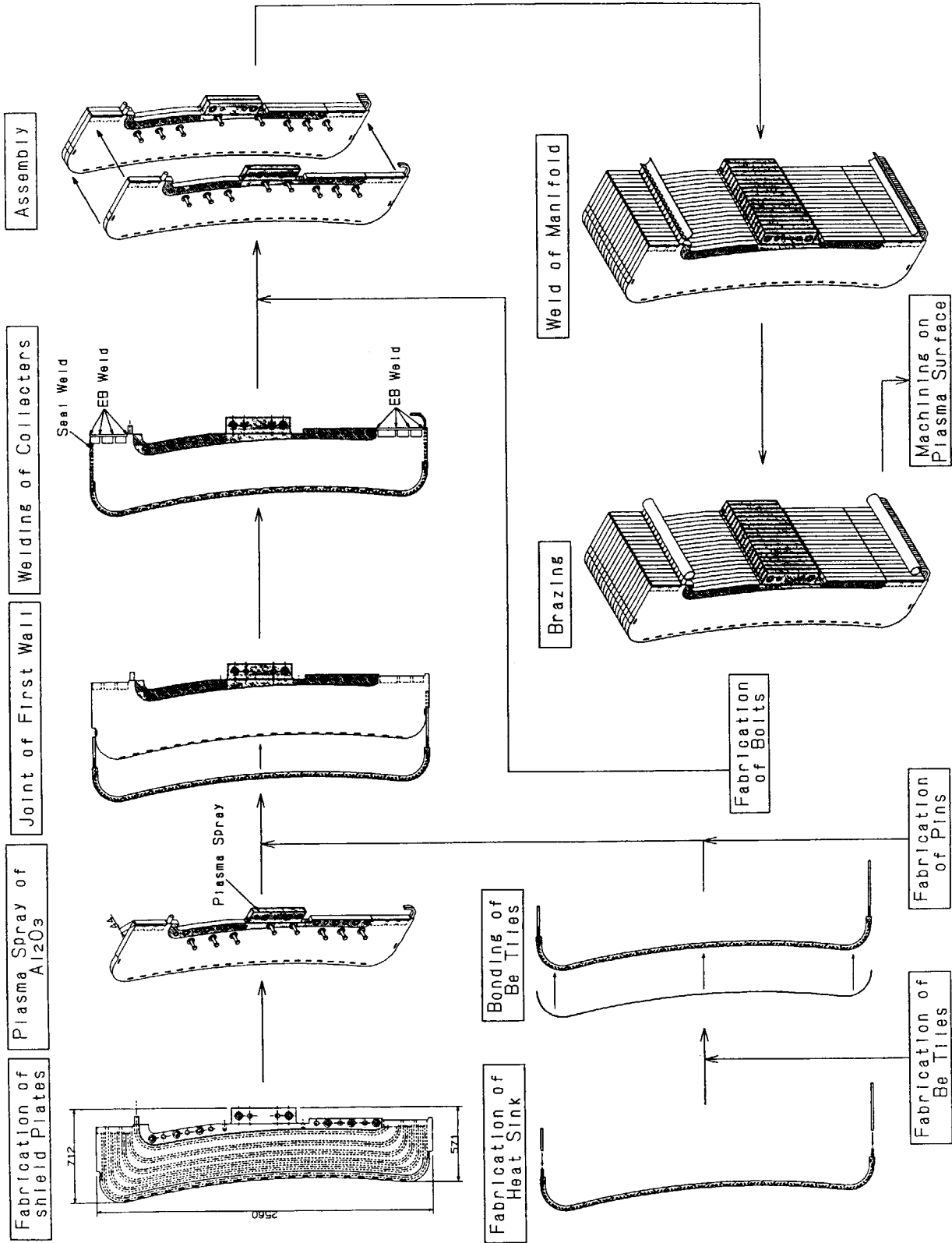


Fig. 6.2.3.6 Fabrication Process of Limiter Module



## 7. Studies on the runaway electrons effects on FW

The thermal response of the First wall with Be armor to the volumetric heat generation due to the runaway electrons impact was investigated in this section. The energy deposition density, i.e. the volumetric heat generation due to the runaway electrons was estimated by using the EGS4 code[7.1]. This volumetric heat is used for the thermal boundary condition in analyses of the transient temperature distribution of FW by FE code ABAQUS.

### 7.1 Outline of EGS4 code system and its validation

The EGS system[1] is a general purpose package for the three dimensional Monte Carlo simulation of the coupled transport of electrons and photons. The most recent and enhanced version of EGS system is called EGS4. The EGS4 code can simulate the electromagnetic processes, and the transport of electrons and photons with the energy above a few keV up to several TeV in arbitrary geometry. This code system provide a stand alone utility program called PEGS code (Preprocessor for EGS) which can generate the material data such as the cross sections which are dependent on the energy of electrons and photons.

A comparison of the results with EGS4 and another Monte Carlo code system called GEANT3[7.2] was performed by Kunugi et. al. [7.3] for energy deposition distribution in a 10mm thick carbon layer on top of a 50mm thick molybdenum layer. The incident electron energies from 10 to 300 MeV and the incident angle from 0.5 to 25 degrees. For both code systems, the results for the peak deposited energy densities and the deposited fraction in carbon and molybdenum are compared. The comparisons are summarized in Table 7.1. The calculations of EGS4 and GEANT3 agree better than 20%.

**Table 7.1. Relative difference of the EGS4 and GEANT3 codes results for runaway electron impact on 10mm carbon on top of 50 mm molybdenum.**

code result	D [%]	$\Delta D$ [%]
Peak energy density in molybdenum	15.6	6.4
Peak energy density in carbon	-4.1	14.7
fraction of energy in molybdenum	-7.3	5.3
fraction of energy in carbon	-9.0	9.5

where,  $D = \frac{E_{\text{GEANT3}} - E_{\text{EGS4}}}{E_{\text{GEANT3}}}$ ,  $\Delta D = \sqrt{\langle D^2 \rangle - \langle D \rangle^2}$ , and E is energy deposition.

### 7.2 Thermal analyses of the runaway electrons impact on FW

Analytical conditions of these simulations were summarized in Table 7.2. The peak energy flux of the runaway electrons reaches maximum at  $t=0$ , the start of the runaway electrons impact and then decays with characteristic time  $\tau_{VDE}$  and the movement of plasma wall contacting point along the wall during VDE. The distribution of the runaway electrons particle was assumed as the following Gaussian shape;

$$n_{RE}(x,t,E) = C_{RE} \exp\left(-\frac{(x - x_s t / \tau_{VDE})^2}{x_{pol}^2} - \frac{t^2}{\tau_{VDE}^2}\right) \exp\left(-\frac{E}{E_o}\right) \quad (1).$$

Here  $x_s$  is magnitude of plasma displacement along the wall,  $x_{pol} (= (2\pi R a \alpha)^{0.5})$  is effective poloidal length of the distribution and  $a$  is the impact angle of the runaway electrons. The value of  $C_{RE}$  is determined by integrating Eq. (1) with respect to coordinate,  $x$ , time,  $t$  and energy  $E$ , is set equal to the peak incident energy density.

**Table 7.2. Analytical conditions of the runaway electrons impact on FW.**

Parameter	value
Energy spectrum	$\exp(-E/E_o)$ $E_o=12.5\text{MeV}$
Impact angle, $\alpha$ [degree]	0.01
Peak incident energy density [ $\text{MJ}/\text{m}^2$ ]	10 - 50
VDE time, $\tau_{VDE}$ [sec]	0.15
Displacement of plasma wall contacting point, $x_s$ [m]	0.5

FW model in Fig.7.1 was used for this simulation. This FW model was assumed to be received the peak incident energy density at the start of the runaway electrons impact as well as steady state heat flux ( $0.5\text{MW}/\text{m}^2$ ) at the surface. The magnetic field effect on the electrons reflected from the surface was considered in the vacuum near the surface. The magnetic field assumed to be uniform and one-dimensional. The material of the armor, heat sink and cooling tube were assumed Be, Cu and SS316. Coolant water temperature was  $140^\circ\text{C}$ . In these thermal analyses, the phase changes such as melting and sublimation were not considered. When the material temperature exceeded the melting or sublimation point, thermal properties of the materials were estimated at the melting or sublimation point.

### 7.3 Heat generation inside of FW due to the runaway electron impact

Fig.7.2 shows the distribution of heat generation inside of FW with CFC armor due to the runaway electrons in three case of the incident energy density of 10, 30 and 50 MJ/m<sup>2</sup>. The heat generation is concentrated near the surface in each case.

#### 7.4 Thermal response of FW due to the runaway electron impact

Fig.7.3 shows the temperature profiles at the edge of the surface in case of the runaway electrons with the incident energy density of 10, 30 and 50MJ/m<sup>2</sup>. It was found that the temperatures at the surface in each condition reached the maximum value after the start of the runaway electrons impact since the electron flux decreased rapidly with time. In case of the runaway electrons impact with the energy of 50MJ/m<sup>2</sup>, surface temperature exceeded the melting point of Be, 1287 °C, because the phase change of material did not considered in these analyses.

Fig.7.4 shows temperature profiles on the edge line of FW with Be armor at 50ms after the runaway electrons with the incident energy density of 10, 30 and 50MJ/m<sup>2</sup>. In the thin layer near the surface, large temperature gradient occurred so that the depth where temperature exceeded the melting point Be was less than 0.5 mm.

#### 7.5 Summary

The runaway electron effects on First wall with Be armor were parametrically investigated by numerical analysis. The numerical results showed that the maximum temperature at the Be armor surface exceeded the melting point in case of the runaway electron impact with the energy density of 50MJ/m<sup>2</sup>, incident angle of 0.01 degree and that the depth of the melting region was less than 0.5mm.

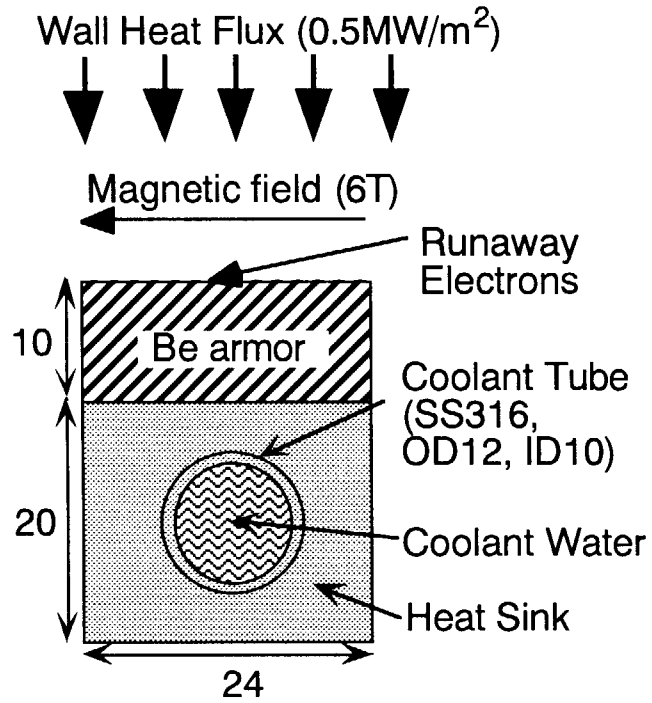


Fig. 7.1. Simulation model of FW with Be armor for the runaway electrons impact.

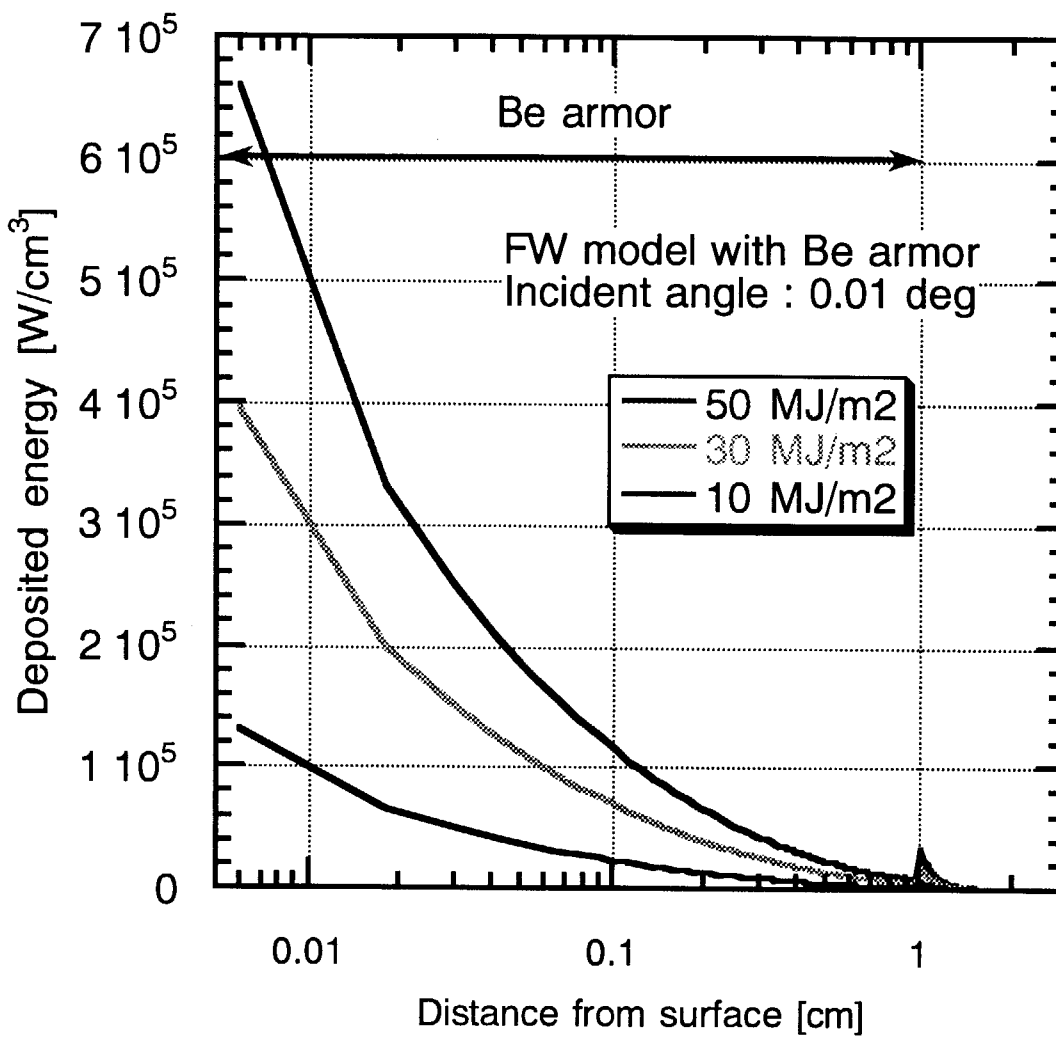


Fig. 7.2. Distributions of heat generation inside of FW with Be armor due to the runaway electrons impact with the incident energy density of 10, 30 and 50MJ/m<sup>2</sup>.

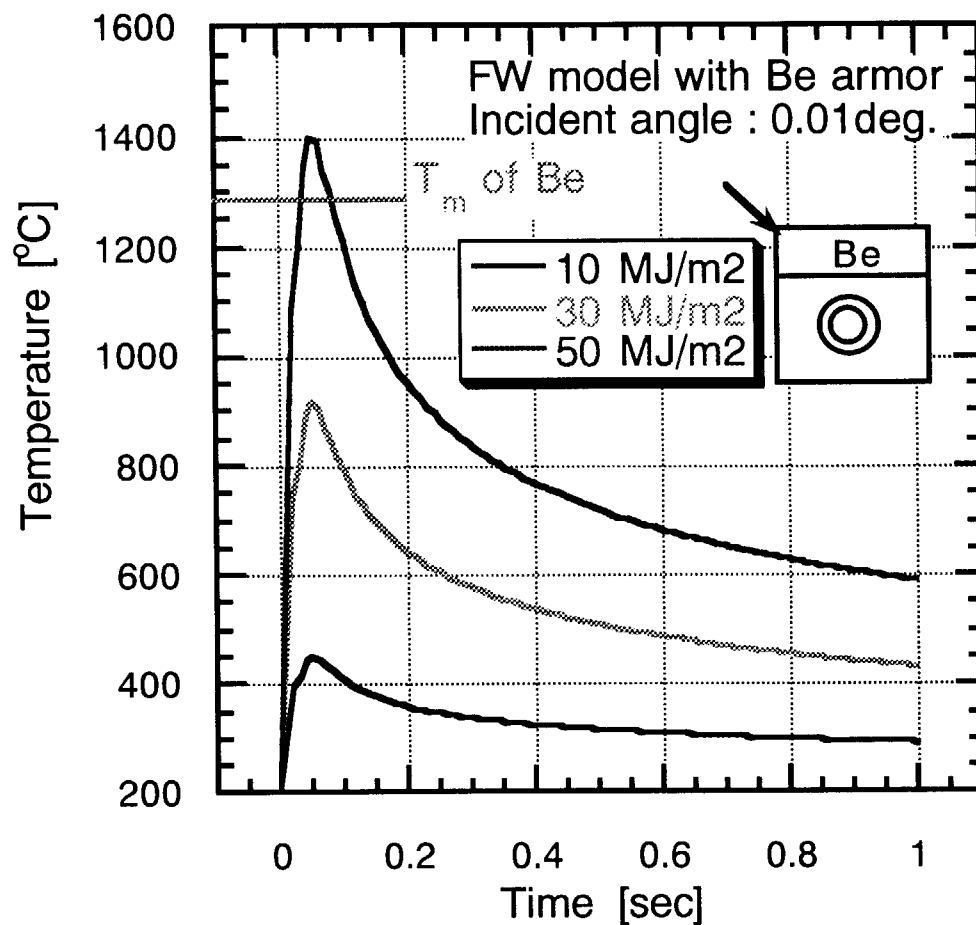


Fig. 7.3. Temperature profiles at the edge of surface in three case of incident energy density of the runaway electrons, 10, 30 and 50MJ/m<sup>2</sup>.

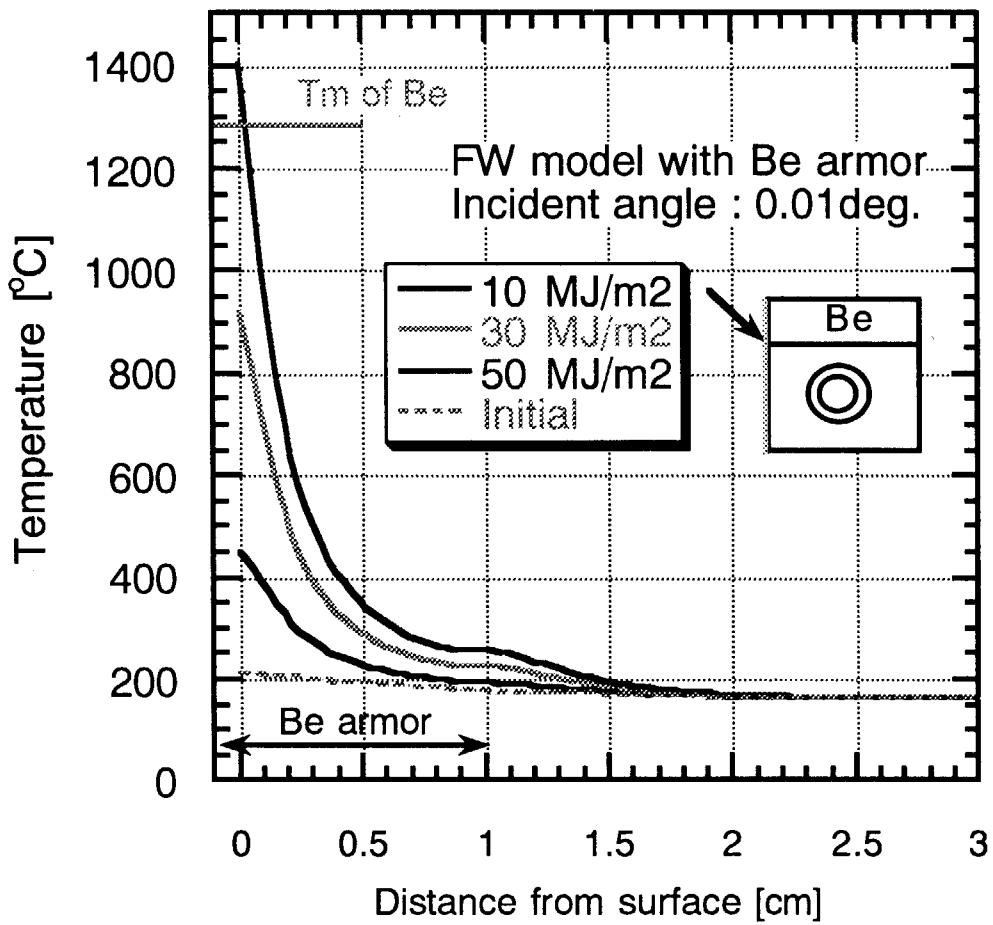


Fig. 7.4. Temperature profiles on the edge line of FW with Be armor at 50ms after the runaway electrons with the incident energy density of 10, 30 and 50MJ/m<sup>2</sup>.

## 8. Summary

Design and analyses have been performed for ITER shield blanket module. Fabrication methods for the shield blanket module and the back plate also have been investigated. Studies on the runaway electron impact for Be armor have been also performed.

Electro-magnetic analysis has been carried out for the shield blanket module to evaluate the effect of the slot on the first wall. Two models are applied to the analyses for stainless steel shield block of the #7 and the #9 modules. The depth and the number of slots are simulated by changing the resistivity of the slotted SS. slotting on the first wall become effective for the #7 module, but it is not effective for the #9 module because the plasma shape does not match with the poloidal curvature of the first wall surface. The number of slot of 10 ~20 with the depth of 2 mm is recommended for the slotted modules.

The fabrication procedure for shield blanket module has been proposed using multi-layered HIP process. The #11 module is selected for the fabrication model with 3-D curvature of the surface. The shield modules are divided into several pieces in order to machine them. The curvature in the toroidal direction is shaped by bending, and the curvature in the poloidal direction by machining. The grooves of the cooling tubes is also machined to make the curvature in the poloidal direction. It is necessary to assemble the module blocks precisely for bonding by HIP at the same time. Issues are pointed out for the fabrication.

Fabrication procedure of the double wall back plate has been developed associated with machining procedure and welding concept. The double wall back plate consist of inner wall, outer wall and cooling rib. The cooling ribs are used for separating inlet and outlet coolant flow. In addition to the cooling ribs, the internal pegs shall be added to support electromagnetic force and water pressure. Additional ribs shall be also provided around port for reinforcement. The welding concept for connecting the rib to the inner wall is discussed and it is concluded that the through wall e-beam welding which needs less machining time is the most efficient welding method. The splice plate welding is the most important process in the back plate manufacturing flow. The back plate shrink deformation for splice plate welding is estimated to be less than 8 mm in toroidal direction and the angular deformation by welding is estimated to be less than 3 degree.

Port limiter design has been performed for the supporting and alignment system. The support structure has a sphere support to provide the vertical and horizontal rotation, and a sliding support for radial translation. Worm and gear system with air motors were applied to support and drive the support structure. As to the vertical plate design, alternative vertical plate designs have been proposed. Bolt connection between FWs and a vertical plate makes the Be-tile bonding to the heat



sink easier than the reference design. The assembly of vertical plates by bolts are designed from the view point of fabrication. The fabrication procedures of the vertical plate are also discussed for low cost fabrication.

The runaway electron effects on First wall with Be armor were parametrically investigated by numerical analysis. The numerical results showed that the maximum temperature at the Be armor surface exceeded the melting point in case of the runaway electron impact with the energy density of 50MJ/m<sup>2</sup>, incident angle of 0.01 degree and that the depth of the melting region was less than 0.5mm.

### Acknowledgments

The authors would like to express their gratitude to Dr. T. Tsunematu and department of ITER Project for their valuable discussions and comments. They would acknowledge Dr. S.Matsuda and Dr. M. Ohta for their support.

### References

- [5.1] Procurement Packages for cost estimation from ITER Director Robert Aymar, Mar 1997.
- [6.1] V.Rozov, 'Port Limiter Alignment and Support System', G16 MD 180 97-11-18 W0.1 1997.
- [7.1] W. R. Nelson, H. Hirayama and D. W. O. Rogers, ' The EGS4 code system,' SLAC-265, US. (1985).
- [7.2] R. Brun, F. Bruyant, M. Marie, A. C. McPherson, and P. Zanarin, GEANT3, CERN Data Handling Division (1987).
- [7.3] T. Kunugi, M. Akiba, M. Ogawa et al., ' The simulation fo the Energy Deposition from Runaway Electrons in Plasma Facing Components with EGS4,' Fusion Technology, 21 (1992)1868.

This is a blank page.

# 国際単位系 (SI) と換算表

表1 SI基本単位および補助単位

量	名称	記号
長さ	メートル	m
質量	キログラム	kg
時間	秒	s
電流	アンペア	A
熱力学温度	ケルビン	K
物質質量	モル	mol
光度	カンデラ	cd
平面角	ラジアン	rad
立体角	ステラジアン	sr

表3 固有の名称をもつSI組立単位

量	名称	記号	他のSI単位による表現
周波数	ヘルツ	Hz	s <sup>-1</sup>
力	ニュートン	N	m·kg/s <sup>2</sup>
圧力, 応力	パスカル	Pa	N/m <sup>2</sup>
エネルギー, 仕事, 熱量	ジュール	J	N·m
工率, 放射束	ワット	W	J/s
電気量, 電荷	クーロン	C	A·s
電位, 電圧, 起電力	ボルト	V	W/A
静電容量	ファラド	F	C/V
電気抵抗	オーム	Ω	V/A
コンダクタンス	ジーメンズ	S	A/V
磁束	ウェーバ	Wb	V·s
磁束密度	テスラ	T	Wb/m <sup>2</sup>
インダクタンス	ヘンリー	H	Wb/A
セルシウス温度	セルシウス度	°C	
光強度	ルーメン	lm	cd·sr
照射度	ルクス	lx	lm/m <sup>2</sup>
放射能	ベクレル	Bq	s <sup>-1</sup>
吸収線量	グレイ	Gy	J/kg
線量当量	シーベルト	Sv	J/kg

表2 SIと併用される単位

名称	記号
分, 時, 日	min, h, d
度, 分, 秒	°, ', "
リットル	l, L
トン	t
電子ボルト	eV
原子質量単位	u

1 eV = 1.60218 × 10<sup>-19</sup> J

1 u = 1.66054 × 10<sup>-27</sup> kg

表4 SIと共に暫定的に維持される単位

名称	記号
オングストローム	Å
バール	bar
ガリ	Gal
キュリー	Ci
レントゲン	R
ラド	rad
レム	rem

1 Å = 0.1 nm = 10<sup>-10</sup> m

1 bar = 100 fm<sup>2</sup> = 10<sup>-28</sup> m<sup>2</sup>

1 bar = 0.1 MPa = 10<sup>5</sup> Pa

1 Gal = 1 cm/s<sup>2</sup> = 10<sup>-2</sup> m/s<sup>2</sup>

1 Ci = 3.7 × 10<sup>10</sup> Bq

1 R = 2.58 × 10<sup>-4</sup> C/kg

1 rad = 1 cGy = 10<sup>-2</sup> Gy

1 rem = 1 cSv = 10<sup>-2</sup> Sv

表5 SI接頭語

倍数	接頭語	記号
10 <sup>18</sup>	エクサ	E
10 <sup>15</sup>	ペタ	P
10 <sup>12</sup>	テラ	T
10 <sup>9</sup>	ギガ	G
10 <sup>6</sup>	メガ	M
10 <sup>3</sup>	キロ	k
10 <sup>2</sup>	ヘクト	h
10 <sup>1</sup>	デカ	da
10 <sup>-1</sup>	デシ	d
10 <sup>-2</sup>	センチ	c
10 <sup>-3</sup>	ミリ	m
10 <sup>-6</sup>	マイクロ	μ
10 <sup>-9</sup>	ナノ	n
10 <sup>-12</sup>	ピコ	p
10 <sup>-15</sup>	フェムト	f
10 <sup>-18</sup>	アト	a

(注)

- 表1-5は「国際単位系」第5版, 国際度量衡局 1985年刊行による。ただし, 1 eV および 1 uの値は CODATA の1986年推奨値によった。
- 表4には海里, ノット, アール, ヘクトールも含まれているが日常の単位なのでここでは省略した。
- barは, JISでは流体の圧力を表わす場合に限り表2のカテゴリーに分類されている。
- EC閣僚理事会指令では bar, barn および「血圧の単位」mmHgを表2のカテゴリーに入れている。

## 換算表

力	N (=10 <sup>5</sup> dyn)	kgf	lbf
	1	0.101972	0.224809
	9.80665	1	2.20462
	4.44822	0.453592	1

粘度 1 Pa·s (N·s/m<sup>2</sup>) = 10 P (ポアズ) (g/(cm·s))

動粘度 1 m<sup>2</sup>/s = 10<sup>4</sup> St (ストークス) (cm<sup>2</sup>/s)

圧	MPa (=10 bar)	kgf/cm <sup>2</sup>	atm	mmHg (Torr)	lbf/in <sup>2</sup> (psi)
	1	10.1972	9.86923	7.50062 × 10 <sup>3</sup>	145.038
力	0.0980665	1	0.967841	735.559	14.2233
	0.101325	1.03323	1	760	14.6959
	1.33322 × 10 <sup>-4</sup>	1.35951 × 10 <sup>-3</sup>	1.31579 × 10 <sup>-3</sup>	1	1.93368 × 10 <sup>-2</sup>
	6.89476 × 10 <sup>-3</sup>	7.03070 × 10 <sup>-2</sup>	6.80460 × 10 <sup>-2</sup>	51.7149	1

エネルギー・仕事・熱量	J (=10 <sup>7</sup> erg)	kgf·m	kW·h	cal (計量法)	Btu	ft·lbf	eV
	1	0.101972	2.77778 × 10 <sup>-7</sup>	0.238889	9.47813 × 10 <sup>-4</sup>	0.737562	6.24150 × 10 <sup>18</sup>
	9.80665	1	2.72407 × 10 <sup>-6</sup>	2.34270	9.29487 × 10 <sup>-3</sup>	7.23301	6.12082 × 10 <sup>19</sup>
	3.6 × 10 <sup>6</sup>	3.67098 × 10 <sup>5</sup>	1	8.59999 × 10 <sup>5</sup>	3412.13	2.65522 × 10 <sup>6</sup>	2.24694 × 10 <sup>25</sup>
	4.18605	0.426858	1.16279 × 10 <sup>-6</sup>	1	3.96759 × 10 <sup>-3</sup>	3.08747	2.61272 × 10 <sup>19</sup>
	1055.06	107.586	2.93072 × 10 <sup>-4</sup>	252.042	1	778.172	6.58515 × 10 <sup>21</sup>
	1.35582	0.138255	3.76616 × 10 <sup>-7</sup>	0.323890	1.28506 × 10 <sup>-3</sup>	1	8.46233 × 10 <sup>18</sup>
	1.60218 × 10 <sup>-19</sup>	1.63377 × 10 <sup>-20</sup>	4.45050 × 10 <sup>-26</sup>	3.82743 × 10 <sup>-20</sup>	1.51857 × 10 <sup>-22</sup>	1.18171 × 10 <sup>-19</sup>	1

1 cal = 4.18605 J (計量法)

= 4.184 J (熱化学)

= 4.1855 J (15 °C)

= 4.1868 J (国際蒸気表)

仕事率 1 PS (仏馬力)

= 75 kgf·m/s

= 735.499 W

放射能	Bq	Ci
	1	2.70270 × 10 <sup>-11</sup>
	3.7 × 10 <sup>10</sup>	1

吸収線量	Gy	rad
	1	100
	0.01	1

照射線量	C/kg	R
	1	3876
	2.58 × 10 <sup>-4</sup>	1

線量当量	Sv	rem
	1	100
	0.01	1

